Lipid storage and trafficking mechanisms in *Plasmodium falciparum*

Jiwon Lee

August, 2025

A thesis submitted for the degree of Doctor of Philosophy of

The Australian National University

Australian National University

Declaration

I hereby declare that this thesis is my own original work and contains no material that has been accepted for the award of any other degree in any university or other institution. To the best of my knowledge, this thesis contains no material previously published or written by another person, except where due reference is made in the text.

Parts of this thesis have been published during the course of my candidature, as indicated in the relevant chapter.

Jiwon Lee

August, 2025

Acknowledgement

First and foremost, I would like to thank my supervisors, Alex Maier and Melanie Rug. Your guidance has helped me shift from a technical mindset to thinking more scientifically. You have reshaped the way I approach research and helped me grow into a true-scientist. Thank you for believing in me and supporting this journey.

To the past and present members of the Maier lab - thank you for always making the lab a lively, energetic, and supportive place. Your presence made even the longest days of experiments enjoyable. I will truly miss the incredible energy and fun atmosphere we shared.

To my colleagues at the Centre for Advanced Microscopy, thank you for supporting me throughout this journey. I'm deeply grateful for your help whenever I faced technical challenges, but even more so for simply being there during moments of exhaustion. Your support made all the difference.

Finally, to my family - Lino, without you, none of this would have been possible. Thank you for being endlessly supportive and for standing by me through every mental and physical meltdown. Mum, finally it's time! The moment you've been waiting for is here. Dad, words can't capture how much I wish you were here to share this moment. I can only imagine how proud and happy you'd be.

This thesis is a product of not just my efforts, but the encouragement, kindness, and support of many people along the way. Thank you all.

Abstract

Plasmodium falciparum, the causative agent of the most severe form of human malaria, undergoes dramatic metabolic shifts across its complex life cycle. Lipid metabolism is critical for membrane biogenesis, energy storage, and developmental transitions. Despite increasing recognition of lipid droplet (LD) biology in other eukaryotes, how *P. falciparum* stores and regulates neutral lipids (NLs) remains poorly understood.

This thesis investigates the formation, composition, and dynamics of neutral lipid storage compartments across blood-stage development. Progressive accumulation of triacylglycerol (TAG)-rich LDs from ring to schizont stage was demonstrated in the asexual stages. Using Nile Red spectral imaging, three-dimensional focused ion beam scanning electron microscopy (3D FIB-SEM) ultrastructural analysis, and metabolic inhibitor assays were used to demonstrate that LD formation and turnover are essential for schizogony, supporting their crucial role in membrane biosynthesis and prevention of lipotoxicity.

A bioinformatic analysis identified candidate LD associated proteins in *P. falciparum*, including conserved lipid synthesis enzymes such as *P. falciparum* diacylglycerol acyltransferase (PfDGAT), acyl-CoA:cholesterol acyltransferase (PfACAT), and phospholipase (PfPL), as well as potential stage-specific regulators such as lysophospholipase 1 (PfLPL1) and ATP-binding cassette transporter G2 (PfABCG2). Analyses of transcriptomic data revealed distinct expression patterns: the TAG synthesis enzyme PfDGAT is enriched in asexual stages and male gametocytes, while the putative cholesteryl ester (CE) synthesis enzyme PfACAT is enriched in female gametocytes, reflecting stage and sex-specific lipid metabolic strategies.

In gametocytes, classical LD structures were not observed. Instead, a female-specific, neutral lipid-rich compartment - termed femLB - was ultrastructurally characterised in this thesis, revealing a densely packed membrane compartment with co-localisation of the ABC transporter PfABCG2.

Altogether, this work demonstrates that *P. falciparum* employs distinct, stage- and sex-specific strategies for neutral lipid storage: TAG-rich LDs are accumulated in asexual stages to support rapid proliferation while female gametocytes store neutral lipids in particular membrane compartments in female gametocytes. These findings provide new insights into the structural and molecular diversity of lipid storage in malaria parasites and lay the foundation for future studies exploring lipid metabolism as a potential target for stage-specific or transmission-blocking antimalarial strategies.

Table of contents

List of abbreviations

3D-EM	three-dimensional electron microscopy
ABC	ATP-binding cassette transporter
ABCA	ABC transporter of the A-subfamily
ABCG	ABC transporter of the G-subfamily
ACAT	Acyl-CoA:cholesterol acyltransferase
ACS	acyl-CoA synthetases
AFS	automated freeze substitution
AGPAT	1-acylglycerol-3-phosphate-O-acyltransferase
ATP	Adenosine Triphosphate
BF	bright field
BiP	binding immunoglobulin protein
BSA	Bovine serum albumin
BSE	backscattered electron
CE	cholesteryl ester
CIDE	cell death-inducing DNA fragmentation factor-like effector
CLEM	correlative light and electron microscopy
COPI	Coat Protein Complex I
DAG	diacylglycerol
DFCP1	Double FYVE domain containing protein 1
DGAT	diacylglycerol acyltransferase
DI	deionised
DIC	Differential Interference Contrast
DMSO	Dimethyl sulfoxide
DNA	deoxyribonucleic acid
DNN	deep neural network
DRM	Detergent-resistant membrane
DV	digestive vacuole
ECL	enhanced chemiluminescence
EDTA	ethylenediaminetetraacetic acid

EM	electron microscopy
ER	endoplasmic reticulum
ESB	energy-selective back-scatter detector
FAs	Fatty acids
FASII	type II fatty acid synthesis
FC	Free cholesterol
FemLB	female lipid body
FIB-SEM	focused ion beam scanning electron microscopy
FIT	fat storage-inducing transmembrane
FS	freeze substitution
FSP27	fat-specific protein 27
G3P	glycerol-3-phosphate
GA	glutaraldehyde
GFP	Green fluorescent protein
GlcNAc	N-acetyl-D-glucosamine
GPAT	glycerol-3-phosphate acyltransferase
GPI	glycosylphosphatidylinositol
GTP	guanosine-5'-triphosphate
HDL	high density lipoprotein
HEPES	4-(2-hydroxyethyl)-1-piperazineethanesulfonic acid
HPF	high pressure freezing
hpi	hours post infection
IC_{50}	half-maximal inhibitory concentration
IgG	immunoglobulin G
iRBCs	infected red blood cells
KDa	kilodalton
LCAT	lecithin-cholesterol acyltransferase
LD	lipid droplet
LDAF1	lipid droplet assembly factor 1
LDL	low-density lipoprotein
LDs	lipid droplets
LM	light microscopy
LPA	lysophosphatidic acid

LPC	lysophosphatidylcholine
LPL	lysophospholipid
MAG	monoacylglycerol
MCS	Membrane contact sites
MFI	mean fluorescence intensity
MGAT	acyl-CoA:monoacylglycerol acyltransferases
MIB	Microscopy Image Browser
mRNA	messenger ribonucleic acid
NA	numerical aperture
NCR1	Niemann-Pick Type C1
NL	neutral lipid
NPC1L1	Niemann-Pick C1 like 1
NRZ	NAG-RINT1-ZW10
ORS	Object Research Systems
OTO	osmium-thiocarbohydrazide-osmium
PA	phosphatidic acid
PAP	phosphatidic acid phosphatase
PBS	phosphate buffered saline
PBS-G	glycine in PBS
PC	phosphatidylcholine
PDAT	phospholipid:diacylglycerol acyltransferase
PE	phosphatidylethanolamine
PEXEL	Plasmodium export element
PG	phosphatidyl glycerol
PL	phospholipid
PLA	phospholipase
PLA2	phospholipase A2
PLIN	Pelilipin
PPM	parasite plasma membrane
PS	phosphatidylserine
PVDF	polyvinylidene difluoride
PVM	parasitophorous vacuole membrane
RalA	Ras-related protein

RBC	red blood cell
RNA-seq	RNA sequencing
ROI	region of interest
RT	room temperature
SD	standard deviation
SDS	Sodium dodecyl sulfate
SDS-PAGE	sodium dodecyl sulfate–polyacrylamide gel electrophoresis
SE	secondary electron
SEM	scanning electron microscopy
SEM	Standard error of the mean
SNARE	soluble N-ethylmaleimide-sensitive factor attachment protein receptor
TAG	triacylglycerol
TBS	tris-buffered saline
TBST	tris-buffered saline with Tween20
TCH	Thiocarbohydrazide
TEM	transmission electron microscopy
TVM	tubulovesicular membrane
TVN	tubovesicular network
UA	uranyl acetate
uRBC	uninfected RBC
UV	ultraviolet
WT	wild type
XN	Xanthohumol
ZFYVE1	zinc finger FYVE domain containing protein1

Chapter 1. Introduction

Plasmodium falciparum

Malaria, caused by infection with *Plasmodium* parasites, remains one of the most severe and widespread parasitic diseases, particularly affecting populations in tropical and subtropical regions. According to the World Malaria Report published by the WHO, approximately 263 million malaria cases and 597,000 malaria-related deaths occurred globally in 2023 (World Malaria Report, 2024). At least six *Plasmodium* species cause malaria in humans: *P. falciparum* and *P. vivax* are the most prevalent, while *P. malariae, P. knowlesi,* and two subspecies of *P. ovale* also contribute to human malaria cases. Among these, *P. falciparum* is the most virulent and is responsible for the most severe, life-threatening forms of the disease.

Efforts to control and eliminate malaria continue to face major challenges, particularly due to the parasite's remarkable adaptability (*via* antigenic variation) and ability to develop resistance to antimalarial drugs. Over time, *P. falciparum* has evolved resistance to nearly every frontline therapy developed against it, including chloroquine, sulfadoxine-pyrimethamine, and more recently, artemisinin derivatives (Sidhu et al., 2002; Gatton Michelle et al., 2004; Ouji et al., 2018). This highlights a fundamental problem: the parasites highly adaptable, and it has repeatedly outpaced human intervention strategies. Its ability to survive in dramatically different environments - from the nutrient-rich human liver and blood to the mosquito midgut - suggests the presence of robust and adaptable cellular mechanisms that are not yet fully understood. Understanding the cell biology of *P. falciparum* is therefore essential for identifying new vulnerabilities that might lead to novel therapeutic avenues. Although there have been significant advances in areas like genomic sequencing, transcriptomics, and high-resolution imaging, many aspects of the parasite’s intracellular organisation, trafficking pathways, and metabolic regulation remain poorly defined. In particular**,** the cellular mechanisms that govern lipid storage and trafficking - processes essential for membrane

biogenesis, energy buffering, and parasite development - are still not well understood. Since lipids are critical to the survival of the parasite during its rapid replication and transmission stages, understanding how *P. falciparum* handles its lipid reserves may provide new insights into parasite adaptation and persistence.

Life cycle stages of P. falciparum

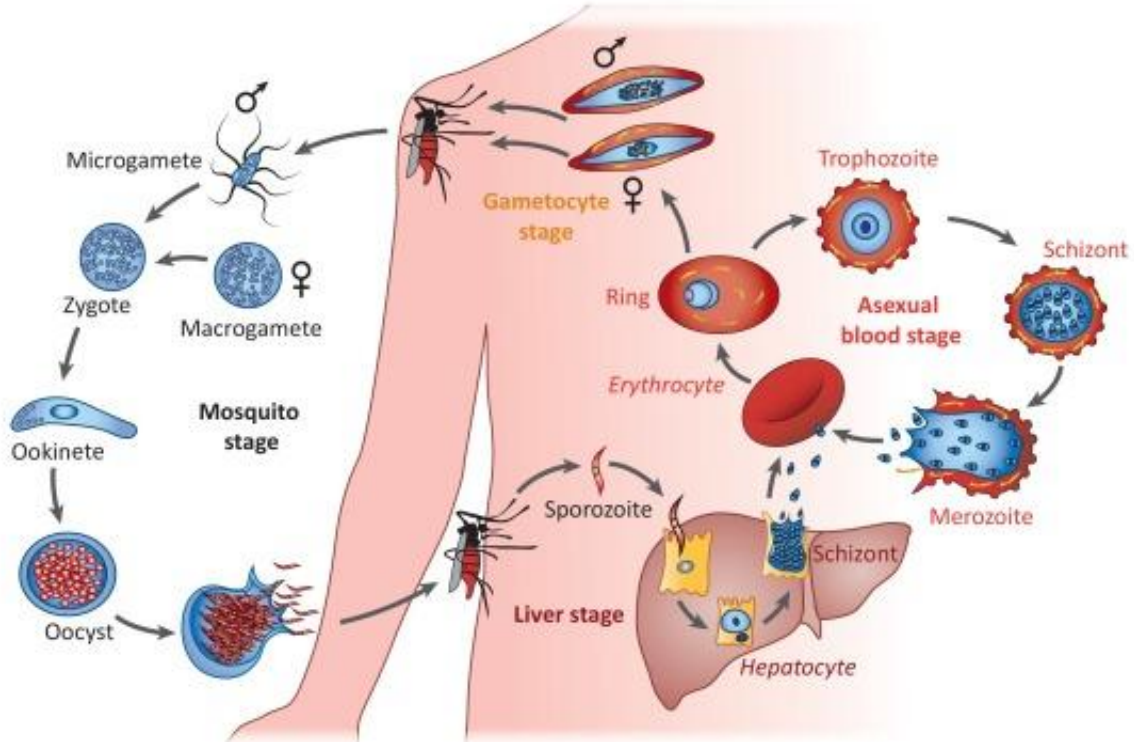

Figure 1. Life cycle stages of *P. falciparum* (*Maier et al.*; 2019). During a blood meal, infected mosquitoes transmit *P. falciparum* sporozoites to the human host. Sporozoites migrate to the liver, where they invade hepatocytes and undergo asexual replication to produce merozoites. These are released into the bloodstream and invade erythrocytes. Within erythrocytes, parasites replicate asexually and releasing daughter merozoites that invade new erythrocytes. A subset of merozoites commits to sexual differentiation, developing into male and female gametocytes. These gametocytes are ingested during a blood meal, where they rapidly mature into male and female gametes and undergo fertilisation. The resulting zygote develops into a motile ookinete that penetrates the mosquito midgut wall and encysts as an oocyst. Sporozoites produced within the oocyst eventually migrate to the mosquito salivary gland, ready for transmission to a new human host during the next blood meal.

P. falciparum has a complex life cycle that alternates between two different hosts: human and mosquito (**Figure 1**). Infection in humans begins when infected mosquito injects sporozoites into the human host as it takes a blood meal. Once the parasites get inside of the human body, sporozoites migrate to the liver, where they invade hepatocytes and replicate asexually. This replication produces thousands of merozoites, which are released into the blood stream to initiate the asexual blood stage cycle.

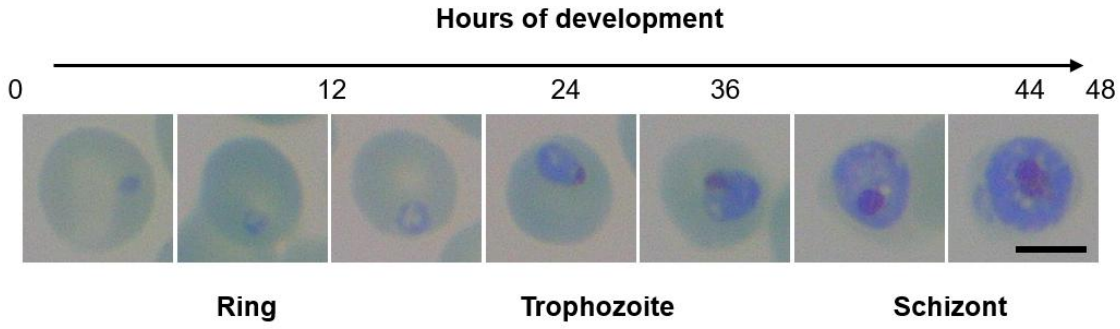

Figure 2. Representative images of Giemsa-stained *P. falciparum*-infected erythrocytes at different developmental stages of the asexual blood stage cycle. During the asexual cycle, parasite transition through the ring, trophozoite, and schizont stages before releasing daughter merozoites. Scale bar: 5 μm.

The asexual blood stage cycle of *P. falciparum* lasts approximately 48 hours and involves three key morphological stages: ring, trophozoites, and schizont (**Figure 2**). After invading a red blood cell (RBC), a single haploid merozoite transforms into a ring stage, which becomes morphologically recognisable by around 6h post invasion (hpi) as a small, ring-shaped form. As the parasite develops, the cytoplasm expands and digestive vacuole (DV) becomes apparent, marking its transition into the trophozoite stage. During schizont stage (around 36-48 hpi), the parasite transforms into multinucleated syncytium as a nuclear division occur in preparation

for merozoite formation. This results in segmentation, where individual daughter merozoites are formed and eventually released as the infected erythrocyte ruptures, enabling reinvasion of new RBCs.

Throughout this developmental cycle, the parasite induces marked structural changes in the host erythrocyte. As the trophozoite and schizont stages progress, knob-like protrusions form on the surface of the infected cell (Gruenberg et al., 1983). These modifications promote cytoadherence - where infected erythrocytes stick to the walls of blood vessels - impairing blood flow and allowing the parasite to evade clearance by the spleen (Smith et al., 2013). Together, parasite replication and erythrocyte deformation contribute to the major clinical symptoms of malaria, such as fever, chills, and anaemia. In severe cases, cytoadherence may lead to complications like cerebral malaria, coma, and death.

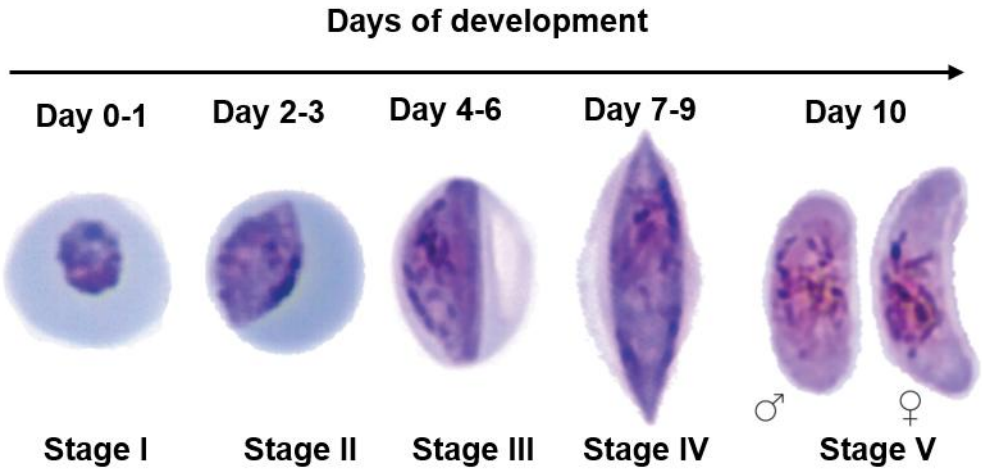

Figure 3. Representative images of Giemsa-stained *P. falciparum* during sexual development (Josling and Llinas, 2015). Gametocyte development is traditionally divided into five morphologically distinct stages. Stage I and II gametocytes are generally challenging to distinguish from asexual trophozoites, while stage III gametocytes begin to elongate and become discernible. In stage IV the gametocyte adopts a more pointed shape. Finally, stage V gametocytes assume their characteristic crescent shape, with females appearing more elongated and curved compared to the thicker, rounded males.

While most merozoites continue the asexual cycle, a subset commits to sexual differentiation, forming gametocytes. This commitment ensures transmission to the mosquito and is critical for the continuation of the life cycle. Only gametocytes are capable of infecting mosquitoes. Gametocyte development takes approximately 10-12 days and is traditionally divided into five morphologically distinct stages, known as stages I-V (**Figure 3**). Stage I and II gametocytes closely resemble asexual trophozoites. Stage III marks the beginning of drastic morphological changes, as the parasite elongates into an oval shape with a single nucleus. In stage IV, the gametocytes are maximally elongated with a crescent shape. By stage V, the gametocyte is fully mature, and it is now possible to distinguish male and female forms. Female gametocytes are generally contain a higher number of osmiophilic bodies, while male gametocytes contain fewer osmiophilic bodies (Ngotho et al., 2019; Evers et al., 2025).

The mature gametocyte is ingested by a mosquito and rapidly egresses from its host erythrocyte. Male gametocytes undergo exflagellation, producing 8 motile and flagellated microgametes. Female gametocytes develop into a single macrogamete. Fertilisation results in the formation of a diploid zygote which develops into a motile ookinete. The ookinete traverses the mosquito midgut and forms an oocyst in the midgut tissue, within which asexual replication produces thousands of sporozoites. These sporozoites migrate to the mosquito's salivary glands, ready for transmission to a new human host during the next blood meal.

Lipid synthesis in P. falciparum

The blood stage of *Plasmodium* parasites involves the invasion and replication within human RBCs (erythrocytes). Unlike most eukaryotic cells, erythrocytes are unusual host cells as they lack organelles and have no biosynthetic machinery including the capacity to synthesise or transport proteins and lipids. Despite these limitations, *P. falciparum* has evolved mechanisms

to survive and replicate within this minimal environment and rely on both *de novo* synthesis and scavenging of host lipids to sustain its metabolic activities within RBCs (**Figure 4**).

Fatty acids (FAs) serves as key building blocks for membrane biogenesis and energy source. *P. falciparum* acquires FAs both through scavenging and through *de novo* biosynthetic pathways. Imported FAs are converted into fatty acyl-CoA by parasite-encoded acyl-CoA synthetases (ACS). This conversion step is essential, as fatty acyl-CoAs serve as the direct substrates for complex lipid biosynthesis. The *Plasmodium* parasite genome encodes multiple ACS homologs, and some of these proteins have been shown to be essential for asexual parasite growth (Bethke et al., 2006; Bopp et al., 2023). However, the specific functions of individual ACS remain to be fully elucidated.

De novo FA acquisition occurs via two main mechanisms. The type II fatty acid synthesis (FASII) pathway functions in apicoplast, but is dispensable for asexual proliferation under nutrient-rich conditions (Vaughan et al., 2009). In contrast, *P. falciparum* also recycles FAs through a phospholipase A2 (PLA_2)-mediated pathway, which is active various cellular compartments including the parasite plasma membrane (PPM), in intracellular vesicular structure, mitochondria and the DV (Singh et al., 2019; Shunmugam et al., 2023; Pietsch et al., 2024). PLA_2 cleaves membrane phospholipids to release free FAs, which can then be reused for the synthesis of new phospholipids and neutral lipids, supporting both membrane remodelling and lipid storage. PLA_2 activity has been shown to be essential for the transition from asexual stages to gametocytes, highlighting its importance in lipid remodelling during sexual development (Flammersfeld et al., 2020).

Fatty acyl-CoAs are directed into *de novo* diacylglycerol (DAG) synthesis pathway. In this pathway, fatty acyl-CoAs are sequentially added to glycerol-3-phosphate (G3P) to form lysophosphatidic acid (LPA), phosphatidic acid (PA), and then DAG (Vial et al., 1982; Ancelin and Vial, 1989). DAG serves as a central branching point: it can be converted into

phospholipids like phosphatidylcholine (PC) and phosphatidylethanolamine (PE). These phospholipids are major components of the parasite membrane and are essential for its growth and replication. DAG can also be further acylated by diacylglycerol acyltransferase (DGAT) to form triacylglycerol (TAG). TAGs are stored in lipid droplets (LDs) and act as reservoirs of metabolic energy.

Cholesterol is another critical lipid for *P. falciparum*, contributing to membrane integrity and successful invasion (Maier and van Ooij, 2022). However, the parasite lacks a complete *de novo* cholesterol synthesis pathway and must acquire cholesterol from external sources (Sherman, 1979; Vial et al., 1984). Since cholesterol is abundant in the erythrocyte membrane, one proposed mechanism is that *P. falciparum* acquires it by reusing existing cholesterol through haemoglobin invagination or vesicle trafficking (Maguire and Sherman, 1990; Hayakawa et al., 2020; Hayakawa et al., 2021). Previous studies support this idea by showing that a part of the cholesterol-rich erythrocyte membrane invaginates and migrates to the cytosol (Elliott et al., 2008; Tokumasu et al., 2014; Hayakawa et al., 2020). Alternatively, cholesterol may also be taken up directly from the external sources through an unknown mechanism (Hayakawa et al., 2021). A recent study identified the *P. falciparum* Niemann-Pick Type C1-related protein (PfNCR1), which localises between the PPM and parasitophosrous vacuole membrane (PVM), and is proposed to mediate cholesterol transfer into the parasite (Istvan et al., 2019; Garten et al., 2020). Once inside the parasite, cholesterol may be esterified with fatty acyl-CoA to form cholesteryl esters (CEs), which are likely stored in neutral lipid compartments such as LDs (Koivuniemi et al., 2009; Vallochi et al., 2018).

Stored TAGs and CEs can be hydrolysed to release free FAs, which are then reused for membrane lipid synthesis or energy production. This breakdown and reuse cycle allow the parasite to buffer its FA supply and respond to fluctuating metabolic demands.

Together, lipid metabolic pathways are tightly interconnected and *P. falciparum* employs a multifaceted strategy - scavenging, synthesising, storing, and recycling FAs - to meet its changing needs and ensure that a reliable supply for membrane assembly, energy storage in stage-specific adaptation.

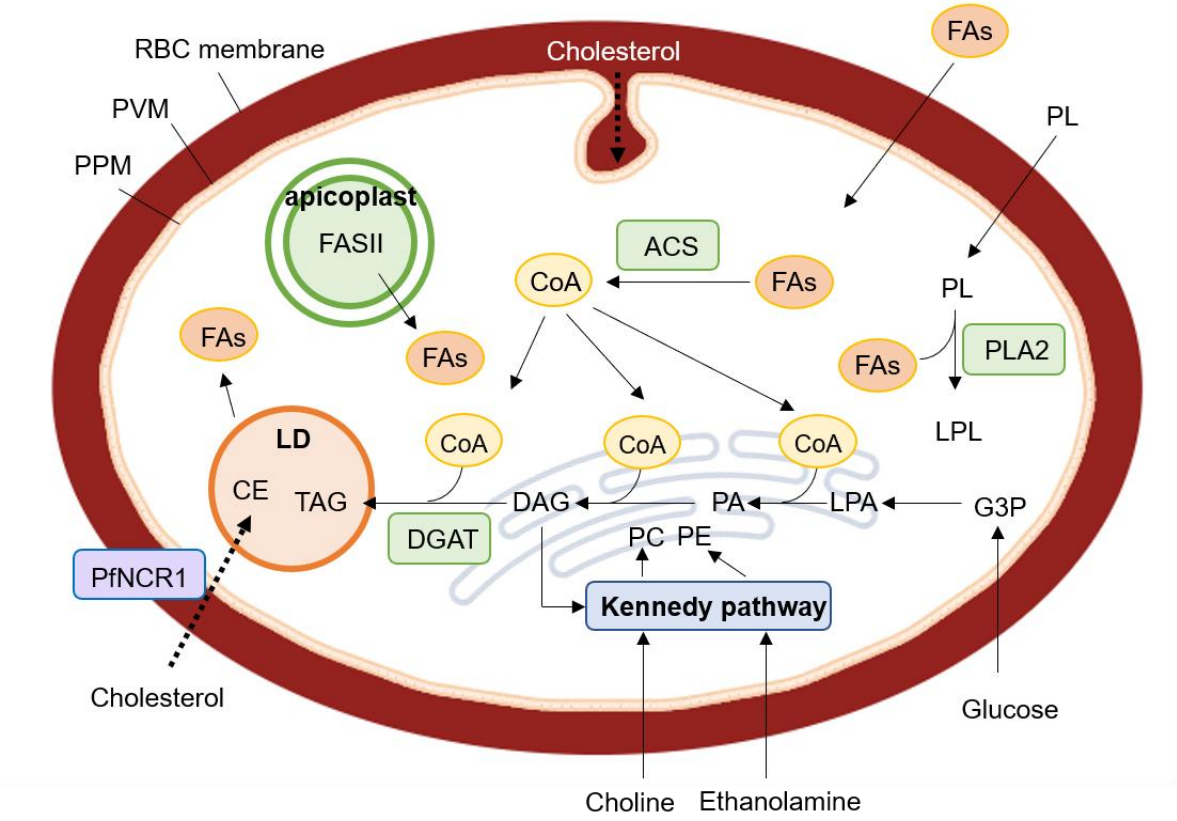

Figure 4. Proposed lipid synthetic pathways in blood stage *Plasmodium falciparum*. *P. falciparum* acquires FAs through scavenging and *de novo* synthesis via the FASII pathway or PLA_2 mediated recycling from membrane phospholipids. FAs are converted into fatty acyl-CoA, which feed into lipid synthetic pathways. Fatty acyl-CoAs are used to generate DAG, a central precursor for the synthesis of membrane phospholipids (e.g., PC, PE) via the Kennedy pathway, and for TAG synthesis. Cholesterol, likely acquired through PfNCR1, can be esterified with FAs to form CE. TAG and CE are stored in LDs and can be hydrolysed to release FAs for membrane biogenesis or energy use.

ACS, acyl-CoA synthetase; CE, cholesteryl ester; CoA, fatty acyl-CoA; DAG, diacylglycerol; DGAT, diacylglycerol acyltransferase; FAs, fatty acids; FASII, type II fatty acid synthesis;

G3P, glycerol-3-phosphate; LD, lipid droplet; LPA, lysophosphatidic acid; LPL, lysophospholipid; PA, phosphatidic acid; PC, phosphatidylcholine; PE, phosphatidylethanolamine; PfNCR1, *Plasmodium falciparum* Niemann-Pick Type C1-related protein; PLA_2, phospholipase A_2; PL, phospholipid; PPM, parasite plasma membrane; PVM, parasitophorous vacuole membrane; TAG, triacylglycerol.

Lipid profile in P. falciparum

Several lipidomic studies have shown that *P. falciparum* dynamically alters its lipid composition throughout the blood stage cycle, particularly in the composition and abundance of neutral lipids (Gulati et al., 2015; Tran et al., 2016; Ridgway et al., 2022).

In uninfected RBC (uRBC), cholesterol is the predominant lipid species (**Figure 5A**). However, following *P. falciparum* infection, the proportion of free cholesterol decreases progressively in both asexual and sexual stages, along with a reduction in sphingolipid content. In contrast, the levels of both phospholipids and neutral lipids increase during these periods.

Among the three main classes of neutral lipids - CE, DAG and TAG - DAG and TAG are the most abundant in asexual parasite-infected RBCs (**Figure 5C**). Each class of neutral lipid appears to be dynamic in asexual blood stage parasites. DAG abundance increases steadily as the parasite develops and proliferates, whereas TAG accumulation peaks between the trophozoite and schizont stages. TAG is then rapidly degraded during merozoite maturation and host cell rupture (Nawabi et al., 2003; Palacpac et al., 2004a; Vielemeyer et al., 2004). Structurally, DAG contains two FA chains, while CE contains only one, making DAG and TAG more efficient forms of FA storage. TAG, in particular, provides the highest energy density and storage efficiency. This suggests that maturing asexual parasites accumulate FA reserves in the form of neutral lipids, which may be rapidly mobilised for membrane

biosynthesis during schizogony. These observations are consistent with studies showing active synthesis of DAG and TAG, but not CE, from exogeneous lipid sources in asexual blood stage *P. falciparum* (Nawabi et al., 2003; Palacpac et al., 2004a; Vielemeyer et al., 2004).

The major phospholipids, PC and PE, also contribute to the overall increase in total lipid content during asexual maturation (Gulati et al., 2015). During the asexual blood stage cycle, the parasite has high demand for lipids to support membrane biogenesis for the growing parasite, daughter merozoites, and intracellular organelles. Given that PC and PE are the main components of these membranes (Schwartz et al., 1987), their accumulation aligns with increasing structural and metabolic demands of the developing parasite.

Gametocytes undergo a remarkable metabolic shift as they prepare for sexual differentiation and transmission. Unlike asexual stage parasites, gametocytes do not divide during development but instead undergo extensive morphological transformation over a 10-12 day period. Previously, gametocytes were considered metabolically dormant, as they can persist in the blood for weeks (Sinden et al., 1997). However, recent lipidomic studies have shown that the lipid profile of gametocytes changes significantly between young and mature gametocytes (Tran et al., 2016; Ridgway et al., 2022). Total lipid abundance increases 3-5- fold compared to uRBC, suggesting that lipid metabolism is active during gametocytogenesis. Importantly, this upregulation of lipid metabolism is not only stage-specific but also appears to be sex-dependent. These differences are likely driven by the distinct biological roles and developmental trajectories of male and female gametocytes.

Phospholipid abundance is comparable between male and female gametocyte-infected RBCs, with no significant differences in the major phospholipid classes (Ridgway et al., 2022). As essential components of cellular membranes, phospholipids are likely required for organelle development in both sexes, and for male-specific cell division during gametogenesis.

Notably, female gametocyte-infected RBCs accumulate significantly more lipids than male gametocyte-infected RBCs (Ridgway et al., 2022). Among the four major lipid categories - phospholipids, sphingolipids, free cholesterol and neutral lipids - only neutral lipids are significantly more abundant in female gametocyte-infected RBCs (Ridgway et al., 2022). In particular, female gametocytes show markedly higher levels of CE compared to male gametocytes (**Figure 5B**). This sex-specific enrichment suggests a distinct role for neutral lipids in female gametocyte biology and transmission. Given that mosquitos lack the ability to synthesise cholesterol *de novo*, CE reserves in female gametocytes may serve as a stored cholesterol source for parasite development within the mosquito vector.

While DAG and TAG are both efficient forms of FA storage, no significant difference in their overall abundance was observed between male and female gametocytes (Ridgway et al., 2022). These neutral lipids may serve as a shared energy reserve to support processes such as organelle biogenesis in both sexes. In males, they may also contribute to the energy demands of exflagellation and rapid cell division. Although CE accumulation shows clear sex-specific enrichment, the relatively similar levels of DAG and TAG in both sexes suggest that these lipids fulfil more generalised roles in gametocyte development and function.

These differences in lipid abundance and composition between male and female gametocytes likely reflect divergent functional demands and highlight the importance of sex-specific lipid storage strategies. While variations in lipid profiles in different life cycle stages of *P. falciparum* reflects the parasite's adaptation to a physiological demand, how these lipids are stored and mobilised remains poorly understood.

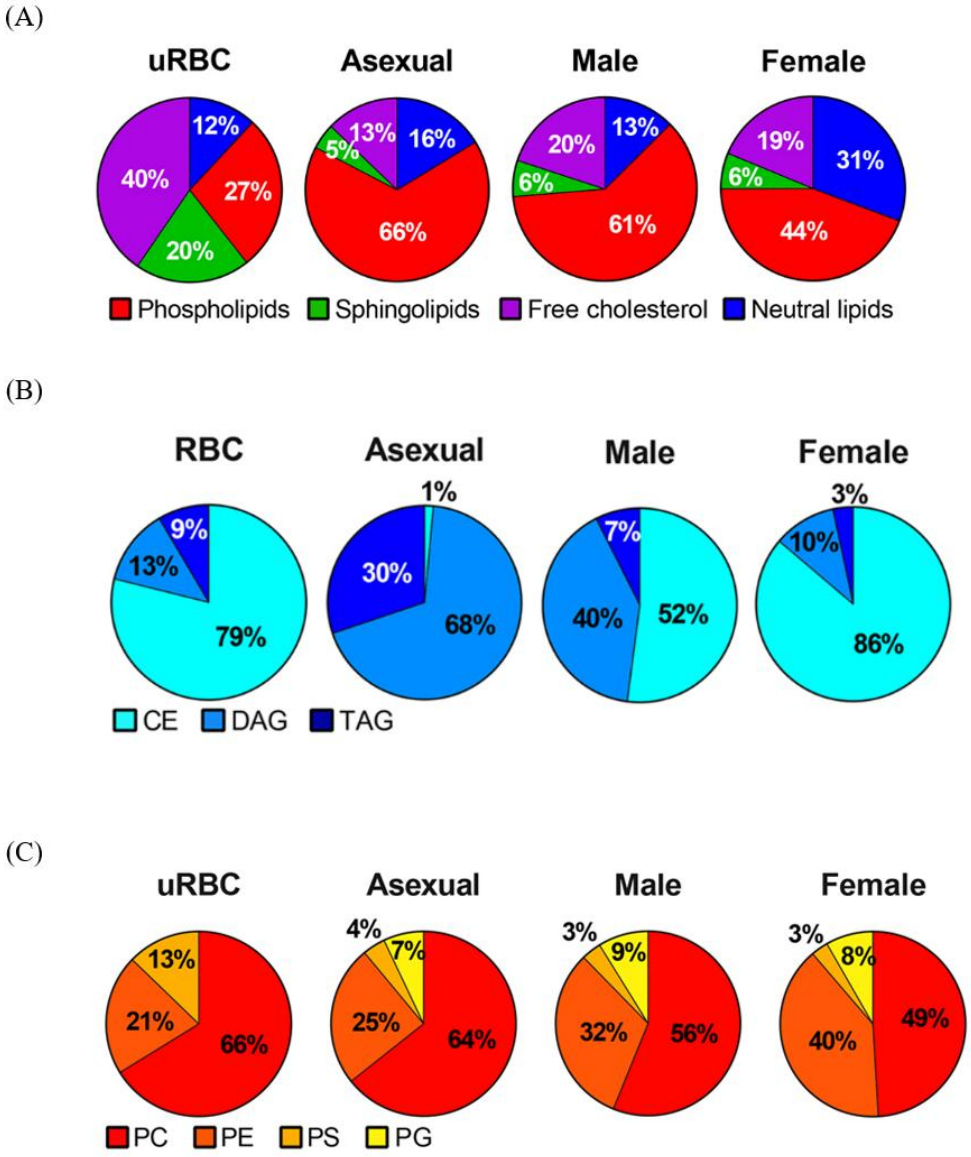

Figure 5. Summary of changes in lipid abundance over the asexual and sexual *P. falciparum* blood stages (from *Ridgway et al.*; 2022). (A) Overview of the lipid classes in uRBC and RBCs infected with mature asexual stages parasites, male and female gametocytes. (B) Analysis of neutral lipids abundance and (C) phospholipids abundance in uRBC, mature asexual, male and female gametocytes. Percentages for each principal component indicate the contribution of each component to overall variation between samples.

CE: cholesteryl Ester, DAG: diacylglycerol, TAG: triacylglycerol, PC: phosphatidylcholine, PE: phosphatidyl ethanolamine, PS: phosphatidylserine, PG: phosphatidyl glycerol.

Lipid droplet

Lipid droplet architecture

Lipids are essential for cellular function, providing energy reserves and building blocks for structural components such as membranes. For many organisms, energy availability fluctuates between periods of surplus and starvation, and the ability to store energy provides a clear evolutionary advantage. In most eukaryotes, neutral lipids such as TAG and CE are stored within specialised intracellular compartments known as lipid droplets (LDs).

Although LDs were initially considered passive fat storage compartments, they are now recognised as dynamic organelles that play central roles, not only in lipid storage but also in energy metabolism and cellular signalling. Structurally, LDs are composed of a highly hydrophobic core of neutral lipids surrounded by a phospholipid monolayer (**Figure 6**). This monolayer is mainly composed of PC and PE, but relatively depleted in sphingomyelin and phosphatidic acid (Leber et al., 1994; Tauchi-Sato et al., 2002; Bartz et al., 2007a). Free cholesterol (FC) is also believed to be incorporated into the LD surface layer (Prattes et al., 2000).

Proteomic studies have identified hundreds of LD-associated proteins across a wide range of organisms, from bacteria to humans. These include enzymes involved in lipid synthesis and metabolism, as well as proteins that mediate membrane trafficking and signal transduction (Yang et al., 2012). Most of these proteins are generally thought to be embedded in or associated with the LD surface, where they contribute to LD biogenesis, lipid turnover, and interactions with other organelles.

Despite their conserved architecture, LDs exhibit considerable variation in number, size, and composition across different cell types and even within the same cells. These variations reflect

differences in metabolic activity and physiological state. For example, LDs can range in size from ~0.1 µm in yeast to over 100 µm in white adipocytes (Suzuki et al., 2011). Their internal composition also differs: LDs in yeast contain approximately equal amounts of TAG and CE, adipocytes predominantly store TAG, and macrophages are enriched in CE (Clausen et al., 1974; Schaffner and Matile, 1981). In yeast and mammalian LDs, PC is the major phospholipid (Tauchi-Sato et al., 2002; Bartz et al., 2007a) while Drosophila LDs contain more PE than PC (Krahmer et al., 2011).

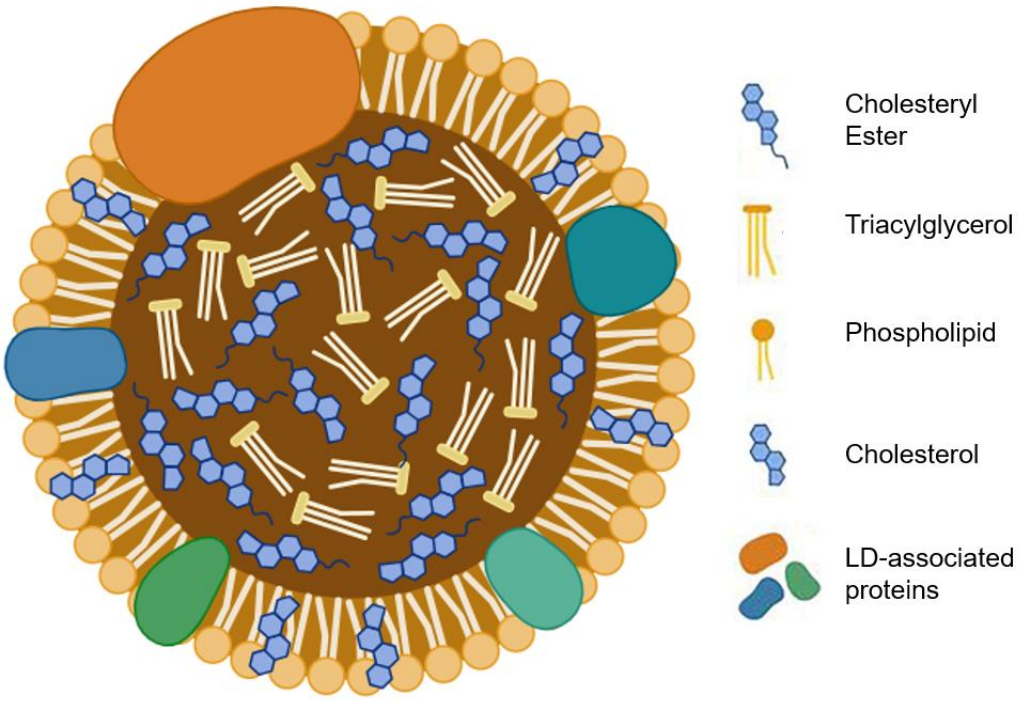

Figure 6. Schematic overview of lipid droplet morphology. LDs consist of a neutral lipid core composed primarily of triacylglycerol (TAG) and cholesteryl ester (CE), surrounded by a phospholipid monolayer. The surface monolayer, composed of phospholipids and free cholesterol, serves as a platform for LD-associated proteins involved in lipid metabolism, membrane trafficking, and signaling. Created with BioRender.com

Lipid droplet biogenesis: proposed models

LDs are thought to originate from the endoplasmic reticulum (ER), although the precise mechanisms underlying their formation remain under investigation. Several models have been proposed to explain how neutral lipids such as TAG are packaged and enclosed within a phospholipid monolayer to form distinct LD structures (Murphy and Vance, 1999; Zweytick et al., 2000).

The most widely accepted model is the ER budding model (**Figure 7A**). In this model, TAGs are synthesised between the two leaflets of the ER membrane through the sequential addition of fatty acids to a glycerol backbone. As neutral lipids accumulate, they form a lens-like structure within the ER bilayer. With continued lipid synthesis, the lens expands and eventually buds toward the cytosol. The resulting LD is enclosed by a phospholipid monolayer derived from the outer ER leaflet. The LD may remain tethered to the ER or become fully released into the cytosol. This model is supported by imaging studies that demonstrate close ER–LD associations in diverse eukaryotic systems (Choudhary et al., 2015; Ladinsky et al., 2019).

While the ER budding model remains the most widely accepted, emerging evidence suggests that LD biogenesis may involve more than one pathway, depending on cell type, physiological state, or metabolic demand. One alternative model is the vesicle efflux model (**Figure 7B**), which proposes that neutral lipids are packed into small ER-derived vesicles that bud into the cytosol. These vesicles may subsequently mature into LDs or fuse with other lipid-rich compartments. It's still not fully understood how these vesicles transition into LDs, but it highlights an alternative pathway of neutral lipid storage. Unlike the ER budding model, this model involves transient bilayer structures and is thought to occur under specific physiological conditions. Efficient formation of these vesicles likely depends on highly organised, compositionally distinct regions of the ER membrane. These microdomains may serve as

platforms for the selective enrichment of lipids and proteins required for vesicle formation. Given that LD formation often occurs at specific membrane sites, raft-like domains enriched in sterols and sphingolipids have been proposed to facilitate the organisation of lipid-synthesising enzymes and structural proteins, potentially influencing where and how LDs emerge from the ER. Supporting this model, several studies have suggested a connection between LDs and intracellular vesicle formation – for example, macrophages have been shown to generate lipid-filled small extra vesicles as a source of lipids (Flaherty et al., 2019).

A third model proposes that LDs may form independently of the ER through the cytosolic aggregation of neutral lipids and lipid-binding proteins (**Figure 7C**). In this scenario, cytosolic proteins capable of stabilising hydrophobic molecules nucleate the formation of small lipid–protein aggregates, which subsequently acquire a phospholipid layer. While this model is not yet well supported by experimental data, it may be particularly relevant in conditions where ER–LD interactions are disrupted or under specific cellular stress. While evidence for this pathway is limited, it remains a plausible alternative, particularly in cases where LDs are observed at locations distant from the ER (Sturley and Hussain, 2012).

Together, these models suggest that LD biogenesis might be a flexible, context-dependent process involving multiple potential routes.

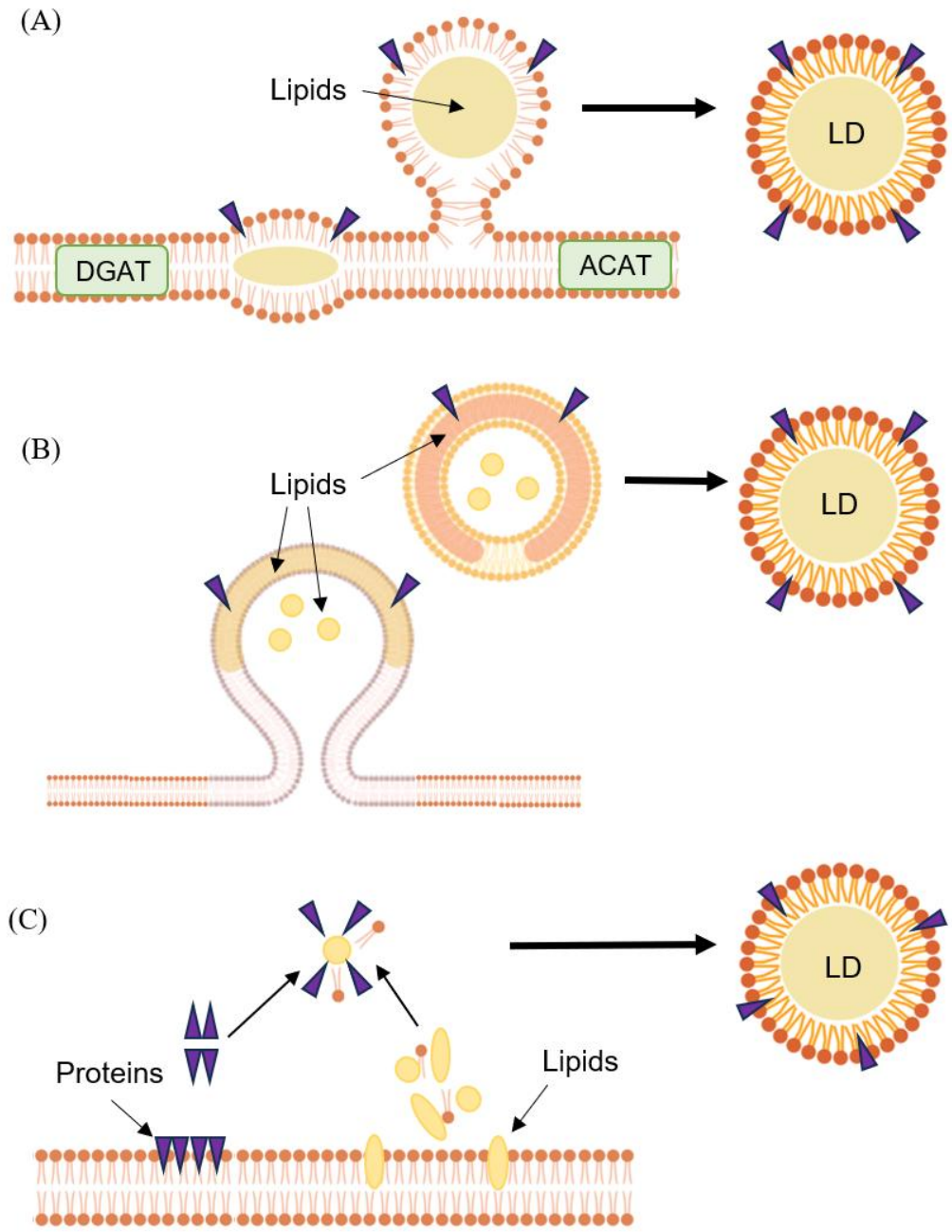

Figure 7. Models for the biogenesis of intracellular lipid droplet. (A) **Budding model**: neutral lipids accumulate within the ER bilayer to form a lipid lens that buds into the cytosol, forming a nascent LD. (B) **Vesicle flux model**: lipid-filled vesicles bud from the ER and are released into the cytosol, where they undergo structural remodelling to form mature LDs. (C) **Aggregation model**: cytosolic lipid-binding proteins aggregate with neutral lipids released from the ER to form LD precursors. Created with BioRender.com. Models adapted from Zweytick et al., 2000; Coppens and Vielemeyer, 2005.

Lipid synthesis and LD formation

The formation of LDs is a complex, tightly regulated process involving multiple enzymatic reactions and dynamic lipid intermediates, including both phospholipids and neutral lipids. The composition and size of LDs often reflect the physiological state of the cell and depend on the coordinated execution of three major process: FA metabolism, neutral lipid synthesis, and phospholipid synthesis and remodelling.

(1) FA metabolism

Many of lipid synthesis steps depend on fatty acyl-CoA, the activated form of FAs. Because free FAs are chemically inert, they must be converted into fatty acyl-CoA via ATP-dependent esterification reaction catalysed by ACS. Once activated, fatty acyl-CoAs are used to make neutral lipids like TAG and CE through acyl-CoA-dependent pathways.

(2) DAG and TAG synthesis

De novo DAG synthesis, also known as the glycerol phosphate pathway, provides precursors for both TAG and phospholipid biosynthesis. This pathway involves the sequential acylation of G3P to form LPA, PA, and DAG. DAG acts as a central intermediate that can be directed towards either TAG synthesis or phospholipid production. Both phospholipid and TAG synthesis are believed to contribute to early LD biogenesis by inducing membrane curvature and accumulating neutral lipids within specific regions of the ER, initiating the nascent LD. In yeast, DAG is essential for LD formation even when the LDs are predominantly CE-rich (Adeyo et al., 2011). More broadly, the balance between DAG and PA influences membrane remodelling and vesicle budding at the Golgi, by modulating membrane remodelling and protein recruitment (Malhotra and Campelo, 2011; Zhukovsky et al., 2019).

Together with the glycerol phosphate pathway, other routes also contribute to DAG production. An acyl-CoA:monoacylglycerol acyltransferases (MGAT) pathway provides an alternative way for generating DAG, particularly in tissues where MAG is abundant or where rapid DAG production is required (Polheim et al., 1973; Phan and Tso, 2021).

Then with the addition of fatty acyl-CoA to DAG, TAG synthesis primarily proceeds via the DGAT pathway (Cases et al., 1998b; Smith et al., 2000; Coleman and Lee, 2004). This is a key mechanism for safely and reversibly storing excess FAs and DAG in the form of TAG (Listenberger et al., 2003). In addition to functioning as energy reserves, these stored lipids serve as precursors for membrane biogenesis during periods of rapid growth (Toker, 2005).

(3) CE synthesis

In eukaryotes, cholesterol can be synthesised *de novo* or acquired exogenously via the low-density lipoprotein (LDL) receptor-mediated endocytic pathway. Once internalised, excess free cholesterol is esterified by acyl-CoA:cholesterol acyltransferase (ACAT), an enzyme that catalyses the formation of CE via an acyl-CoA-dependent pathway (grey square in **Figure 8B**), and resulting CEs are stored in LDs (Luo et al., 2020).

In addition to these acyl-CoA-dependent reactions, acyl-CoA-independent pathways also proposed to contribute to neutral lipid synthesis (blue box in **Figure 8**). In mammalian cells, lecithin cholesterol acyltransferase (LCAT) catalyses the transfer of an acyl group from phospholipids (particularly PC, also known as lecithin) to free cholesterol, forming CEs without requiring acyl-CoA (Rousset et al., 2009). In addition to its esterification role, LCAT functions as a phospholipase, cleaving phospholipids and contributing to membrane lipid remodelling.

In yeast and plants, TAG synthesis can also occur via the phospholipid:diacylglycerol acyltransferase (PDAT) pathway, another acyl-CoA-independent pathway. PDAT catalyses the

transfer of an acyl group from phospholipids to DAG, generating TAG. In yeast, the CoA-dependent synthesis of TAG via DGAT is sufficient to maintain TAG levels under normal conditions, suggesting that PDAT may serve a more specialised role. Beyond TAG synthesis, PDAT also catalyses the breakdown of major membrane phospholipids implying a potential function in regulating membrane lipid composition in response to changing growth conditions (Dahlqvist et al., 2000).

(4) Phospholipid synthesis

As LDs expand, their phospholipid monolayer must also increase to maintain structural stability of the neutral lipid core. This is particularly critical during early stages of rapid LD growth. Two main pathways contribute to phospholipid biosynthesis: the Kennedy pathway (*de novo* synthesis, yellow box in **Figure 8**) and the Land cycle (remodelling pathway, orange box in **Figure 8**).

The Kennedy pathway synthesis PC and PE starting with the phosphorylation of choline or ethanolamine, followed by conversion to CDP-choline or CDP-ethanolamine (Gibellini and Smith, 2010). DAG acts as the backbone for attaching headgroups in this process.

The Land cycle, which involves de-acylation of PLs by PLA and subsequent re-acylation by LPL, mediates phospholipid remodelling. This cycle not only supplies DAG but also modulates membrane fluidity and curvature. Inhibition of PLA_2 enzymes has been shown to significantly reduced LD formation, suggesting the land cycle plays an active role in initiating LD biogenesis (Gubern et al., 2008).

Together, these interlinked pathways coordinate lipid metabolism and LD formation, ensuring proper lipid storage, energy buffering, and membrane precursor supply under changing cellular demands.

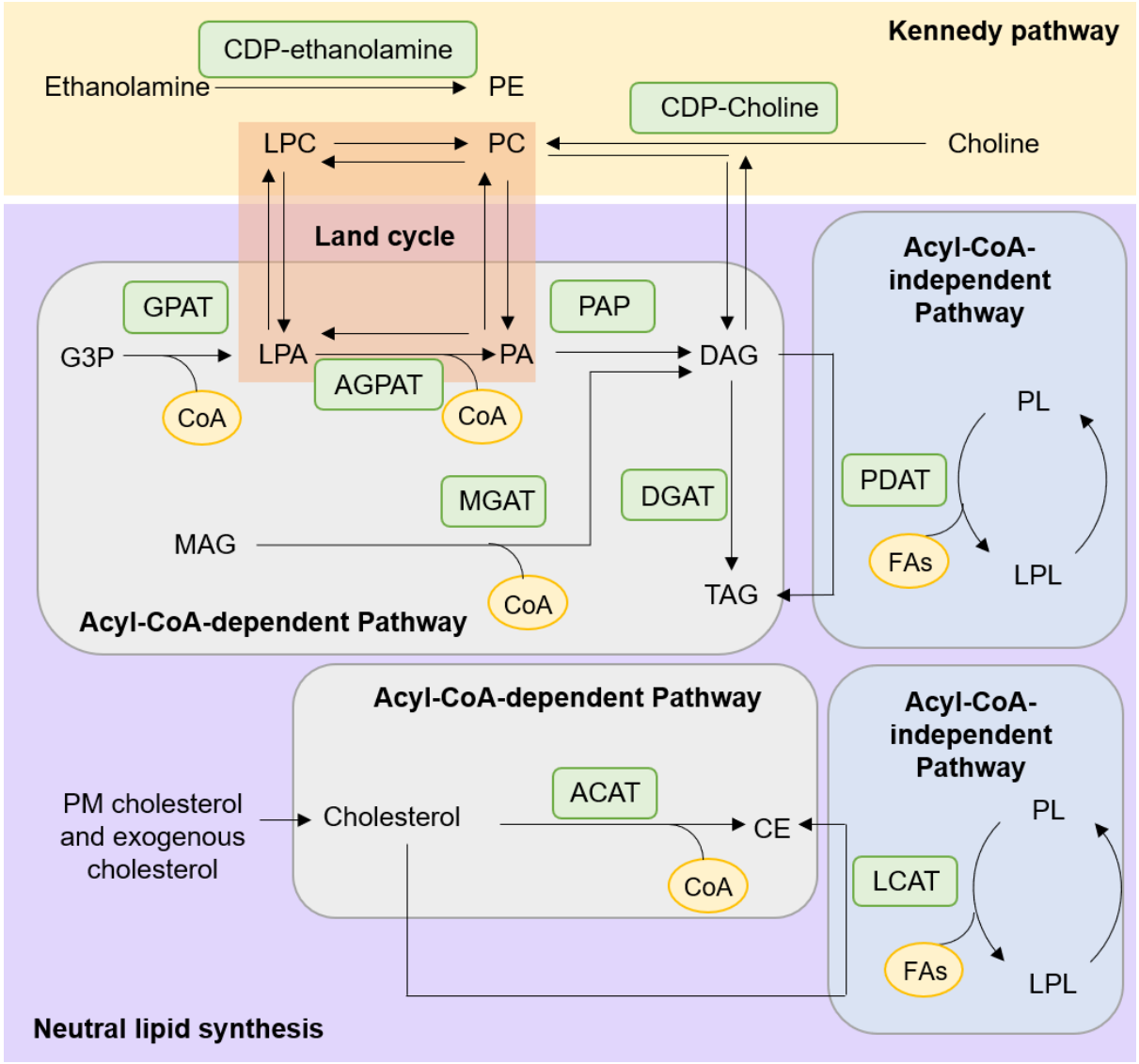

Figure 8. General lipid biosynthesis and LD formation. LD biogenesis requires the coordinated synthesis of both neutral lipids and phospholipids. Two main pathways contribute to phospholipid biosynthesis: the Kennedy pathway (*de novo* synthesis, yellow box) and the Land cycle (remodelling pathway, orange box). Neutral lipid synthesis (purple box) occurs via both acyl-CoA dependent (grey box) and acyl-CoA independent pathways (blue box).

ACAT, acyl-CoA:cholesterol acyltransferase; AGPAT, 1-acylglycerol-3-phosphate O-acyltransferase; CDP, cytidine diphosphate; CE, cholesteryl ester; CoA, fatty acyl-CoA; DAG, diacylglycerol; DGAT, diacylglycerol acyltransferase; FA, fatty acid; G3P, glycerol-3-phosphate; GPAT, glycerol-3-phosphate acyltransferase; LCAT, lecithin:cholesterol acyltransferase; LPA, lysophosphatidic acid; LPC, lysophosphatidylcholine; LPL, lysophospholipid; MAG, monoacylglycerol; MGAT, monoacylglycerol acyltransferase; PA, phosphatidic acid; PAP, phosphatidic acid phosphatase; PC, phosphatidylcholine; PE, phosphatidylethanolamine; PDAT, phospholipid:diacylglycerol acyltransferase; PL, phospholipid; TAG, triacylglycerol.

LD contact sites and their cellular functions

Beyond their role as lipid storage organelles, LDs are increasingly recognised as multifunctional hubs that participate in diverse additional metabolic processes. To fulfil these roles, LDs interact closely with other organelles through membrane contact sites. Electron microscopy studies have revealed that LDs often remain physically associated with various organelles, and proteomic analyses have identified shared proteins between LDs and other organelles, suggesting dynamic exchange and coordination (Yu et al., 2015; Benador et al., 2018; Ma et al., 2021; Dudka et al., 2024). These contact sites facilitate lipid transfer, signal transduction, and metabolic regulation, contributing to overall cellular homeostasis (**Figure 9**).

For example, LD-ER contact sites are thought to play a key role in LD biogenesis and in the continued exchange of lipids and proteins. LD-mitochondria contacts have been implicated in FA transfer, which supports mitochondrial β-oxidation and may help protect against lipotoxicity (Benador et al., 2019). LD-peroxisome contacts involve the fusion of the peroxisome's outer phospholipid bilayer leaflet with the LD phospholipid monolayer, allowing protrusions bordered by the inner bilayer leaflet to invade the LD core (Binns et al., 2006). This unique structural arrangement enables the direct transfer of lipids for peroxisomal FA metabolism. LD-endosome and LD-autophagosome contacts have been linked to lipid remobilisation and lipophagy, particularly under nutrient stress condition (Singh et al., 2009). In addition, LD-nucleus interactions may participate in the trafficking of nuclear envelope-derived lipids or in lipid-mediated transcriptional regulation. LD-LD contacts allow transfer of lipids from small LD to large LD (Nishimoto and Tamori, 2017). The ability of LDs to form contact sites with multiple organelles highlights their active role in lipid sensing, trafficking,

and signalling. These interactions allow LDs to respond dynamically to changes in the cellular environment.

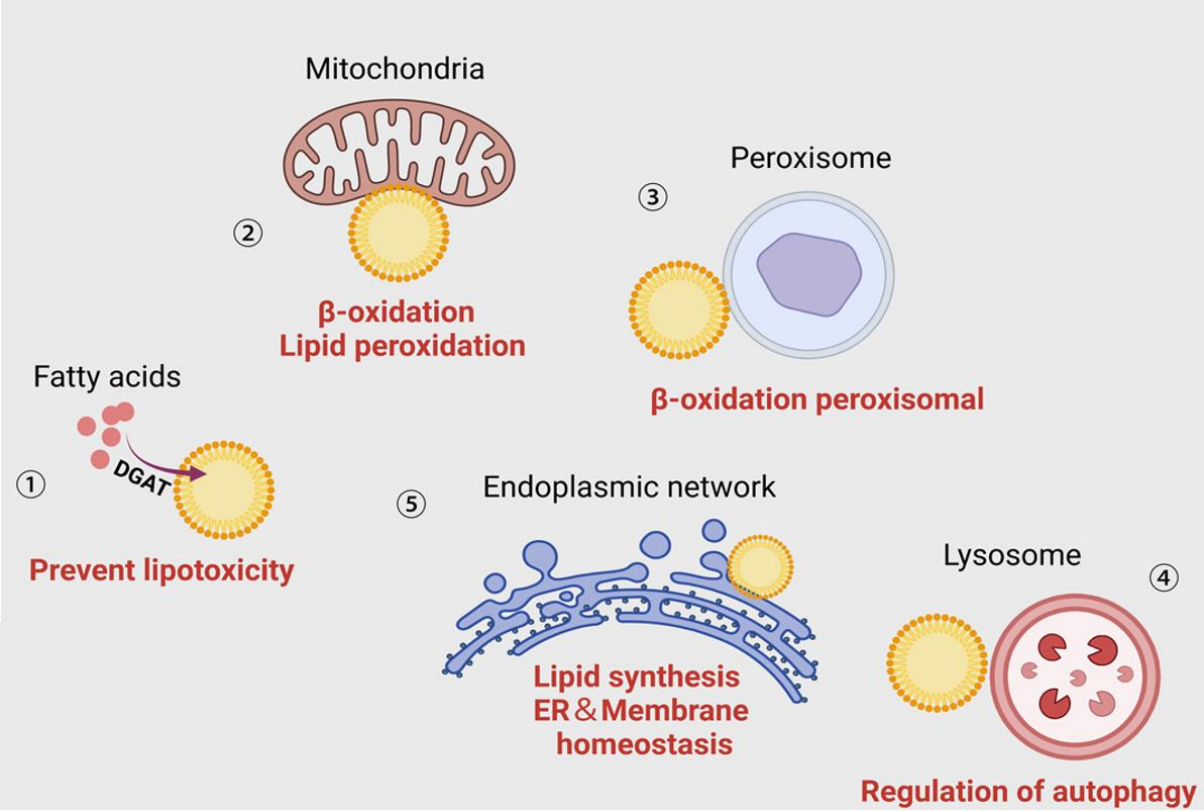

Figure 9. LDs contact sites and their functions in eukaryotes. LDs interact with various organelles to support cellular metabolism and homeostasis: (1) LDs prevent lipotoxicity by sequestering excess FAs through DGAT-mediated TAG synthesis. (2) LDs supply FAs to mitochondria for β-oxidation and help lipid peroxidation. (3) LDs contribute to peroxisomal β-oxidation and redox homeostasis. (4) LDs are involved in the regulation of autophagy via interactions with lysosomes. (5) LDs maintain ER and membrane homeostasis by participating in lipid synthesis and buffering ER stress. Figure adapted from (Tan et al., 2024)

Significance and scope

LDs are highly dynamic organelles that store neutral lipids and have been extensively characterised in many eukaryotic organisms. They share a conserved structure, yet their size, number, and composition vary widely depending on cell type, physiological state, and function. For instance, TAG-rich LDs dominate in metabolically active tissues like adipose, liver, and muscle, serving as energy reservoirs, while CE-rich LDs are prevalent in steroidogenic tissues and foam cells, supporting cholesterol metabolism and hormone synthesis. These examples highlight how LD content and function are highly specialised and context-dependent.

In contrast, the presence, morphology, and function of LDs in the malaria parasite *P. falciparum* remain poorly defined. As an intracellular parasite with a tightly regulated and complex life cycle, *P. falciparum* relies heavily on lipid metabolism for membrane biosynthesis, energy storage, and stage-specific remodelling. Previous reports have shown that lipid requirements shift dramatically between the asexual replication stages and the sexual transmission stages, with distinct lipid profiles across stages (Gulati et al., 2015; Tran et al., 2016). This raises questions about whether *P. falciparum* employs distinct lipid storage strategies in a stage-specific manner. Yet, we still lack a detailed understanding of how the parasite stores and mobilises neutral lipids, what organelles are involved, and how these processes are regulated across life cycle stages.

This gap in knowledge is particularly critical given the parasite's extraordinary adaptability to environmental changes and therapeutic pressures. *P. falciparum* has evolved resistance to nearly every frontline antimalarial therapy, underscoring the need for new strategies that target essential biological processes. Lipid metabolism - central to survival, replication, and transmission - is a promising but underexplored vulnerability.

Despite recent advances in *Plasmodium* cell biology, studying small and dynamic organelles like LDs remains technically challenging due to the parasite's small size (~5-7 µm) and complex intracellular organisation. However, the development of new tools - such as lipid-specific probes, genetically tagged parasite lines, and high-resolution imaging techniques - now makes it possible to visualise LDs and study their dynamics with unprecedented resolution.

This thesis leverages on recent advances to investigate neutral lipid storage organelles in *P. falciparum* across both asexual and sexual intraerythrocytic stages. By integrating fluorescence and electron microscopy with biochemical assays, it aims to characterise the structural features, distribution, and composition of these compartments throughout the blood-stage life cycle. A detailed analysis of their morphology, lipid content, and regulatory mechanisms provides insight into how the parasite manages its lipid resources-offering potential targets for stage-specific or transmission-blocking antimalarial strategies.

Research hypothesis and aims

Previous lipidomic studies suggest that the parasite alters its lipid profile to meet the requirements for each life cycle stage (Gulati et al., 2015; Tran et al., 2016; Ridgway et al., 2022). However, how these neutral lipids are stored and used throughout the life cycle stages hasn't been studied yet. This thesis is based on the hypothesis that *P. falciparum* uses distinct, stage-specific lipid storage compartments tailored to its physiological needs across blood cycle stages. This study aims to investigate how *P. falciparum* stores and regulates neutral lipids throughout its life cycle and whether structurally and functionally distinct lipid storage compartments exist. The work is structured into three results chapters, each aligned with a specific research aim:

(1) Chapter 3 investigates LD dynamics during asexual blood stages. The aim is to determine the role of LD formation and turnover in parasite replication, using split emission fluorescence microscopy, 3D focused ion beam scanning electron microscopy (FIB-SEM), and metabolic inhibitor assays.

(2) Chapter 4 explores whether *P. falciparum* possesses homologs of known LD-associated proteins from other eukaryotes. This chapter aims to identify candidate proteins in *P. falciparum* that may contribute to LD biogenesis and function in stage-specific manner, based on literature review and published transcriptomic data.

(3) Chapter 5 aims to characterise a female specific neutral lipid storage compartment by defining its ultrastructure, composition, and potential function during gametocytogenesis. This will be achieved using split emission fluorescence microscopy, correlative light and electron microscopy (CLEM), and 3D FIB-SEM, along with chemical inhibitor treatments to assess functional relevance.

Taken together, this thesis aims to advance our understanding of how *P. falciparum* stores and utilises lipids across different life cycle stages. By investigating the structure, composition, and regulation of lipid storage organelles, this work seeks to uncover stage-specific mechanisms that may represent novel targets for therapeutic intervention.

Chapter 2. Material and Methods

Materials

Chemical reagents

Chemical	**Supplier**
16% Paraformaldehyde	Electron Microscopy Sciences
70% Glutaraldehyde	Electron Microscopy Sciences
AlbuMAX™ II	Gibco
Anti-GFP mouse	Roche
Artemisinin	Sigma
Bovine serum albumin (BSA)	Sigma
Chloroquine	Sigma
D-glucose	Sigma
Dimethyl sulfoxide (DMSO)	Sigma
D-sorbitol	Sigma
Epon Resin	Electron Microscopy Sciences
Ethanol	Merck
Ezetimibe	Cayman Chemical
Gentamicinin	Invitrogen
Giemsa	POCD Healthcare GiemsaSNP
Glycerine	Sigma-Aldrich
Hoechst 33342	Thermo Fisher
Human serum	Australian Red Cross Blood Service
Hypoxanthine	Sigma

HM20 Resin	Electron Microscopy Sciences
Horseradish peroxidase-coupled goat anti-mouse IgG	Thermo Fisher
NuPAGE™ LDS Sample Buffer (4X)	Novex
Lead Citrate	AJAX
Methanol	ChemSupply
Mouse monoclonal 98-6H1-1	WEHI monoclonal antibody facility
Mitotracker™ Deep Red FM	Thermo Fisher
N-acetyl-D-glucosamine	Biosynth Carbosynth
Nile Red	Sigma
Orlistat	Selleckchem
Osmium tetroxide	ProSciTech
Potassium ferrocyanide	Sigma
RPMI 1640-HEPES with GlutaMAX™	Invitrogen
Sodium dodecyl sulfate (SDS)	Sigma
SYBR Safe DNA Gel Stain	Invitrogen
T863	Selleckchem
Thiocarbohydrazide (TCH)	Eastman
TRIS (tris(hydroxymethyl) aminomethane)	Amresco
Triton X-100	Sigma
Uranyl Acetate	Thermo Fisher
Xanthohumol (XN)	Selleckchem
β-mercaptoethanol (BME)	Sigma

Ethics approvals and biological reagents

Human type O^+ RBCs and human serum were provided by the Australian Red Cross Blood Bank and approved for experimental use by the Australian National University ethics committee agreement 2017/351 and the Australian Red Cross agreement 23-02ACT-03.

The *P. falciparum* 3D7 wildtype parasites used for all experiments were originally received from the Walter Reed Army Institute of Research, Silver Spring, MD, USA.

The pGREP-1/PfgABCG2 cell line (3D7 parasites expressing a GFP tagged version of the gametocyte ATP binding cassette transporter family member 2 (ABCG2) protein (PF3D7_1426500), expressed from the endogenous locus) and the pCC-1/PfgABCG2 cell line (*gABCG2* disruption) were generated by Tran et al. (2014). They are referred to as PfABCG2-GFP expressing cell line and ΔPfABCG2 cell line in this thesis.

Methods

P. falciparum culturing

2.1. Culture of asexual blood stage of P. falciparum

Asexual blood stage parasites were cultured following established procedures (Maier and Rug, 2013). The cultures were maintained at 4% haematocrit resuspended in complete medium: RPMI 1640-HEPES with Glutamax medium supplemented with 10 mM glucose, 480 µM hypoxanthine, 20 µg/ml gentamicin, 2.5% (v/v) human serum and 0.375% (w/v) Albumax II. The cultures were maintained at 37°C under microaerophilic conditions (1% O_2, 5% CO_2, 94% N_2).

2.2. Culture of gametocytes of P. falciparum

Parasites were induced to form gametocytes as previously described with modifications (Fivelman et al., 2007). To induce sexual commitment, a sorbitol synchronised culture containing 2% trophozoites at 4% haematocrit was stressed by replacing only 25% of the culture medium. Approximately67% of the medium was replaced on the following day. The appearance of ring stage parasites under this nutrient stress condition was defined as day 0 of gametocytogenesis. On day 0, a high parasitemia ring stage culture was treated with sorbitol to remove mature stage asexual parasites and passed through a magnetic column to eliminate remaining mature asexual parasites and mature gametocytes, retaining only ring stage parasites. On the subsequent day (day 1), the culture was again treated with sorbitol to remove late-stage asexual parasites. The culture medium was supplemented with 50 mM N-acetyl-D-glucosamine (GlcNAc) to inhibit asexual parasite proliferation, as at this concentration GlcNAc is toxic to trophozoites and schizonts and blocks merozoite invasion, without affecting

gametocyte development (Gupta et al., 1985; Ponnudurai et al., 1986; Fivelman et al., 2007). The medium was replaced daily thereafter.

To collect gametocytes on either day 6 or day 8, the culture was treated with 5% (w/v) sorbitol one day prior to the collection. Gametocytes were magnetically enriched using a sterile column with a SuperMACS^{TM} II magnet (Miltenyi), and eluted in culture medium containing 50 mM GlcNAc. Collected gametocytes were incubated for at least 1 hour in complete culture medium with 50 mM GlcNAc at 37°C under microaerophilic conditions prior to experiments.

2.3. Sorbitol synchronisation

Parasite cultures were synchronised by selectively lysing mature asexual parasites, as described previously (Lambros and Vanderberg, 1979). This method takes advantage of the differential permeability of the RBC membrane following parasite infection. While uninfected RBCs and ring stage-infected RBCs are impermeable to sorbitol, mature-stage infected RBCs become increasingly permeable due to parasite-induced modifications of the host membrane. Sorbitol enters these permeable cells, causing osmotic lysis and thereby selectively eliminating mature forms without affecting ring stages or uninfected cells. To synchronise the culture, ring stage *P. falciparum*-infected RBCs were centrifuged at 524 x g for 5 min, and the resulting pellet was resuspended in 5% (w/v) sorbitol and incubated at 37°C for 10 min. The treated cultures were then washed and resuspended in complete culture medium.

2.4. Magnetic enrichment of **P. falciparum**

Mature gametocytes and late-stage asexual parasites of *P. falciparum* exhibit magnetic properties due to the conversion of non-magnetic Fe^{2+} in haem into magnetic Fe^{3+} during haemozoin crystallisation. As a result, these stages are retained in a magnetised column of iron

particles, while uninfected RBCs and ring-stage parasites are not. Magnetic enrichment was conducted using a SuperMACS^{TM} II magnet with a MACS® column. Prior to use, the column was sterilised with 80% ethanol, rinsed with PBS, and then with incomplete culture medium. A high-density *P. falciparum* culture (approximately 10% parasitemia) was applied onto the magnetic column. The retained late-stage asexual and gametocyte-infected RBCs were then eluted from the demagnetised column using culture medium.

Light Microscopy

2.5. Giemsa-stained thin smear analysis

Giemsa staining was used to assess parasitemia and examine the morphology and life cycle stage of *P. falciparum*. Thin smears prepared from the parasite cultures were fixed with methanol (100%) and stained with 10% Giemsa solution (in DI H_2O). Giemsa contains eosin and methylene blue (azure); eosin stains cytoplasmic acidophilic/positively charged components (e.g., haemoglobin) light pink, while methylene blue stains negatively charged residues (e.g., DNA) blue to purple.

2.6. Fluorescence microscopy

For live cell fluorescence microscopy, fluorescence probes such as Nile Red (4 µg/ml, neutral lipid staining) and Hoechst (1 µg/ml, nuclear staining) were added directly to the culture medium, and cells were imaged following incubation.

For fixed cell imaging, cultured cells were fixed with 2% paraformaldehyde in PBS and washed twice with PBS before applying a fluorescence probe such as Nile Red (4 µg/ml) and Hoechst (1 µg/ml). Fluorescently stained cells were applied to pre-cleaned microscope slides

(Hurst) and sealed under a No. 1.5 coverslip using nail polish to prevent them from drying out during imaging. Unless otherwise specified, images were acquired using a Leica Stellaris 8 confocal microscope with 63x oil immersion objective lens, NA 1.4.

2.7. Standard Nile Red stained fluorescence imaging

Cultured parasites were fixed with 2% paraformaldehyde and subsequently stained with Nile Red (4 µg/ml) and Hoechst (1 µg/ml) for nucleic acid staining which allowed distinguishing the different specified stages. Hoechst fluorescence was detected at 352 nm excitation / 455 nm emission, while Nile Red fluorescence imaging was initially performed with standard settings at 559 nm excitation / 636 nm emission.

2.8. Nile Red spectral shift imaging

Nile Red fluorescence has been observed to be highly dependent on the polarity of its environment, with excitation and emission spectra shifting depending on lipid hydrophobicity (Greenspan and Fowler, 1985; Diaz et al., 2008; Teo et al., 2021). Less polar lipids shift its emission spectrum to shorter wavelengths, and to longer wavelengths as the polarity of the lipid environment increases (**Figure 10**A).

To evaluate and distinguish lipid species according to their polarity, a split excitation/emission regime was established for Nile Red-stained cells (**Figure 10**B). Nile Red stained cells were imaging using a Lecia Stellaris 8 confocal microscope with a white light laser and a 63x oil immersion objective lens (NA 1.4). Three excitation/emission settings were used: one for visualising non-polar head groups like TAGs (excitation at 506 nm, emission at 520-590 nm) and another for visualising polar head groups like phospholipids (excitation at 598 nm,

emission at 610-750 nm). When GFP-expressing cell lines were used, an additional channel was included to visualise GFP (excitation 473 nm, emission 485–515 nm).

Spectral overlap between the three channels was evaluated using spectral spillover table (https://www.thermofisher.com/order/fluorescence-spectraviewer) to confirm minimal bleed-through under the chosen settings (**Figure 10**C).

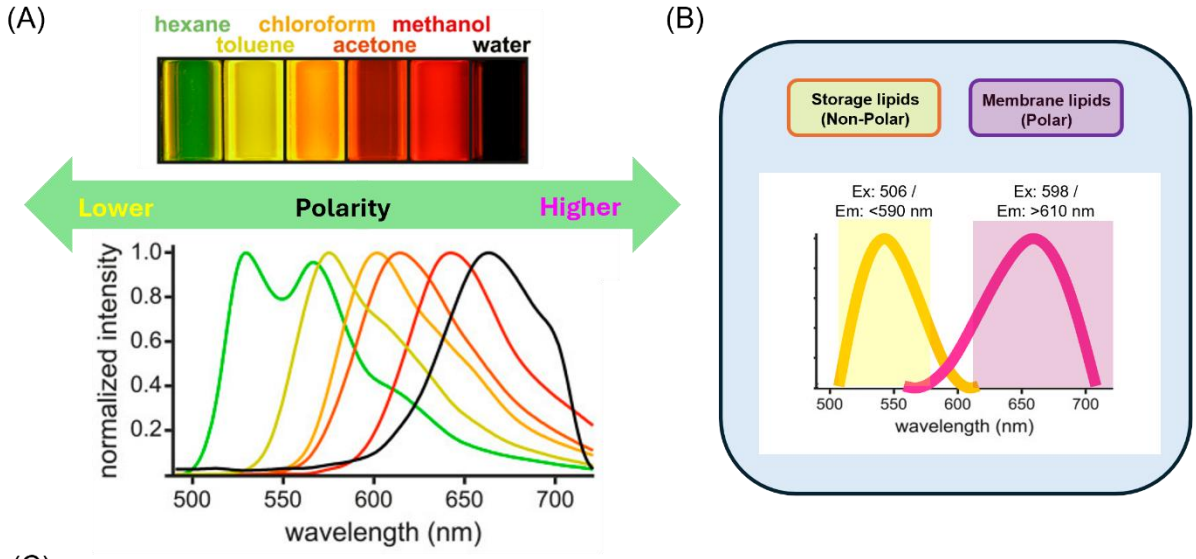

(C)

	Fluorophore	Channel	Emission	GFP	Nile red (Polar)	Nile red (Non-polar)
473 Laser	GFP	500/30	580	46.1%	-	-
506 Laser	Nile red (Non-polar)	555/70	583	8.6%	1.8%	33.2%
598 Laser	Nile red (polar)	680/140	727	-	87.4%	1.2%

Figure 10. Nile Red spectral shift imaging. (A) Demonstration of a substantial colour shift of emitted fluorescence with cuvettes of Nile Red dissolved in solvents of varying polarity and excited with 380 nm light and also normalized fluorescence emission spectra from the six solvents (Teo et al., 2021) (B) Spectra setting to distinguish neutral lipids (non-polar) and phospholipid (polar lipids) (C) Fluorescence spill out table at three different excitation and emission (https://www.thermofisher.com/order/fluorescence-spectraviewer).

2.9. Image analysis of fluorescence microscopy data

Throughout each experiment, images were consistently acquired under identical conditions. Z-stack imaging was employed to cover 3D volumes of entire parasites, and the final images are presented as maximum intensity projections. Quantification of Nile Red fluorescence was performed by using ImageJ (https://imagej.nih.gov/ij/). The parasite area was selected based on an intensity threshold of Nile Red, and the relevant area was measured by using 'analyse particles'. The mean fluorescence intensity (MFI) of Nile Red was measured based on maximum intensity projection images. The integrated intensity was calculated by multiplying MFI by the area occupied by the parasite (Shihan et al., 2021).

Ratio maps were created by using RatioloJ, a plugin for ImageJ (Michelis et al., 2022). Maximum intensity projection images of z-stack were used for this process.

Focused Ion Beam Scanning Electron Microscopy (FIB-SEM)

2.10. Sample preparation for FIB-SEM

To enhance the contrast of intrinsically contrast-poor resin embedded biological specimen for backscattered electron imaging (BSE) at low accelerating voltage, various contrasting agents were added in this protocol. Samples for FIB-SEM analysis were prepared using the osmium-thiocarbohydrazide-osmium (OTO) method (Tapia et al., 2012; Rudlaff et al., 2020) with some modifications. Since osmium binds to lipids and oxidises unsaturated fatty acids, it increases electron density in lipid-rich regions. The OTO method enhances the contrast of neutral lipid-enriched structures, such as LDs, making them easier to distinguish from other organelles with similar shapes and sizes (**Figure 11**).

Mature gametocyte or mature asexual parasites were magnet purified and rested in the incubator for at least 1 hour before processing further (Ribaut et al., 2008). The magnet-purified

cells underwent a brief wash with PBS and were subsequently fixed using 2.5% glutaraldehyde and 2% paraformaldehyde in PBS. The fixed parasites were washed with PBS, then post-fixed with 2% osmium tetroxide and 1.5% potassium ferrocyanide in PBS for 1 hour. Next, the samples were washed in milliQ water, incubated in an aqueous solution of thiocarbohydrazide (TCH) for 20 minutes, followed by a second incubation in a 2% aqueous solution of osmium tetroxide for 30 min after washing with milliQ water. The heavily fixed cells were incubated overnight in 1% uranyl acetate in milliQ water, then washed in milliQ water with subsequent dehydration using increasing concentrations of ethanol and two washes with 100% acetone in the final dehydration step. Following dehydration, samples were incubated in a gradually increasing concentration of EPON 812 resin in acetone. The cell pellets were polymerised after overnight incubation in 100% resin at 60ºC.

The resin embedded trimmed samples were mounted on SEM stubs using a mixture of super glue and silver paste (providing conductivity) and trimmed further to a small sample surface area (1 mm^2). Subsequently, the trimmed block was sectioned with an ultra-microtome (Leica EM UC7) to expose the region of interest (ROI). To confirm that the exposed area contained a suitable density of target cells, 0.5 – 1 μm thick sections were stained with toluidine blue and observed under LM prior to the FIB-SEM experiment. Finally, to improve stability under FIB-SEM conditions, the samples were sputter coated with a ~ 10 nm thick layer of gold.

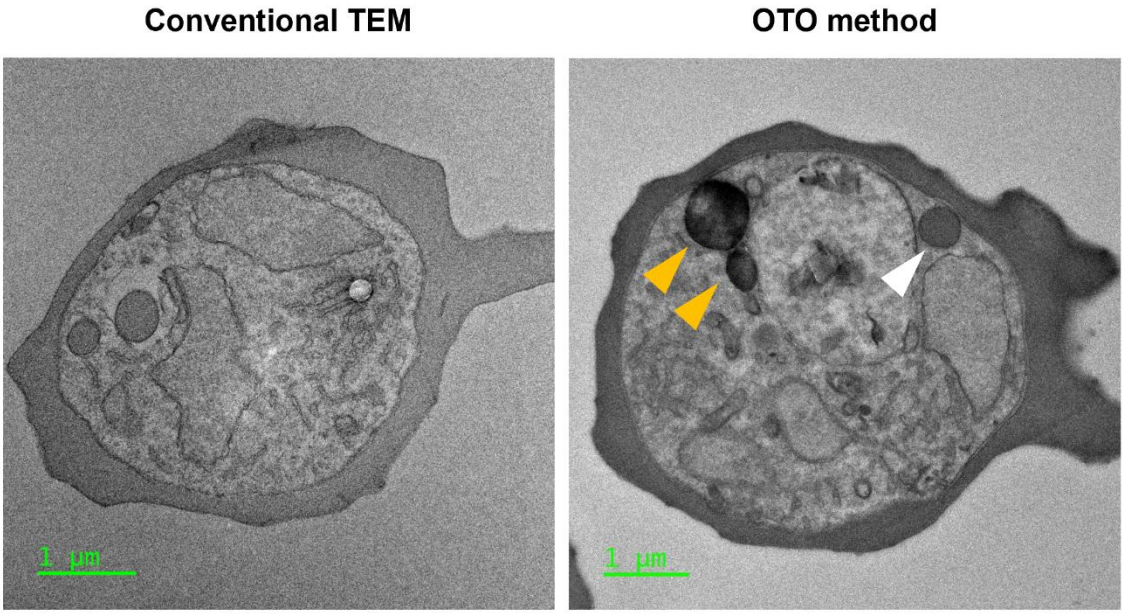

Figure 11. Comparison between conventional TEM sample preparation and the OTO method samples. Conventional TEM samples were initially fixed with 2.5% glutaraldehyde and 2% paraformaldehyde in PBS, followed by secondary fixation with 1% osmium tetroxide, dehydration, and resin embedding (Hayat, 1973). In contrast, the OTO method enhances contrast in lipid rich regions, resulting in significantly higher electron density. For example, LDs (yellow arrows) exhibit higher electron density compared to haemoglobin-containing compartments (white arrow) which enabling improved visualization and distinction of lipid structures.

2.11. FIB-SEM volume imaging

A region with high cell density, additionally confirmed via a secondary electron image, was selected for processing in a FIB-SEM (Zeiss Crossbeam 550). The sample stage was tilted at 54° and the coincident point of the electron beam and the ion beam was determined and set in order to align the field of view for imaging (SEM) and milling (FIB). The sample was positioned at a 90º angle in relation to the ion beam and 36º to the electron beam. The area for volume imaging was selected by SE or BSE imaging, according to the number of cells located within the field of view. Initially, a platinum layer of approximately 1 µm thickness was deposited on top of the selected ROIs using the Crossbeam's gas injection system. Subsequently, trapezoid shaped trenches (30 µm x 40 µm) were created with an accelerating

voltage of 30 kV and a current of 30nA to expose ROIs for imaging and also prevent redeposition during the milling process. The selected areas were polished with a 30 kV ion beam at a current of 7 nA prior to serial imaging. Finally, the serial milling was set at 30 kV and a current of 700 pA with 10 nm slice thickness. Cross sectional images were obtained by detecting backscattered electrons with the energy-selective back-scatter detector (ESB) using an electron accelerating voltage of 1.5 kV, a current of 2 nA and an 8 µs dwell time, with a frame resolution of 3072 x 2304. The FIB-SEM experiment was conducted three times (biological replicates) and three technical replicates in each run. Each raw dataset comprised an average of 800 images with an approximate 10 nm^3 voxel size.

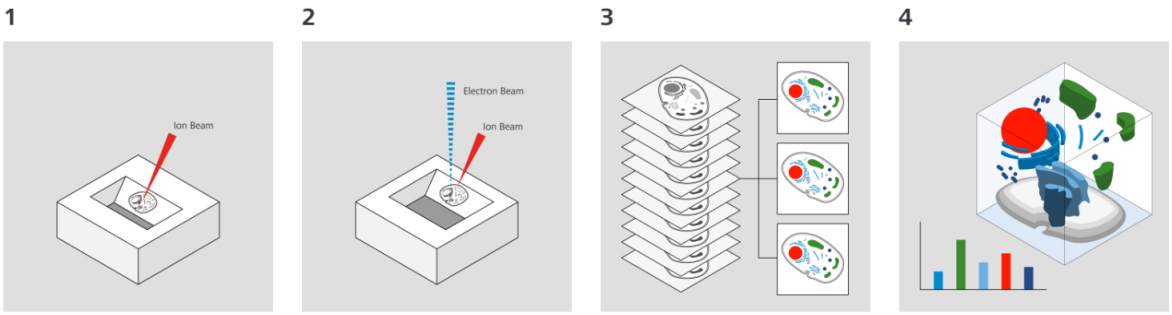

Figure 12. Workflow of 3D imaging by focused ion beam-scanning electron microscopy (FIB-SEM). 1) A trench is milled into a resin-embedded sample using a focused ion beam (FIB) until the structure of interest is exposed. 2) The newly exposed surface is imaged by scanning electron microscopy (SEM), and this milling-imaging cycle is repeated to capture serial images through the volume of the structure. 3) The acquired image stack is digitally aligned and reconstructed into a 3D dataset. Subcellular structures can be identified and segmented. 4) The segmented 3D volume can then be visualised, explored, and quantitatively analysed to investigate cellular architecture.

Volume EM with Focused Ion Beam Scanning Electron Microscopy (https://www.zeiss.com/microscopy/en/applications/life-sciences/volume-em/fib-sem.html)

2.12. FIB-SEM data post processing and analysis

All processing, visualisation and analysis were conducted using the Microscopy Image Browser (MIB) (Belevich et al., 2016) and Dragonfly 2020.2 (Object Research Systems (ORS) Inc, Montreal, Canada, 2020). Images of each run were aligned using cross-correlation, and denoising was performed with a deep neural network (DNN) denoisefilter. A Gaussian filter was applied prior to segmentation. The data analysis focussed on single infected cells, encompassing entire cells. A total of 9 trophozoites, 10 early schizonts, 11 mid schizonts, and 3 late schizonts were used for quantification. Life cycle stages were defined as follows: ring stage cells contained a single nucleus (no DV observed), trophozoite stage cells contained a single nucleus (DV observed), early schizont cells displayed 2 to 5 nuclei, mid schizont stages contained 6 or more nuclei (without fully segmented merozoites), while late schizont cells contained more than 20 nuclei with fully segmented merozoites. Manual or semi-automatic graphcut segmentation in MIB and Dragonfly were used for 3D segmentation and rendering.

To quantify the relative volume of LDs in different life cycle stages, the LD volume per parasite was calculated as the ratio of LD volume over the volume of the whole parasite using segmented models from renderings in MIB and Dragonfly.

To determine the frequency of contacts between LDs and other organelles, we tallied the number of contacts, counting each instance as one, even if multiple contact occurred with the same organelle. The membrane contact occurrence was then calculated as follows:

$$LD\ membrane\ contact\ occurrence\ for\ each\ organelle(\%) = 100 \times \frac{Number\ of\ LD\ contacts\ with\ each\ organelle}{Number\ of\ LD\ contacts\ with\ all\ organelles}$$

Correlative Light and Electron Microscopy (CLEM)

Correlative light and electron microscopy (CLEM) enable fluorescently labelled proteins to be placed in their ultrastructural context. Throughout the process of high pressure freezing (HPF), freeze substitution (FS), and resin embedding, the fluorescence is retained such that sections can be imaged with confocal microscopy to localise the fluorescently labelled proteins followed by EM to obtain high resolution ultrastructural detail.

2.13. Sample preparation for CLEM

Magnet purified gametocytes were cryo-fixed with HPF (EM ICE, Leica). Cryo-fixed cells were then transferred into an automated FS system (EM AFS2, Leica) for freeze substitution at -90°C. Samples were dehydrated in a graded ethanol series and gradually infiltrated by acrylic resin (HM20) in the AFS2. Eventually samples were polymerised under UV at low temperature.

Polymerised resin blocks were then sectioned with an ultramicrotome (Leica UC7) to produce ~70 nm thin sections. The sections were collected on a TEM finder grid (London Finder Grids 200 mesh, EMS). The TEM grids were mounted on a microscope slide with 50% glycerine in water and coverslipped for fluorescence microscope imaging. After imaging on the fluorescence microscope (Zeiss LSM800 confocal microscope), the grids were washed with milliQ water and then post-stained with 2% uranyl acetate and lead citrate for 10 minutes each prior to TEM imaging. An overview of the CLEM workflow is shown in **Figure 13**.

2.14. Imaging for CLEM

Fluorescence imaging of thin sections were acquired using a Zeiss LSM 800 confocal microscope with 63x oil immersion objective lens (NA 1.4). GFP signal was acquired using 488 nm excitation and 400 – 500 emission settings. To obtain corresponding ultrastructural information, the same sections were imaged using a JEOL F200 transmission electron microscope (TEM), operated at 80 kV accelerating voltage. TEM images were acquired using a Gatan Rio camera and Digital Micrograph software (Gatan Inc.) at a resolution of 4024 × 4024 pixels. Fluorescence and TEM images were then imported into ZEN software, and ZEN Connect was used to generate precise overlay images for correlative analysis.

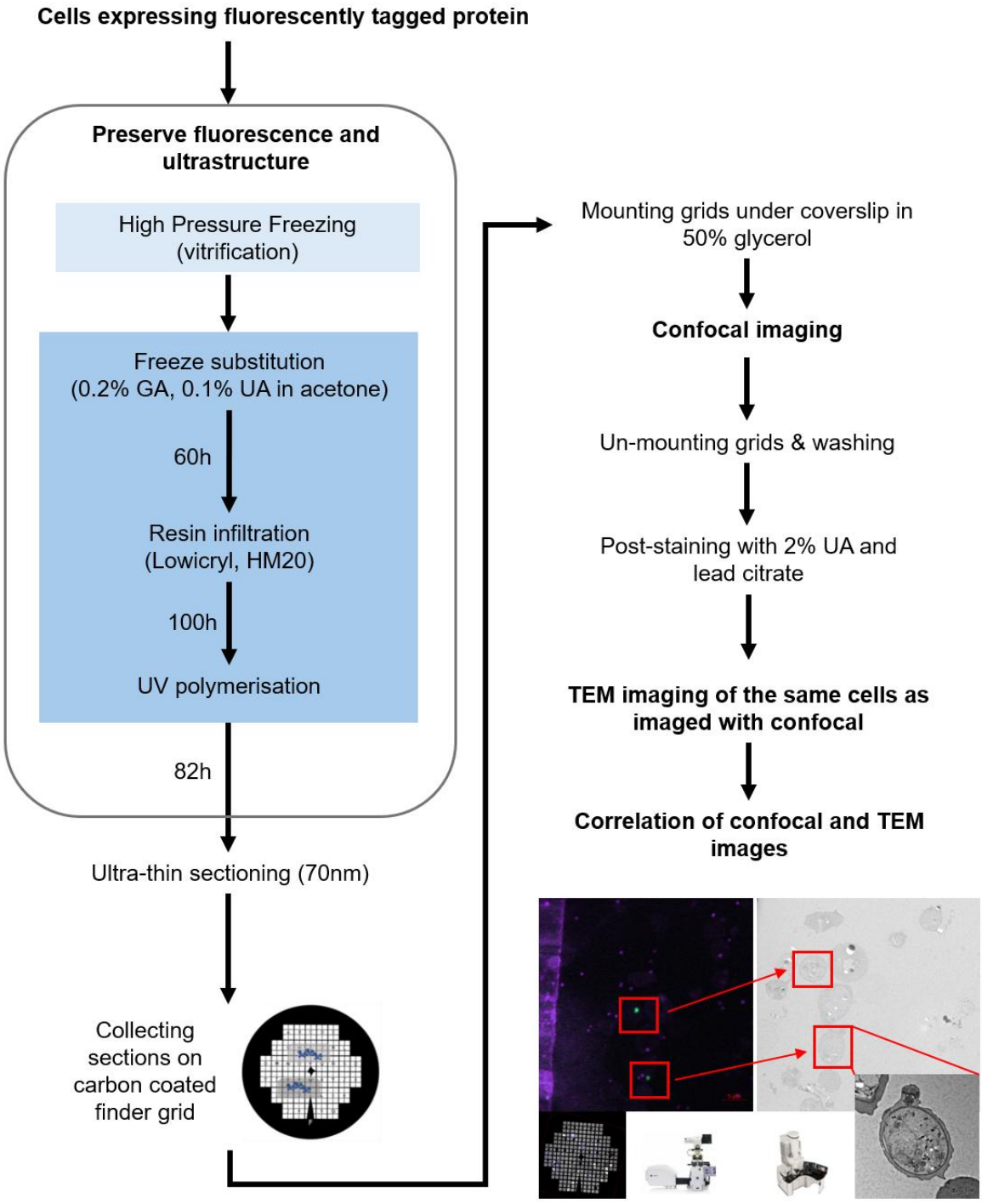

Figure 13. Overview of correlative light and electron microscopy (CLEM) workflow. PfABCG2-GFP expressing gametocytes were processed using cryo-fixation by using high pressure freezing, freeze substitution, resin embedding, and ultrathin sectioning. Processed cells are first imaged by fluorescence microscopy to visualise fluorescent markers (PfABCG2-GFP) and identify regions of interest for further ultrastructural analysis using transmission electron microscopy. GA: glutaraldehyde, UA: uranyl acetate.

Inhibitor assays

2.15. Growth inhibitor assays for asexual stage

In order to achieve synchronised parasite cultures, 5% w/v D-sorbitol treatment was applied two days prior to experiments (Lambros and Vanderberg, 1979). IC_{50} values were determined using a SYBR green I based fluorescence assay (Smilkstein et al., 2004). Test inhibitors were serially diluted 2-fold across flat-bottom 96 well plates. A 200 µM chloroquine treatment was included as a negative control to determine background fluorescence. A 100 µL culture was added to each well at a final parasitemia of 0.5% and final haematocrit of 1% in a total volume of 200 µL per well. Plates were incubated at 37 °C under microaerophilic conditions. At 72 hours post-treatment, plates were transferred to a freezer to halt parasite growth and lyse the cells. After thawing, the lysate was mixed 1:1 with SYBR Safe DNA Gel Stain (final concentration 1:10,000) diluted in SYBR lysis buffer. Fluorescence was measured at 490 nm excitation and 520 nm emission using a FLUOstar Optima fluorescence plate reader (BMG Labtech).

2.16. Gametocyte viability assay

Gametocyte viability was assessed as previously described, with modifications (Ridgway Melanie et al., 2020). Test inhibitors were serially diluted across 96-well round bottom plate in complete culture media with 50 mM N-acetyl-D-glucosamine. 100 mM artemisinin was used as a negative control to determine background gametocyte fluorescence. Magnet enriched gametocytes (Day 7, stage IV) were added to the plate and incubated for 72 hours at 37ºC under microaerophilic conditions. Parasites were then stained with 500 nM MitoTracker™ Deep Red FM (to label viable gametocytes) and 5 µg/ml Hoechst 3342 (to label parasite nuclei) in PBS-G. Hoechst staining was used to identify all parasitised red blood cells, enabling total parasite

count regardless of viability. For quantification, events were measured on an LSR II Flow Cytometer (BD Biosciences). MitoTracker™ Deep Red FM fluorescence, detected at 633 nm excitation and 780/60 nm emission. Data were processed using FlowJo™ software, and gametocyte viability was determined based on MitoTracker™ fluorescence intensity relative to the total Hoechst-positive population.

In vitro inhibitor assay and analysis for asexual stages

2.17. *Inhibitor treatment*

Highly synchronised culture at the early ring stage were treated with inhibitor concentrations approximately 8 x IC_{50} value: 60 µM of Orlistat, 40 µM of Xanthohumol, and 200 µM of T863, based on a prior growth inhibition assay as described in section **2.15** (data not shown). The parasite stages were assessed using Giemsa stained smears, and the initial stage, referred to as 8 hours (h), was defined based on morphological features (van Biljon et al., 2018; Si et al., 2023). Each Inhibitor or DMSO (maximum DMSO concentration during the inhibitor assay, i.e., 0.1% DMSO) for control were added at 12 hour intervals (8h, 20h, 32h, and 44h), and parasite development was monitored at each stage using both light and fluorescence microscopy. Once the inhibitor was added at each time point, it was maintained until the final imaging time point at 84h (no medium change).

2.18. Light microscopy analysis

Imaging was performed throughout one complete intraerythrocytic cycle (at 20h, 32h, and 44h), with additional time points at 60h and 84h to assess parasite development in the subsequent cycle. Parasitemia was assessed on Giemsa-stained smears at the time point when

the parasite completed invasion and had established itself in the cell (60h). The parasitemia was assessed by counting a total of 500 cells at each inhibitor addition points (8h, 20h, 32h, and 44h). The cell growth compared to control was calculated as follows:

$$Growth\ compared\ to\ control(\%) = 100 \times \frac{parasitemia\ of\ treated\ culture}{parasitemia\ of\ control\ culture}$$

For fluorescence microscopy, each time point cultures were fixed with 2% paraformaldehyde and subsequently stained with Nile Red (4 µg/ml) and Hoechst (1 µg/ml). Imaging and analysis were performed as described in Section **2.8** and **2.9**.

2.19. *Ultrastructural analysis*

Highly synchronised parasite-infected RBCs at approximately 10% parasitemia were cultured as described in Section **2.1.** Inhibitors, including 60 µM Orlistat, 40 µM XN, and 200 µM T863, as well 0.1% DMSO (control), were added to the cultures at 32 hours post invasion. Cells were collected at 44 hours (12 hours after inhibitor addition) and at 60 hours (24 hours after inhibitor addition) for TEM analysis. Samples were prepared using the OTO method, as detailed in Section **2.10**. The resin embedded samples were sectioned using an ultra-microtome (Leica EM UC7) to obtain 70 nm ultrathin sections for imaging in a JEOL F200 TEM at 200kV. The images were captured with a Gatan Rio16 camera.

In vitro inhibitor assay and analysis for gametocyte

2.20. *Inhibitor treatment*

Enriched PfABCG2-GFP expressing mature gametocytes (Day 8, stage IV) of were collected using magnetic purification (refer Section **2.4**) and incubated for 1 day at 37ºC under microaerophilic conditions. Approximately 1 x IC_{50} value of each inhibitor was added to the gametocyte culture on day 9 (stage IV): 120 µM of Orlistat, 30 µM of XN, and 110 µM of Ezetimibe, based on a prior growth inhibition assay as described in section **2.16** (**Figure 34**). Two controls were included: a DMSO control (0.1%, matching the maximum DMSO used in inhibitor treatments) and Primaquine (20 µM) which is a widely used antimalarial that kill mature *P. falciparum* gametocytes. Inhibitors were added to the culture and incubated for 24 hours. Once the inhibitor was added at each time point, it was maintained until the final imaging time point at 24 hours.

2.21. Fluorescence microscopy analysis

Inhibitors were added into magnet enriched gametocytes (stage IV), and after 24 hours of incubation, cells were fixed with 2% paraformaldehyde and stained with Nile Red (4 µg/ml). To assess changes in lipid polarity following each treatment, images were acquired as described in Section **2.8**.

2.22. Detergent resistant membrane isolation

Detergent-resistant membrane (DRM) fractions were isolated from PfABCG2-GFP expressing gametocytes using a sequential extraction method using Triton X-100 and SDS (Van Schravendijk et al., 1993; Maier et al., 2006).

Magnet enriched PfABCG2-GFP expressing gametocytes (5.7×10^7) were lysed by snap freezing in liquid nitrogen and subsequent thawing. Lysed cells were pelleted and pellets were resuspended in ice-cold 1% Triton X-100 (in PBS) supplemented with 1× protease inhibitor cocktail (25× Roche Complete Mini EDTA-free), and incubated on ice for 20 minutes with intermittent mixing. Negative control and GFP control samples were directly resuspended in an equal volume of 2× LDS sample buffer containing 5% BME to achieve a final concentration of 1× LDS and 2.5% BME.

Lysates of PfABCG2-GFP expressing gametocytes and WT 3D7 parasites were centrifuged at 13,000 × g for 5 minutes at 4°C. The supernatant, representing the Triton X-100–soluble fraction, was collected and mixed with LDS sample buffer containing BME (final concentration of 1× LDS and 2.5% BME).

The pellet was washed once with ice-cold 1% Triton X-100 (in PBS) supplemented with 1× protease inhibitor cocktail, then centrifuged again at 13,000 × g for 5 minutes at 4°C. The supernatant was discarded, and the pellet was further resuspended in 2% SDS in PBS containing protease inhibitor cocktail at room temperature. The suspension was incubated at room temperature for 20 minutes, followed by centrifugation at 13,000 × g for 10 minutes. The resulting supernatant, containing the Triton X-100–insoluble but SDS-soluble proteins (enriched in DRM-associated proteins) was collected (Maier et al., 2006), and mixed with LDS sample buffer containing BME (final concentration of 1× LDS and 2.5% BME).

To extract the final insoluble fraction, the remaining pellet was washed with 2% SDS in PBS supplemented with 1× protease inhibitor cocktail, followed by centrifugation at 13,000 × g for 10 minutes. The supernatant was carefully removed, and the pellet was resuspended in an equal volume of 2× LDS sample buffer containing 5% BME to achieve a final concentration of 1× LDS and 2.5% BME.

All collected fractions were stored at –80°C until further analysis by SDS-PAGE and immunoblotting.

2.23. SDS-PAGE and immunoblotting

Each fraction from the DRM isolation was thawed on ice and then boiled at 70 °C for 10 minutes on a heat block with intermittent mixing. After heating, fractions were cooled to room temperature. As a control for GFP signal, BiP(S)-GFP-SDEL expressing (expected size ~27 kDa) was used (van Dooren et al., 2005). PfEMP1 from WT 3D7 cell line was included (expected size ~300 kDa) as a DRM marker control (Maier et al., 2006), and uRBCs were included as a negative control. All fractions were loaded onto a 4-12% Bis-Tris NuPAGE precast gel (Invitrogen, Life Technologies). Gels were run at 200 V for 30–60 minutes.

Proteins were transferred from the SDS-PAGE gel to polyvinylidene difluoride (PVDF) membrane using the iBlot system (Invitrogen, Life technologies) according to manufacturer's instructions. Following the transfer, the membrane was blocked with TBS solution containing 10% milk powder for 1 hour and then incubated with a primary antibody solution at 4ºC overnight. The membrane was then washed 3 times with TBST and incubated with a secondary antibody at RT for 1hour. Primary and secondary antibodies were diluted in TBST containing 5% BSA and 5% milk respectably.

For immunoblotting, duplicate membranes were prepared: one for GFP and the other for PfEMP1 labelling. The following primary and secondary antibodies were used for immunodetection. To detect GFP, membrane was incubated with mouse anti-GFP (1:2000, Roche), followed by horseradish peroxidase-coupled goat anti-mouse IgG (1:1000) as secondary antibody. For PfEMP1 detection, anti-PfEMP1 ATS (mAb 1B/98-6H1-1, 1:200; WEHI monoclonal antibody facility) was used as a primary antibody (Maier et al., 2006), followed by the horseradish peroxidase-coupled goat anti-mouse IgG secondary antibody (1:1000).

After secondary antibody incubation, membranes were washed with 3 times TBS and incubated with enhanced chemiluminescence (ECL) solution for 1 min before exposure using a ChemiDoc imaging system (Bio-Rad).

Statistical Analysis

Except where otherwise specified, data were analysed in Prism 8 using one-way ANOVA.

Chapter 3. Lipid droplet dynamics are essential for the development of the malaria parasite *Plasmodium falciparum*

Published as:

Lee, J., Matuschewski, K., van Dooren, G., Maier, A.G., Rug, M. (2024) Lipid droplet dynamics are essential for the development of the malaria parasite *Plasmodium falciparum*. *Journal of Cell Science* 137(20): jcs262162

Introduction

Plasmodium falciparum, the deadliest species of malaria parasites infecting humans, has a complex life cycle which requires transition between two intrinsically different hosts (human and mosquito). Hence, the parasite faces the challenges of having to navigate growth, proliferation, transmission, and sexual reproduction in vastly different host environments. Each of these cellular processes rely on coordinated lipid access and metabolism mechanisms, with the parasite either synthesising essential lipids *de novo* or acquiring them from its host environment (Sherman, 1979; Shears et al., 2015; Shunmugam et al., 2022). During the asexual blood stage cycle, which is solely responsible for pathogenesis in the human host, the parasite invades a mature erythrocyte (Maier et al., 2019). Once inside, the parasite grows from a ring stage, *via* a trophozoite stage to a schizont stage. During the last stage, the parasite undergoes an unusual process of asexual multiplication called schizogony. While most eukaryotes divide by binary fission, *Plasmodium* undergoes a closed mitosis with rounds of DNA replication and nuclear division without cell division (cytokinesis), which leads to multinucleated cells (Francia and Striepen, 2014; Voß et al., 2023). Schizogony is the 'mode' of multiplication which occurs in both the liver and the blood stage of the parasite life cycle in the mammalian host. During intraerythrocytic schizogony, the parasite eventually segments into 8-32 individual daughter merozoites. After egress from the infected cell, each merozoite will invade a new erythrocyte to continue the asexual blood cell cycle. In order to provide building blocks for the fast growth and multiplication of *P. falciparum* within each 48h asexual replication round, the parasite requires a ready supply of lipids to synthesise new cellular membranes. At the same time *P. falciparum* needs to prevent excess lipid accumulation to counteract potential lipid toxicity.

Previous studies have shown a drastic change in lipid composition throughout the asexual blood stage cycle. In particular, the neutral lipid species DAG and TAG were elevated compared to uninfected erythrocytes (Gulati et al., 2015; Tran et al., 2016; Ridgway et al., 2022), while the other major group of neutral lipids (CE) were reduced to almost undetectable levels (Vielemeyer et al., 2004; Tran et al., 2016).

Since neutral lipids serve as crucial repositories of energy and building material in eukaryotic cells (Olzmann and Carvalho, 2019), the remarkable enrichment of DAGs and TAGs in *P. falciparum* might be reflected in the dynamics of the major lipid storage organelles - lipid droplets (LDs). Despite early recognition at the end of the 19th century (Altmann, 1894), LDs were long considered as being inert fat particles (Coleman, 2020). In more recent studies, LDs have been shown to be very dynamic organelles, crucial for lipid homeostasis in many different cell types (Farese and Walther, 2009; Fujimoto and Parton, 2011; Pol et al., 2014). They have a distinct structure, consisting of a hydrophobic core composed mainly of the neutral lipids TAG and CE, surrounded by a monolayer of phospholipids containing embedded proteins. Since the enzymes for the last steps of TAG and CE synthesis reside in the ER, the ER is regarded as key for the formation of LDs (Coleman and Lee, 2004; Fujimoto and Parton, 2011). Similarly, several cellular organelles are in need of neutral lipids that are contained within LDs and hence, interactions of LDs with other organelles can be observed (Murphy et al., 2009; Schuldiner and Bohnert, 2017; Rakotonirina-Ricquebourg et al., 2022). The role of LDs goes beyond being a mere lipid storage compartment: they have been implicated in a range of additional functions including the degradation of hydrophobic proteins (Fujimoto and Ohsaki, 2006) and haem detoxification in *P. falciparum* (Hoang et al., 2010).

Given the significant growth and changes occurring during the maturation of the parasites, I hypothesised that size, composition and dynamics of LDs vary significantly across the *P.*

falciparum intraerythrocytic cell cycle.

While fluorescence microscopy and lipidomic studies have explored the general distribution of neutral lipids in asexual stages (Palacpac et al., 2004a; Vielemeyer et al., 2004; Gulati et al., 2015; Tran et al., 2016), LD dynamics in the malaria parasite remain underexplored.

In this chapter, I applied a combination of advanced light microscopy techniques and volume imaging using Focused Ion Beam Scanning Electron Microscopy (FIB-SEM) in combination with inhibitors of essential enzymes in neutral lipid metabolism to characterise the dynamics and importance of LDs in the parasite's asexual life cycle stages.

Results

LDs accumulate during the parasite's schizogony

In order to characterise the content of LDs, I made use of a particular trait of the lipophilic fluorescent dye Nile Red (9-(Diethylamino)-5*H*-benzo[*a*]phenoxazin-5-one), which displays altered sensitivity of the dye depending on the lipid environment (Greenspan, 1985). Previous studies in other organisms showed that an excitation/emission profile of 506 nm/550 nm allows for observation of mainly non-polar head groups, while an excitation/emission profile of 598 nm/>610 nm shows a higher specificity for polar head groups (Greenspan, 1985; Diaz et al., 2008; Gao et al., 2014). Hence, signals appearing in the emission >610 nm range (termed magenta emission) indicate polar lipids (*e.g.* phospholipids (PL)), whereas the signals observed in the <590nm emission range (termed yellow emission) represent neutral lipids (*e.g.* acyl-glycerols and/or esterified cholesterol).

In order to gain information on the lipid distribution of RBCs infected (iRBCs) with different asexual blood cycle stages of *P. falciparum*, I stained the cells with Nile Red (**Figure 14** and **15A**). RBCs infected with ring and trophozoite stages exhibited a few small

intense punctae in the parasite cytoplasm at yellow emission. These punctae, reminiscent of LDs, increase in number and size in schizont stages and were often in close proximity to the DV (as indicated by the dark hemozoin crystals observed in the DIC images). When the polar lipid excitation/emission (magenta) settings were applied, I observed a diffuse overall staining of the cytoplasm, likely representing intracellular membranes of a vast array of organelles, which are mainly composed of PL (**Figure 15A**). Most of the punctae we observed in the yellow emission also appeared under these imaging conditions. However, their intensity was faint and, particularly in later stages of the parasite development, these could no longer be distinguished from the overall fluorescence signal within the parasite. Interestingly, smaller punctae appeared around the periphery of the segmented schizont (**Figure 14** and **Figure 15A**; yellow arrowheads), indicating that the content of these punctae can easily be distinguished from LDs by applying these differences in spectral analysis settings.

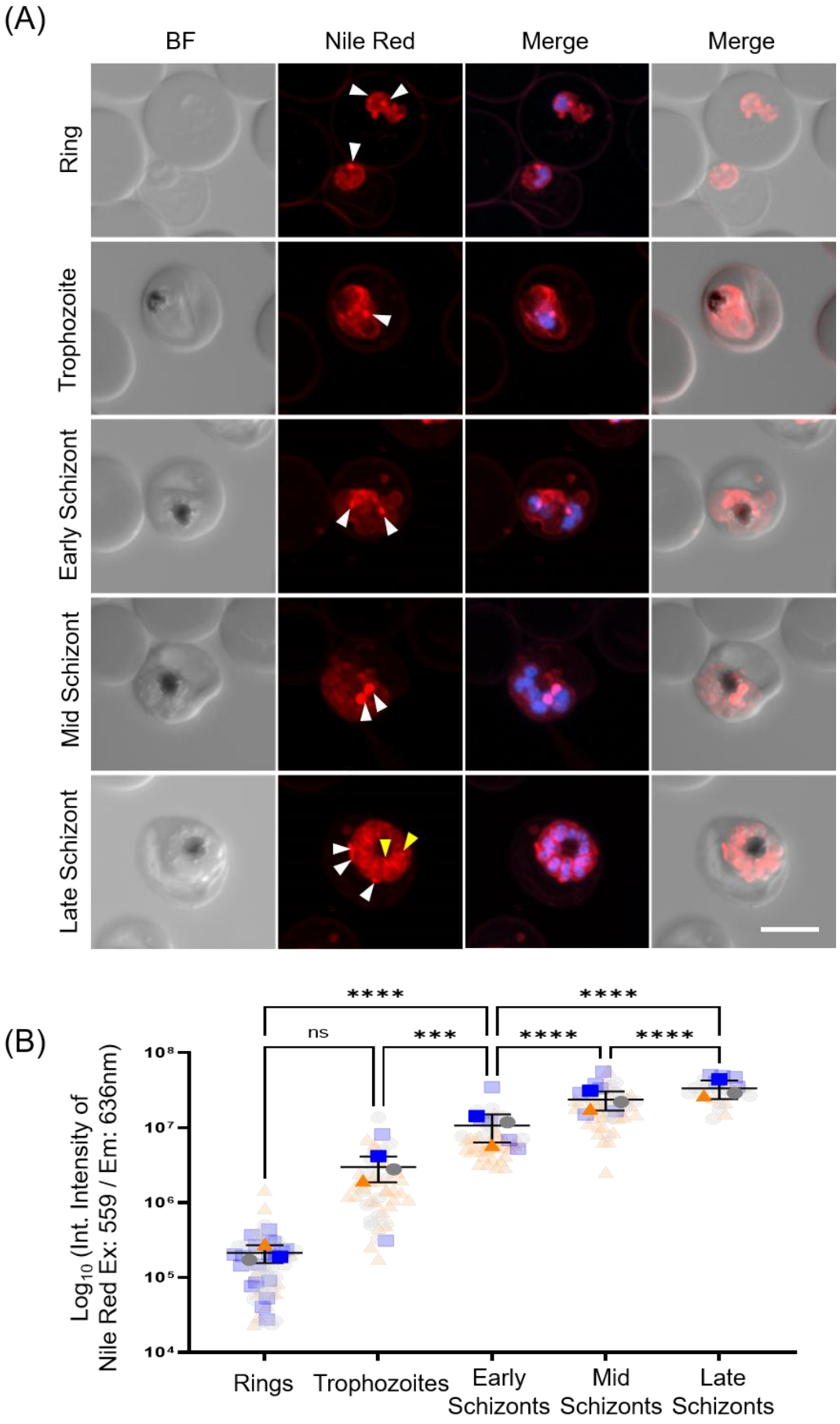
(A)
BF
Nile Red
Merge
Merge
Ring
Trophozoite
Early Schizont
Mid Schizont
Late Schizont
(B)
****
****
ns
***
****
****
Log10 (Int. Intensity of Nile Red Ex: 559 / Em: 636nm)
10⁸
10⁷
10⁶
10⁵
10⁴
Rings
Trophozoites
Early Schizonts
Mid Schizonts
Late Schizonts

Figure 14. Neutral lipid distribution during asexual blood stages of *Plasmodium. falciparum* using traditional Nile Red excitation and emission settings. (A) Representative maximum intensity projection confocal images of Nile Red-stained parasite-infected RBCs in ring (shortly after invasion), trophozoite, early schizont, mid schizont, and late schizont stages (with segmented daughter cells). White arrowheads point to punctate structures with high fluorescence intensity at excitation: 559 nm/ emission: 636 nm settings. BF: brightfield image; Nile Red (neutral lipid) staining is depicted in red, nuclei in blue (Hoechst stain); third column shows a merge of Nile Red and Hoechst fluorescence and the far right column depicts merges of Nile Red with BF images which clearly shows close association with various organelles, e.g. the digestive vacuole of the parasite. In the late schizont stage, high intensity Nile Red fluorescence surrounds the individual merozoites with multiple foci at the tip of daughter merozoites (yellow arrowheads). Scale bar: 5 μm. (B) Neutral lipid content in asexual blood stages of *P. falciparum*. Integrated (Int.) intensity of Nile Red fluorescence (excitation: 559 nm/ emission: 636 nm) was calculated as mean intensity over the parasite area. Three biological replicates were performed, and the different bold colour symbols represent the mean value of individual experiments, while the transparent symbols represent individual data points (cells) within each experiment. Total sample size (combined three biological replicates) of each life cycle stage: rings = 66, trophozoites = 46, early schizonts = 48, mid schizonts = 48, and late schizonts = 23. An ordinary one-way ANOVA was performed where **** = $p < 0.0001$; *** = $p < 0.002$, ns=0.4; shown are mean values (± SEM).

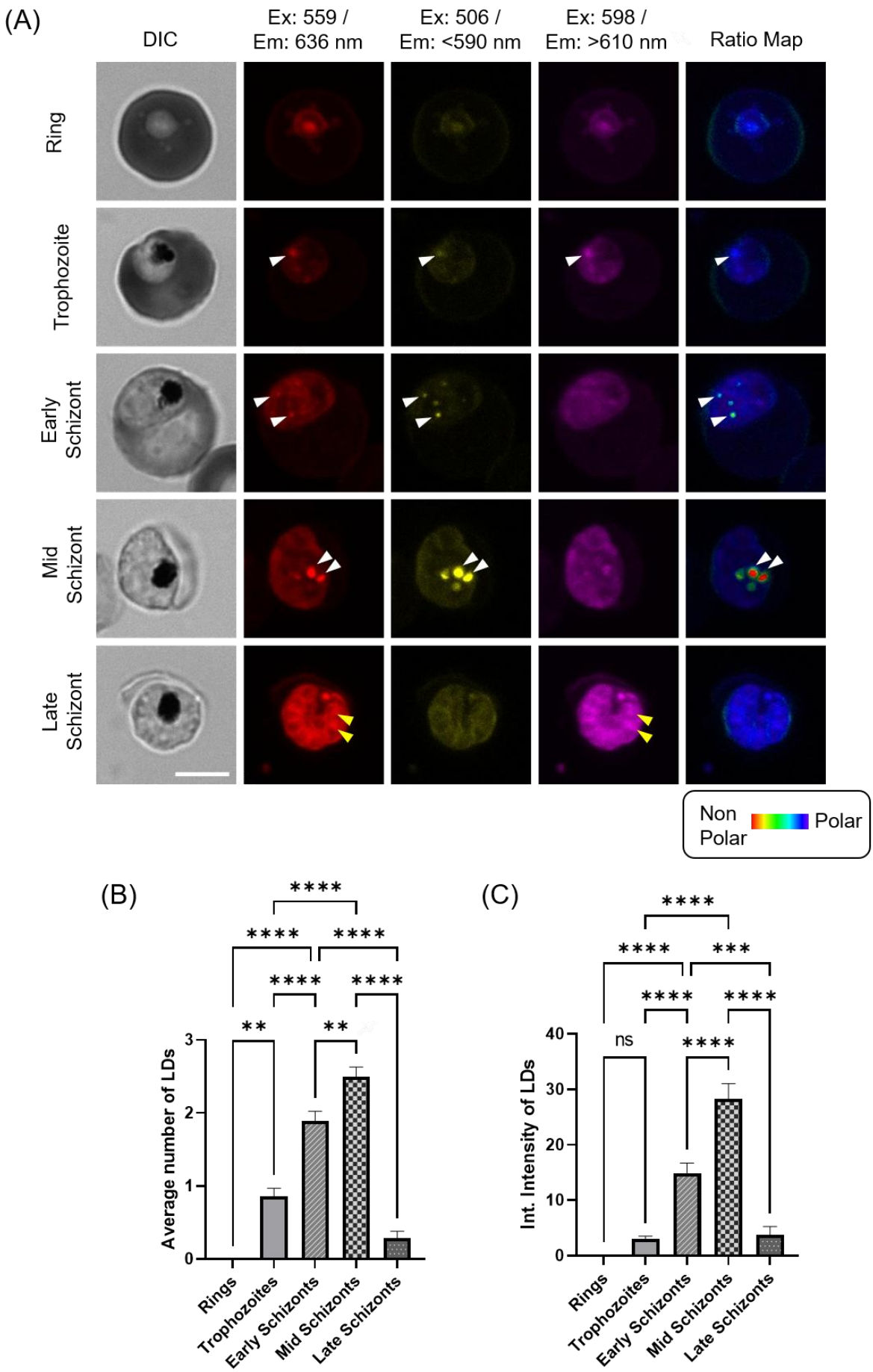
(A)
DIC
Ex: 559 / Em: 636 nm
Ex: 506 / Em: <590 nm
Ex: 598 / Em: >610 nm
Ratio Map
Ring
Trophozoite
Early Schizont
Mid Schizont
Late Schizont
Non Polar
Polar
(B)
Average number of LDs
Rings
Trophozoites
Early Schizonts
Mid Schizonts
Late Schizonts
(C)
Int. Intensity of LDs
ns

Figure 15. Differentiating polar and non-polar lipids in Nile red stained *P. falciparum*-infected red blood cells. (A) Representative confocal images of Nile Red-stained parasite-infected red blood cells, employing different excitation and emission settings on ring (shortly after invasion; *n*=66), trophozoite (1 nucleus; *n*=70), early schizont (2-5 nuclei; *n*=60), mid schizont (>6 nuclei without fully segmented merozoites; *n*=60), and late schizont stages (>20 nuclei; with segmented daughter cells; *n*=30). Differential Interference Contrast (DIC) images of parasitised RBCs are depicted in the first column, Nile Red fluorescence signal under traditional settings are depicted in red (excitation: 559 nm/ emission: 636 nm; second row), non-polar (e.g. TAG) lipid-enriched features are depicted in yellow (excitation: 506 nm/emission: 520-590 nm; third row), polar lipids (*e.g.* phospholipids) are depicted in magenta (excitation: 598 nm /emission: 610-750 nm, forth row) and a ratio map is depicted in the far right column. The ratio images, created by dividing yellow (non-polar) intensity by magenta (polar) intensity, is presented in a rainbow scale. Regions closer to the blue end of the spectrum indicate higher polarity, whereas those shifted towards the red end signify lower polarity. All images, except DIC, are maximum intensity projections. White arrowheads: LDs; yellow arrowheads: polar lipid accumulations in individual merozoites. Scale bar: 5µm. (B) Average number of LDs in different life cycle stages, presented as mean values (± SEM). *p = 0.03, **p = 0.006, ****p < 0.0001. (C) Average integrated intensity of total LDs in different life cycle stages, depicted as Mean ± SEM. Ns, not significant (p=0.9932); ***p = 0.0001; ****p < 0.0001. Quantification of LDs derived from yellow emission signals. LDs were identified using intensity thresholding and particle analysis (size threshold > 0.05 µm) in ImageJ by using maximum intensity projection images from z-stack. Total sample size of each cycle stage: rings = 24, trophozoites = 36, early schizonts = 37, mid schizonts = 71, and late schizonts = 39. All images were acquired with the same setting with counting mode for the quantification.

The data in **Figure 15** (supported by **Figure 14**) indicate that the spectral properties of Nile Red can be exploited to examine the intracellular distribution of different lipid classes across the intraerythrocytic cycle. This enabled us to distinguish between neutral lipid (NL)-containing LDs and other lipid-rich structures in the parasite, while traditional Nile Red spectral analysis (**Figure 14** and **Figure 15A**; red panel) obscures the differential signals. This is particularly obvious in the schizont stages, where the overall amount of lipids increases due to requirements of new membranes around developing daughter merozoites (**Figure 15A**; red and magenta).

To quantify the observed changes in number and size of NL-enriched LDs during the

asexual cycle of the parasite, I first measured the intensity of the overall Nile Red signal (traditional, non-differentiating settings) in iRBCs across the different asexual cycle stages (**Figure 14B**). To this end, I tightly synchronized parasite cultures and defined the analysed stages as follows: ring stages contained one nucleus (no haemozoin visible), trophozoites contained one nucleus (haemozoin clearly visible), early schizonts displayed up to five nuclei whereas mid schizonts contained 6 or more nuclei, but did not contain fully segmented merozoites. The late schizont stages clearly displayed segmented daughter merozoites. The integrated intensity increases steadily as the parasite matures, reflecting the increase in lipid abundance during intraerythrocytic development. Strikingly, employing the split excitation/emission experiment and analysing the yellow fluorescence signal from Z-stack projections of the cells, the average number of LDs observed per cell increases as the parasite matures, from being completely absent in ring stages to having, on average, over two LDs in the mid-schizont stage. However, the average number of LDs drops significantly in late schizont parasites (**Figure 15B**). Using this methodology, I also determined the integrated intensity of the observed LDs and found that, similarly to the number of LDs/cell, the intensity of the LDs also increases as the parasite matures, however, with a significant drop in intensity in the late schizont stages (**Figure 15C**). Taken together, I observed a steady increase in LD number and LD fluorescence intensity during the growth phases intraerythrocytic cycle, peaking in mid schizont stages but declining rapidly in late schizont stages. The decrease in late schizont stages indicates that NL may be recruited from the storage LDs for assembly in merozoite membranes.

3D FIB-SEM imaging allows for quantification of LD dynamics

To increase the spatial resolution and to eliminate the discrepancies observed with the differential analysis of lipid groups, I employed osmium tetroxide staining and electron microscopy to visualise LDs. Osmium tetroxide preserves lipids throughout the preparation process for electron microscopical investigation and preferentially binds to unsaturated bonds in fatty acids, imparting electron density that is observable via electron microscopy (Hayes et al., 1963; Adams et al., 1967). A correlation between electron density of LDs and NL content was demonstrated previously, allowing ready identification of LDs at an ultrastructural level (Cheng et al., 2009; Fujimoto et al., 2013). Using an osmium-thiocarbohydrazide-osmium (OTO) staining method (Tapia et al., 2012), I was able to identify high electron density material in droplet-like organelles throughout the examined asexual stages on electron microscopy sections in 2D that we designated as LDs (**Figure 16 A-D**).

To overcome limitations of 2D imaging in determining the exact number and/or size of LDs in any given parasite we analysed, we exploited a focused ion beam (FIB)/scanning electron microscopy (SEM) volume imaging technique, henceforth referred to as 3D FIB-SEM imaging. Here, LDs of asexual stages were segmented from 3D volume data, identified based on their high contrast threshold and morphology (**Figure 16 A-D & A'-D'**). I subsequently determined numbers and volumes of LDs from these 3D data sets to identify potential differences in LD numbers and/or volumes in the various asexual life cycle stages (**Figure 16 E and F**). While no high density LDs were observed in ring or early trophozoite stages, multiple LDs were identified in the parasite cytoplasm in trophozoite stages, increasing in number in early and, more significantly, in the mid schizont stage (**Figure 16 E**). These numbers correspond with the number of LDs in our confocal analysis (**Figure 15A, B and C**), supporting the notion that NL-enriched LDs increase from trophozoites to

mid schizont stage.

High resolution 3D volume data sets furthermore permit the quantification of additional parameters. I subsequently determined the average volume of LDs in our 3D volume data sets (**Figure 16F**). I found that the relative LD volume/parasite area increased almost 10-fold in mid schizont stages when compared to LD volumes in trophozoite stages (**Figure 16F**). However, the average volume of LDs decreased again at late schizont stages (**Figure 16F**), corroborating our confocal microscopy findings of a very small pool of NL available in late schizont stages (**Figure 15A**, lowest panel and **15B**). Notably, LDs were only observed in the residual body, closely associated with the remnant DV in the analysed late schizont stages (**Figure 16D**, arrowhead). Again, this is in line with our confocal data (**Figure 14** and **15**), where NL-enriched LDs were also sometimes found in close proximity of the DV. Rhoptries, apically-localised organelles that first appear in daughter merozoites during late schizogony, also contained electron dense material (**Figure 16D**; red arrowheads) but with a much lower density than LDs, and can therefore be clearly distinguished via this method. This indicates that the small punctae found at the periphery of late schizonts by fluorescence microscopy (**Figure 15A**) most likely represent rhoptries. Of note, no high electron density (NL-enriched) droplets were detected in merozoites within the late stage schizonts, suggesting that merozoites do not contain LDs. Together, high resolution 3D FIB-SEM permitted accurate quantification of tempo-spatial LD dynamics during the 48 h *P. falciparum* growth cycle inside erythrocytes.

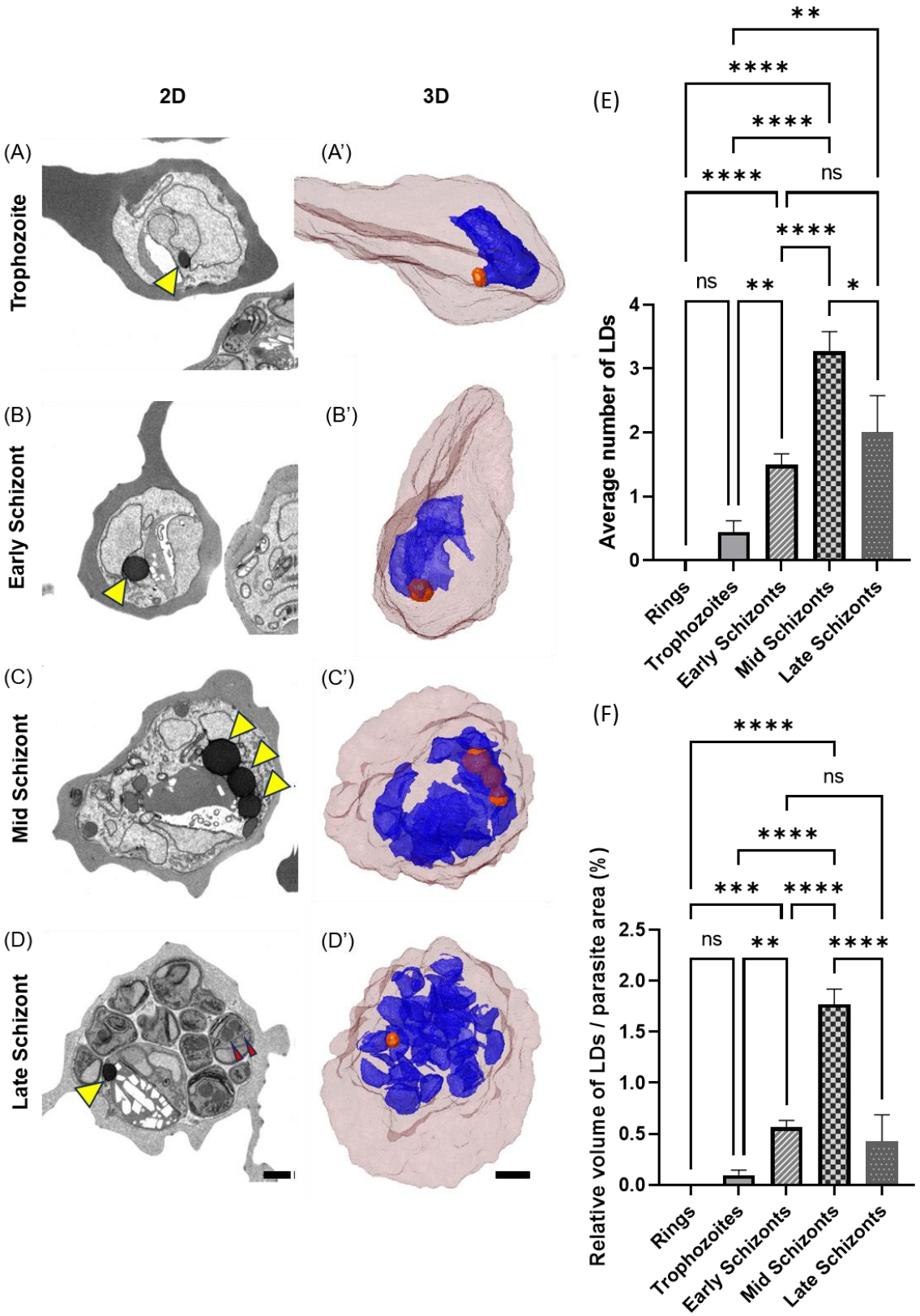

Figure 16. Ultrastructural characterisation with quantitative analysis of LDs in the asexual stages of *P. falciparum*. Representative 2D images (A-D) from a 3D FIB-SEM volume imaging data set and (A'-D') corresponding rendered and flattened 3D volumes. (A-D) Yellow arrowheads indicate location of LDs in the different parasite stages. Note that

in (D) the LD is located in the residual body. (A'-D') LD, orange; nuclei, blue. Scale bar: 1µm. (E) Average number and (F) relative volume of LDs/parasite area in different life cycle stages derived from 3D FIB-SEM data. The life cycle stages of the cells we observed were defined as follows: trophozoite stage cells contained a single nucleus, early schizont cells displayed 2 to 5 nuclei, mid schizont stages contained 6 to 15 nuclei, while late schizont cells contained more than 20 nuclei. n = 3-13; 13 rings, 9 trophozoites, 10 early schizonts, 11 mid schizonts, and 3 late schizonts were analysed to ascertain LD number and volume. Mean values (± SEM). Ns, not significant ($p > 0.04$); *$p < 0.04$; **$p = 0.009$; ****$p < 0.0001$.

LDs are closely associated with various cellular organelles through the asexual stages

Membrane contact sites (MCS) refer to regions where the membranes of two organelles come into close proximity without merging (Scorrano et al., 2019; Prinz et al., 2020). These contact sites facilitate direct communication and exchange of lipids and other molecules between organelles, contributing to various cellular functions. In the FIB-SEM data, the tight interaction of LDs and other cellular organelles appear as a high electron density regions that connect LDs with various organelles (**Figure 17** and **18**).

I set out to determine whether LDs have preferential contact sites with particular organelles and also whether these preferences might differ across the asexual cycle stages. This quantitative approach could potentially offer clues about LD functions as parasites develop within their host cell. LDs were often in close contact with other cellular organelles (sometimes with several at the same time) (**Figure 19**). I observed frequent contact sites of LDs with the ER across all studied intraerythrocytic stages, and with the nucleus in trophozoites and early/mid schizonts (combined 43-53% of all observed interactions). In trophozoites and the various studied schizont stages, contact sites of LDs with the DV were also commonly observed, with 27-36% of all observed MCS occurring between these two organelles. Similarly, contact between LDs and the mitochondrion occurred in 7-18% of cases and between LDs and invaginations of the parasite plasma membrane in 7-18% of

analysed LDs. These invaginations resembled cytostomes, the sites at which haemoglobin and other host cell material is taken up by parasites (**Figure 19** A-D & A'-D').

The ER is known to be an LD biosynthesis site in mammalian cells and a range of other eukaryotes (Fujimoto and Parton, 2011; Jacquier et al., 2011; Hugenroth and Bohnert, 2020; Choudhary and Schneiter, 2021). Interestingly, when studying LD-ER contact sites through our 3D data sets, I frequently observed small LDs that appeared to be budding from the ER, and could represent sites of LD formation (**Figure 17** (A) (A') & (B) (B')). To my knowledge, signatures of LD biogenesis have not been shown before in P. falciparum. The consistent occurrence of contact sites with the mitochondrion, DV, ER and uptake sites throughout the asexual erythrocytic life cycle (**Figures 17**, **18** and **Figure 19** E) suggests that LDs contribute to numerous aspects of the parasite's biology and its development.

I notice an apparent absence of LD contact sites with the nucleus in late schizont stages (**Figure 19**E). However, since the ER has its origin around the nuclear envelop and stays intricately linked with the nucleus, it is difficult to distinguish between LDs that might provide lipids for the growth of the nuclear envelope or being associated with the nascent ER close to the nucleus. In late schizont stages the majority of LDs was associated with the DV and ER in the residual body– a structure that contains parasite material such as hemozoin that has not been incorporated into daughter merozoites after segmentation (Rudlaff et al., 2020). This might indicate that remnants of organelles, including 'unused' LDs, end up in this disposal site.

Together, I observed dynamic interactions of the LDs with several organelles during the course of intra-erythrocytic growth, indicative of central roles for organelle functions.

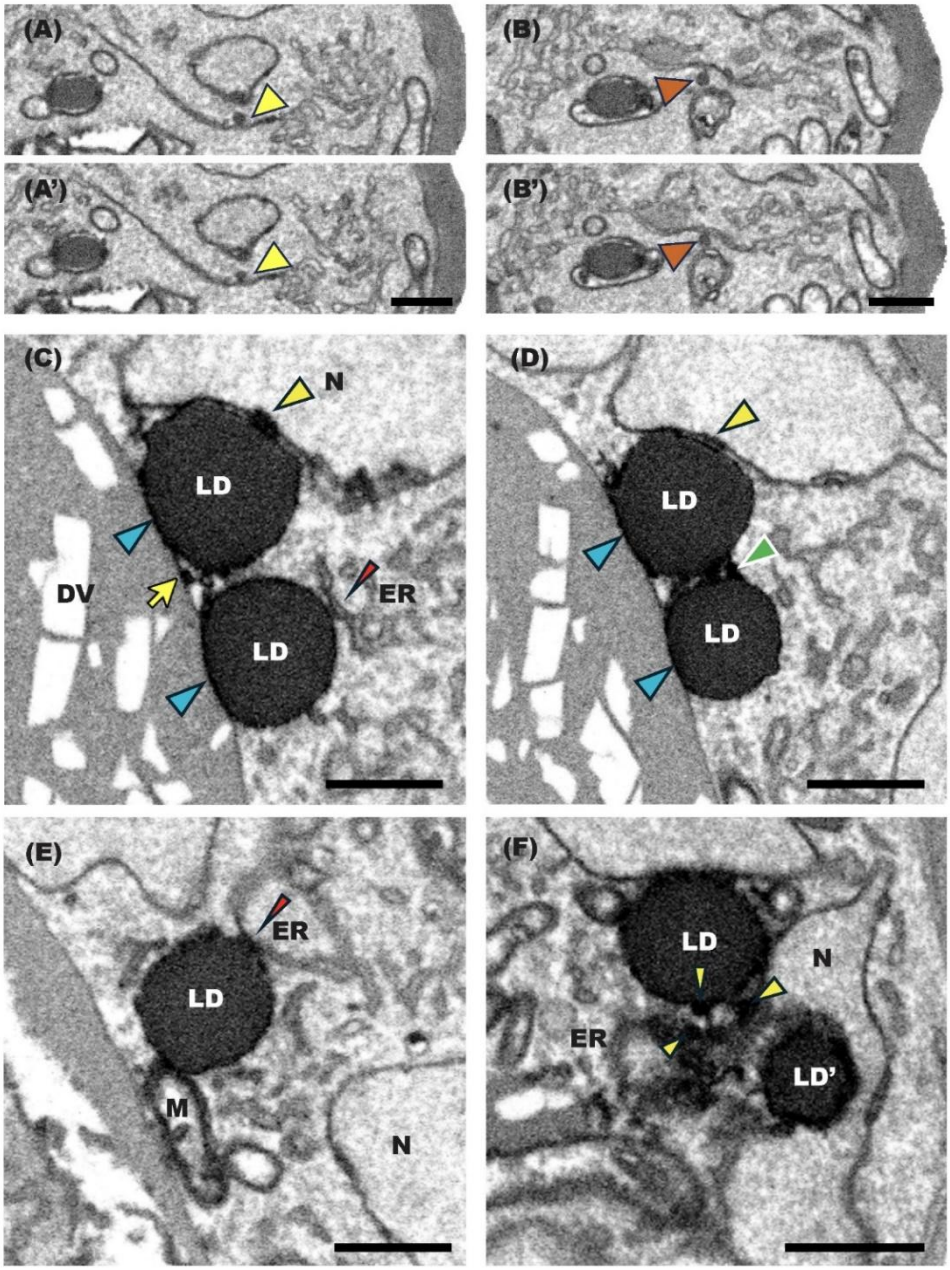

Figure 17. Membrane contact sites (MCS) of LDs with other organelles in *Plasmodium falciparum* asexual blood cycle stages (selected from 3D FIB-SEM image series) (A) (A') and (B) (B') LD budding sites from ER (yellow and orange arrowheads): small budding LDs in two adjacent serial sections from two different data sets (A & B). (C) MCS are visible between LD and nucleus (yellow arrowhead), LD and digestive vacuole (DV; blue arrowheads) and LD and ER (red arrowhead). Trafficking of small LDs between DV and LD is depicted with a yellow arrow. (D) MCS between two LDs, potentially indicating imminent fusion event (green arrowhead). LD and nucleus MCS (yellow arrowhead), LD and digestive vacuole (DV) MCS (blue arrowheads). (E) MCS between LD and mitochondrion (M) and LD and ER (red arrowhead). (F) LD biosynthesis site on ER with some LDs potentially trafficked to or fusing with larger existing LDs (yellow arrowheads). LD' is closely associated with the nucleus and seems to be nestled in a groove of the nuclear membrane when observed through the 3D stack of images. Scale bar: 500 nm.

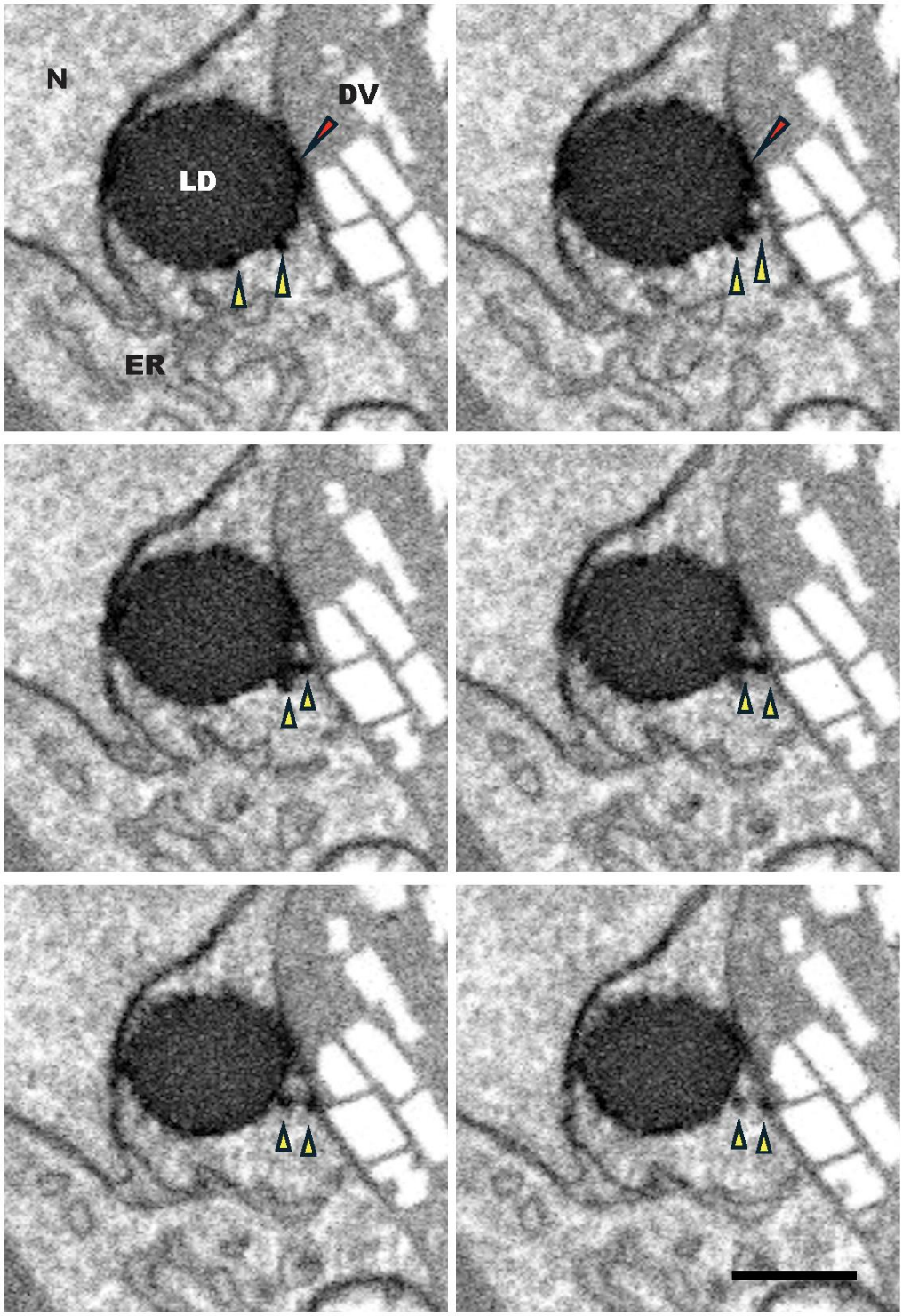

Figure 18. LD content transfer between LDs and Digestive vacuole (DV). Series of images through 3D FIB-SEM data set which shows trafficking of small LDs from large LD by budding events (yellow arrowheads). MCS between large LD and DV is depicted with a red arrowhead. ER: endoplasmic reticulum; DV: digestive vacuole; n: nucleus; LD: lipid droplet. Scale bar: 500 nm.

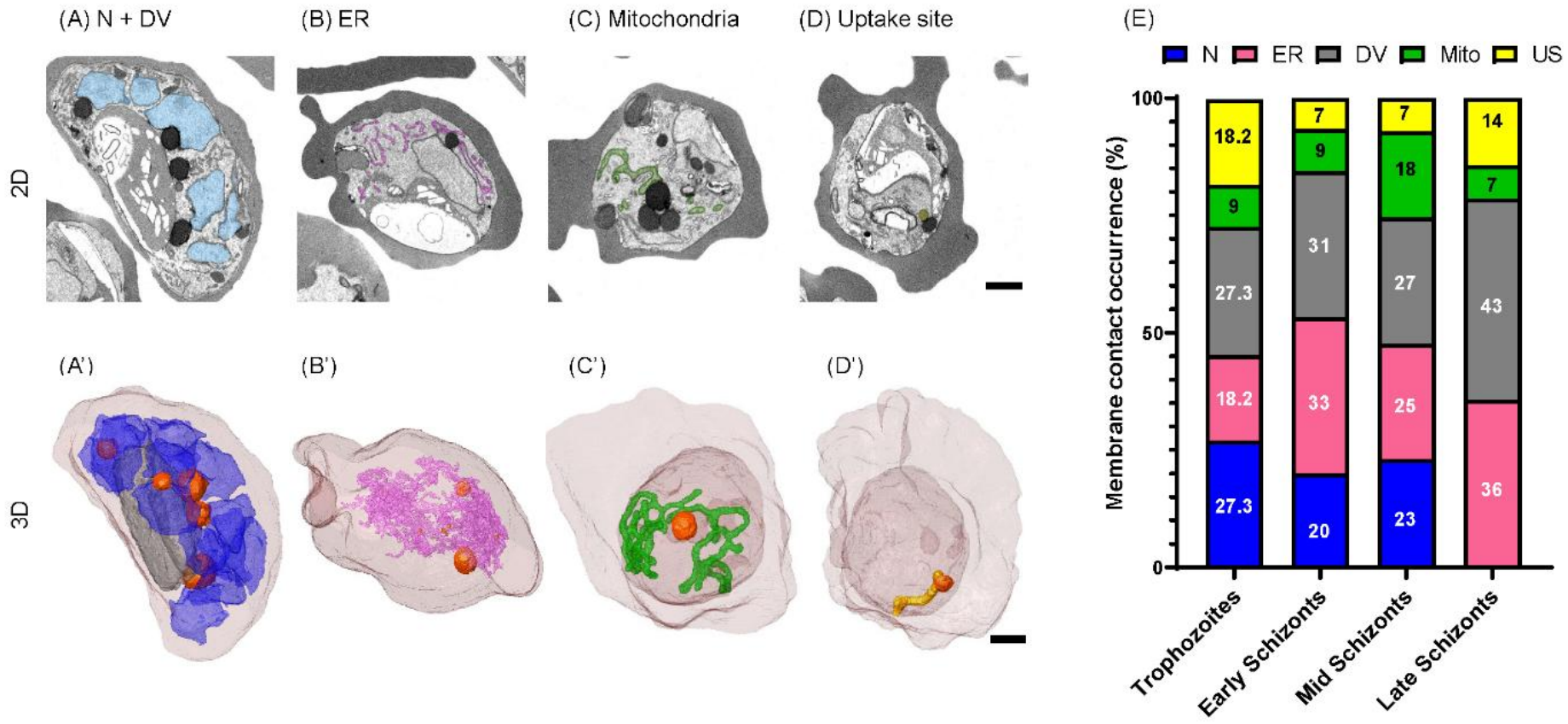

Figure 19. Visualisation and quantification of membrane contact sites (MCS) between LDs and other organelles. (A-D) Representative 2D images from a 3D FIB-SEM volume imaging data set and (A'-D') relevant rendered organelles within the parasite and host cell from corresponding 3D FIB-SEM volume data at various asexual parasite stages: (A) (A') depict multiple LDs (black/orange) in close proximity to nuclei (N, blue) and digestive vacuole (DV, haemozoin crystals visible/grey), (B) (B') with the endoplasmic reticulum (ER, pink), (C) (C') with the mitochondrion (Mito, green) and (D) (D') with an uptake site (US, yellow). (E) Normalised data of membrane contact occurrence between LDs and other parasite organelles. *n* = 3-11; 9 trophozoites, 10 early schizonts, 11 mid schizonts, and 3 late schizonts of 3D FIB-SEM data sets were analysed. Scale bars: 1 µm.

TAG hydrolysis is essential for merozoite formation

TAG hydrolysis is a universal lipid metabolic process whereby TAGs are broken down into glycerol and FAs. Orlistat, a commercially available anti-obesity drug, irreversibly inhibits the lipase responsible for this breakdown and has been demonstrated to inhibit malaria parasite growth (Yuan et al., 2011) (**Figure 20A**). This was shown to be a consequence of elevated TAG levels in late schizont stages, resulting in a subsequent inhibition of merozoite egress from the host RBC (Gulati et al., 2015).

I hypothesised that the TAGs present in LDs may be contributing to merozoite formation, which could explain the reduction of LD number and volume in segmenting schizonts. I reasoned that, if my hypothesis is correct, inhibiting TAG catabolism through the addition of Orlistat would inhibit merozoite formation, and that adding Orlistat after the depletion of LDs in segmenting schizonts would not lead to an impairment in merozoite formation. To this end, I added 60µM (8xIC_{50} concentration) of Orlistat to synchronised parasites at 8, 20, 32 and 44 hours after invasion and determined their appearance at 60 hours, compared to a DMSO control (**Figure 20** B & C). When Orlistat was added between 8 and 32 hours after invasion, the parasites progressed to the schizont stage where they stalled, unable to complete merozoite formation, eventually resulting in death of the parasites, as observed at the 84 hour time point. In contrast, when the drug was added at 44 hours into the cycle, I observed that >40% of parasites were able to survive, resulting in abundant rings at 60 hours into the assay (**Figure 20** B&C). These findings corroborate the results of Gulati et al., (2015) indicating that TAG hydrolysis and FA release is crucial at the time point of merozoite membrane formation.

Since I had observed a decrease in the volume of NL-enriched LDs from mid to late schizont stages (**Figure 16F**), I wanted to test whether LDs instead accumulate in the

presence of Orlistat in late schizont stages. The split emission fluorescence microscopy data of Nile Red stained parasites (yellow emission) showed a delay in nuclear division when Orlistat was added between 8 and 32 hours post invasion (**Figure 20** B&D). Nuclear division occurred eventually, yet the majority of parasites remained arrested at the mid schizont stage, failing to successfully undergo full merozoite formation (**Figure 20** B&D, 44 hours and 60 hours). While the control cells showed the typical membrane pattern surrounding each individual merozoite at 44 hours (late schizont stage, **Figure 20** E), treated cells displayed a much higher number of intensely fluorescing large punctae (**Figure 20** D). These punctae had accumulated non-polar lipids (likely TAGs, **Figure 20** E), typical for LDs which were still present at 60 hours in the presence of Orlistat, except when the drug was added after merozoite formation as indicated above (**Figure 20** E, lowest panel). These results support the hypothesis that TAG is consumed from LDs in support of the parasite's schizogony. The observations indicate that lipids derived from TAG hydrolysis in LDs (i.e. FA release from LDs) are essential for merozoite development.

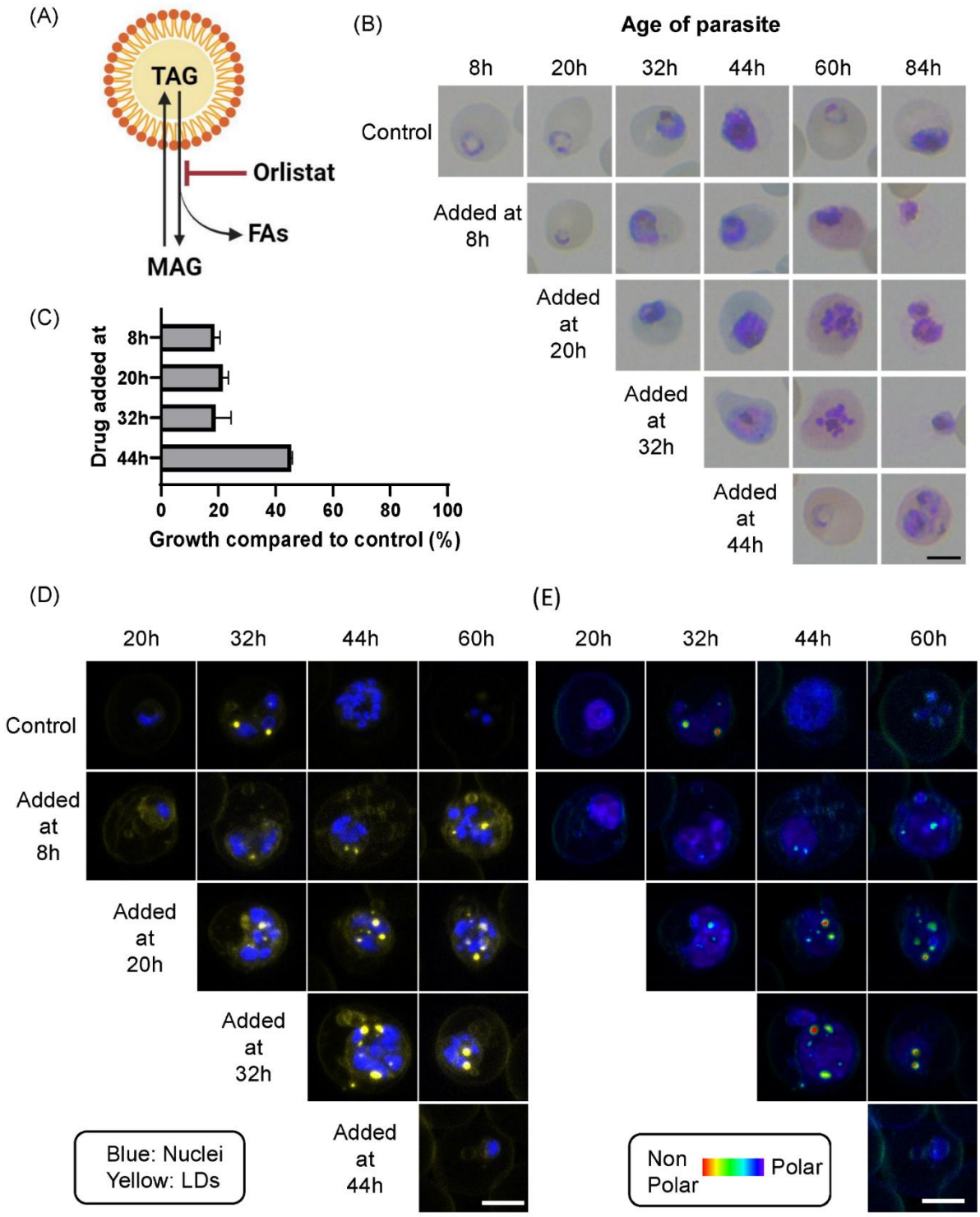

Figure 20. ***In vitro*** **assay with TAG hydrolysis inhibitor, Orlistat.** (A) Schematic representation illustrating the effects of Orlistat, which prevents TAG hydrolysis by inhibition of lipases. (B) Light microscopy of highly synchronised Giemsa-stained iRBC were treated with Orlistat at different time points. Cells were serially assessed for development every 12 hours following the addition of 60µM Orlistat (8xIC_{50}), at 8 hours, 20 hours, 32 hours, and 44 hours and representative images for each time point are depicted. (C) Parasite growth compared to control was assessed on Giemsa-stained smears at 60

hours. Three biological replicates were performed and each data point represents analysis out of 500 cells. (D, E) Effect of Orlistat on LD development. (D) Cells were stained with Nile Red for analysis of LD distribution. Non-polar lipid accumulation in LDs is depicted in yellow (excitation: 506nm/emission: 520-590nm). Hoechst staining indicates parasite nuclei (blue). (E) Polarity ratio map from images shown in (D). The ratio map, created by dividing yellow (non-polar) intensity by magenta (polar) intensity, is presented in a rainbow scale. Regions closer to the blue end of the spectrum indicate higher polarity, whereas those shifted towards the red end signify lower polarity. Figures (D) and (E) depict representative images of maximum intensity projection of cells captured through z-stack imaging. Scale bars: 5 µm.

Decreased capacity for TAG synthesis and storage promotes cell death

The majority of TAG is synthesised at the ER membrane through the glycerol 3-phosphate (Kennedy) pathway (Lehner and Kuksis, 1996), and the resulting TAG is then packaged into LDs. LDs may undergo expansion through the activity of TAG synthesis enzymes (Olzmann and Carvalho, 2019). One of the crucial enzymes involved in TAG biosynthesis is DGAT (Bell and Coleman, 1980). This enzyme catalyses the formation of an ester linkage between fatty acyl CoA and the free hydroxyl group of DAG to synthesise TAG (**Figure 21** A). In *Plasmodium*, TAG synthesis occurs mainly during the late trophozoite stage (Palacpac et al., 2004a; Vielemeyer et al., 2004). This is the stage at which we start to observe prominent LDs (**Figure 15** and **16**).

Xanthohumol (XN), a prenylated chalcone from *Homulus lupulus*, has been shown to inhibit both the DGAT1 and DGAT2 enzymes of mammalian and yeast cells (Tabata et al., 1997; Inokoshi et al., 2009). In *P. falciparum*, XN inhibited the parasite's in vitro replication and interfered with the process of haemin degradation (Frölich et al., 2005). I hypothesised that XN inhibition of the parasite DGAT enzyme would impair the development of LDs. To determine the effects of XN on LD development, I added XN at different time points post-invasion, and performed Nile Red labelling to visualise LDs (**Figure 21**). In contrast to our results with Orlistat, we observed immediate arrest of parasite development, irrespective of

the time point of XN addition (**Figure 21** B&C). Interestingly, we observed an absence of LDs when XN was added prior to the onset of LD formation in late trophozoites (**Figure 21** D&E). Small amounts of neutral lipids surrounding the nucleus in the pyknotic parasite cells were observed, resembling the pattern observed during the untreated control ring stages. However, no obvious LD accumulation was observed in cells treated earlier than 32 hours post infection (**Figure 21**E). These results support the hypothesis that XN interferes with TAG synthesis or its storage or both, which seems to be essential for development of the parasite through the asexual part of its life cycle. When treated at 32 or 44 hours after invasion, TAG-containing LDs seemed to form (**Figure 21** D&E) but parasite development was still impaired, with mostly pyknotic parasites observed at the 60 hour time point (**Figure 21**C) which could be due to another mode of action of XN. Overall, these results support the hypothesis that XN interferes with TAG synthesis and NL storage, which seems to be essential for development of the parasite through the asexual part of its life cycle.

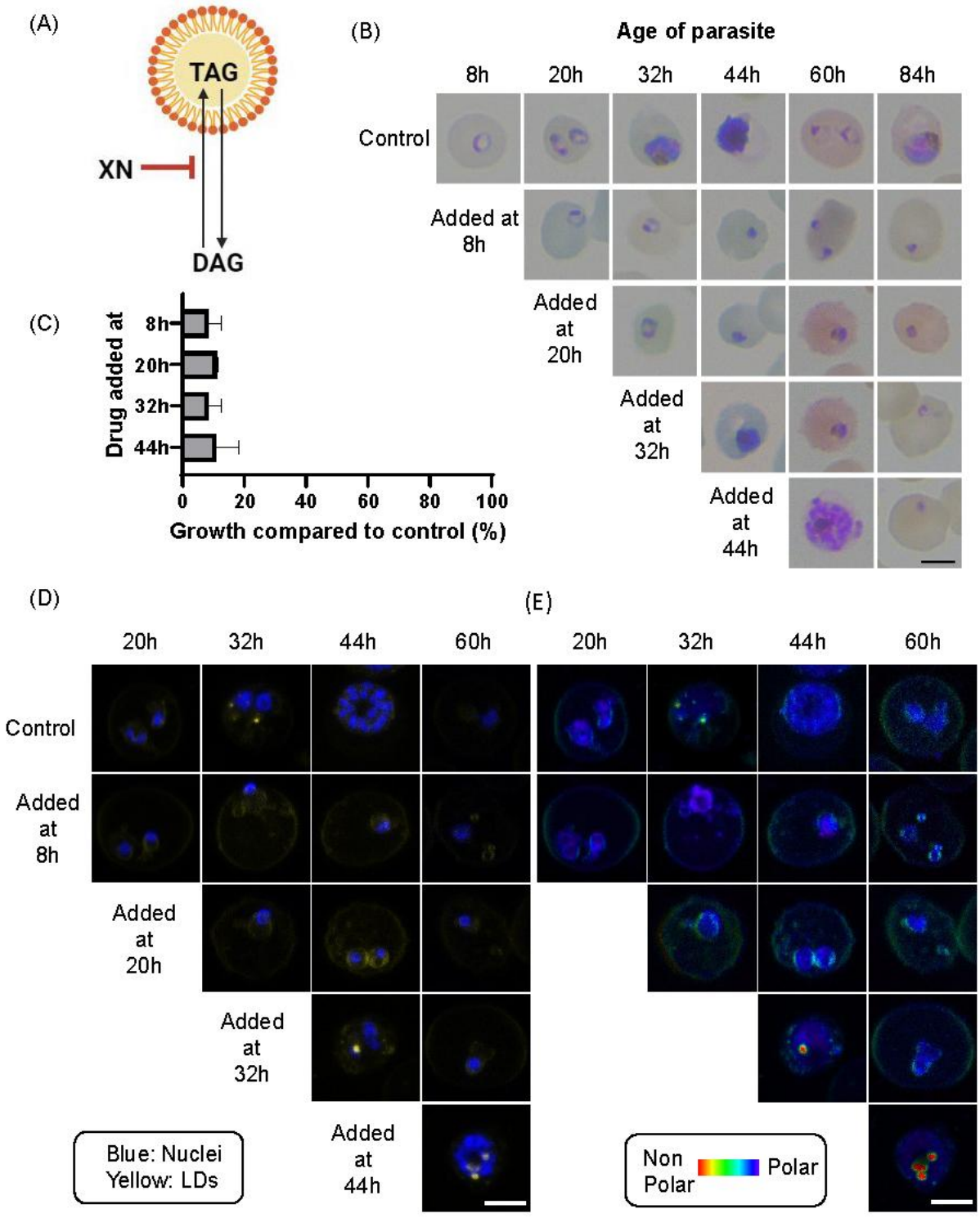

Figure 21. *In vitro* assay with DGAT inhibitor, Xanthohumol (XN). (A) Schematic representation illustrating the effects of XN by inhibiting major enzymes involved in TAG catalysis (DGATs). (B) Light microscopy of highly synchronised Giemsa-stained iRBC treated with XN at different time points. Cells were serially assessed for development every 12 hours following the addition of 40µM XN (8xIC_{50}), at 8 hours, 20 hours, 32 hours, and 44 hours and representative images for each time point are depicted. (C) Parasite growth

after XN treatment compared to control was assessed on Giemsa-stained smears at 60 hours. Three biological replicates were performed, and each data point represents analysis out of 500 cells. (D, E) Effect of XN on LD development. (D) Cells were stained with Nile Red for analysis of LD distribution. Non-polar lipid accumulation in LDs is depicted in yellow (excitation: 506nm/emission: 520-590nm). Hoechst staining indicates parasite nuclei (blue). (E) Polarity ratio map from images shown in (D). The ratio map, created by dividing yellow (non-polar) intensity by magenta (polar) intensity, is presented in a rainbow scale. Regions closer to the blue end of the spectrum indicate higher polarity, whereas those shifted towards the red end signify lower polarity. Figures (D) and € depict representative images of maximum intensity projection of cells captured through z-stack imaging. Scale bar: 5 µm.

DGAT1 inhibition primarily affects Plasmodium falciparum ring stages

Earlier reports have shown that *Plasmodium* contains only one DGAT enzyme which most closely resembles the DGAT1 enzyme of mammalian cells (Palacpac et al., 2004b; Vielemeyer et al., 2004; Vial and Ben Mamoun, 2005). In order to identify whether XN affects the parasite by interfering with the parasite DGAT or haemin degradation I repeated the experiment with T863 (**Figure 22**A). T863 is a potent, selective inhibitor of DGAT1 that acts on the acyl-CoA binding site of DGAT1 and inhibits DGAT1-mediated TAG formation in cells (Cao et al., 2011). When added to ring stage parasites, T863 arrested parasite development in a similar, rapid fashion to XN (**Figure 22**B) leading to the formation of pyknotic cells (**Figure 22**C) without any significant accumulation of LDs throughout the assay (**Figure 22**D). However, in contrast to XN, when T863 was added at 20 or 32 hours after invasion, parasites seemed to develop and divide, although slower than the control cells and with only ~25% of cell survival at the 60 hour time point (**Figure 22**B&C). When T863 was added at 44 hours post invasion, the parasites seemed to develop similarly to the ones treated with Orlistat, with the survival rate (~50%) being very similar to this treatment as well (**Figure 22** B&C). In contrast to Orlistat treatment this late in the cycle though, no LDs could be observed in our split emission and ratio analysis (**Figure 22** D&E). This suggests that the inhibitory effect of T863, which selectively targets DGAT-1, prevents LD formation

when added at an early stage, where TAG is not abundant yet. However, when added at a stage where LDs are already present (32 hours post invasion), the parasites can still develop for a while, utilising the available TAG for membrane formation. Depending on the window of synchronisation, this explains the >50% survival rate when observed at 60 hours. For parasites which were earlier in the cycle when the inhibitor was added, not enough TAG could be accumulated in the presence of T863, hence the amount of TAG was not sufficient for merozoite membrane formation and subsequent merozoite release. These results also indicate that the effect of XN in later stage parasites is independent of DGAT inhibition (and might be a reflection of insufficient haemin digestion or lipid toxicity due to non-segregated lipids in the cytoplasm).

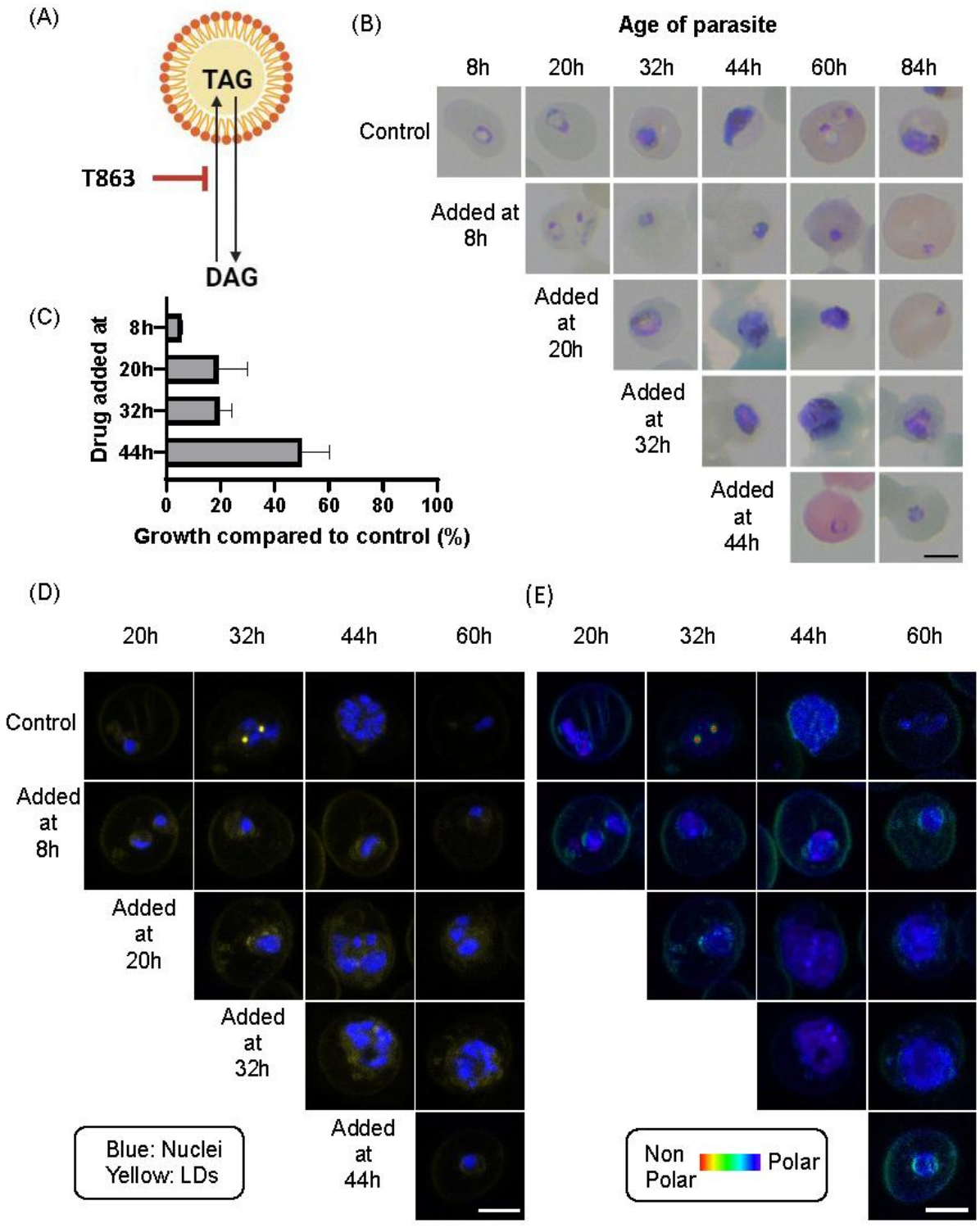

Figure 22. *In vitro* assay with DGAT inhibitor, T863. (A) Schematic representation illustrating the effects of T863. (B) Light microscopy of highly synchronised Giemsa-stained iRBC treated with T863 at different time points. Cells were serially assessed for development every 12 hours following the addition of 40µM XN ($8xIC_{50}$), at 8 hours, 20 hours, 32 hours, and 44 hours and representative images for each time point are depicted. (C) Parasite growth after T863 treatment compared to DMSO control was assessed on

Giemsa-stained smears at 60 hours. Three biological replicates were performed, and each data point represents analysis out of 500 cells. (D, E) Effect of T863 on LD development. (D) Cells were stained with Nile Red for analysis of LD distribution. Non-polar lipid accumulation in LDs is depicted in yellow (excitation: 506nm/emission: 520-590nm). Hoechst staining indicates parasite nuclei (blue). (E) Polarity ratio map from images shown in (D). The ratio map, created by dividing yellow (non-polar) intensity by magenta (polar) intensity, is presented in a rainbow scale. Regions closer to the blue end of the spectrum indicate higher polarity, whereas those shifted towards the red end signify lower polarity. Figures (D) and (E) depict representative images of maximum intensity projection of cells captured through z-stack imaging. Scale bars: 5 μm.

Drugs targeting TAG metabolism cause ultrastructural changes in P. falciparum LDs and impair merozoite formation

To substantiate the observations from light microscopy regarding the effects of Orlistat, XN and T863 on LDs, I exposed highly synchronised infected erythrocytes to each of the individual drugs at 32 hours post invasion. I then sampled and prepared cells for transmission electron microscopy (TEM) analysis 44 hours and 60 hours post invasion.

While control parasites revealed fully formed merozoites ready for egress in most cells observed at 44 hours post invasion (**Figure 23**A, left panel), the inhibitor-treated cells all displayed multiple parasite nuclei but none of them had progressed to segmentation into individual merozoites within the host erythrocyte (**Figure 23**B-D). In Orlistat-treated cells, multiple large LDs were observed at 44 hours post invasion, with some of them closely associated with the DV (**Figure 23**B, yellow arrows). Cells treated with XN displayed large (mostly single) LDs at 44 hours post-invasion, clearly identifiable by their electron dense content (**Figure 23**C). In contrast, cells treated with the inhibitor T863 displayed some globular organelles without discernible double membrane, reminiscent of LDs, but with a much lower electron density (**Figure 23**D). These observations corroborate our findings from the split emission experiments. Cells treated with Orlistat and XN displayed multinucleated parasites interspersed with non-polar lipid containing LDs when treated with

the inhibitors at 32 hours post invasion and observed at 44 hours. In contrast, T863-treated cells displayed LDs depleted of non-polar lipids (**Figures 22**E & **23**D).

In order to study the fate of the cells after inhibitor treatment into the next erythrocytic cycle, cells were also sampled at 60 hours post-invasion (**Figure 23**, right panel). While control cells developed into rings as expected (**Figure 23**A), Orlistat- and XN-treated cells exhibited plasma membrane disintegration, and membrane whorls, blebs and aggregations were visible in the cytoplasm, all hallmarks of cellular degradation. In contrast, when cells were treated with T863 at 32h post-invasion, parasite development was delayed (no rings observed at 60 hours post invasion) but segmentation of the parasite into daughter merozoites was clearly visible (**Figure 23**D).

The ultrastructural analysis of cells treated with the three different inhibitors support the light microscopy results. In the absence of TAG hydrolysis (Orlistat treatment) or decreased TAG synthesis and storage capacity (XN treatment), cell segmentation is prevented, leading to parasite death. In contrast, cells treated with T863 at this later stage in the erythrocytic cycle, where TAG-enriched LDs would have already formed, the inhibitor delayed parasite development but did not prevent segmentation, suggesting that the inhibitory effect of T863 mainly targets early TAG synthesis.

Overall, the data from our inhibitor studies suggest that the NLs in parasite LDs are comprised mainly of TAGs, and that interference with TAG synthesis, storage or hydrolysis results in detrimental effects for the parasite. This highlights the fundamental importance of TAG metabolism for parasite survival.

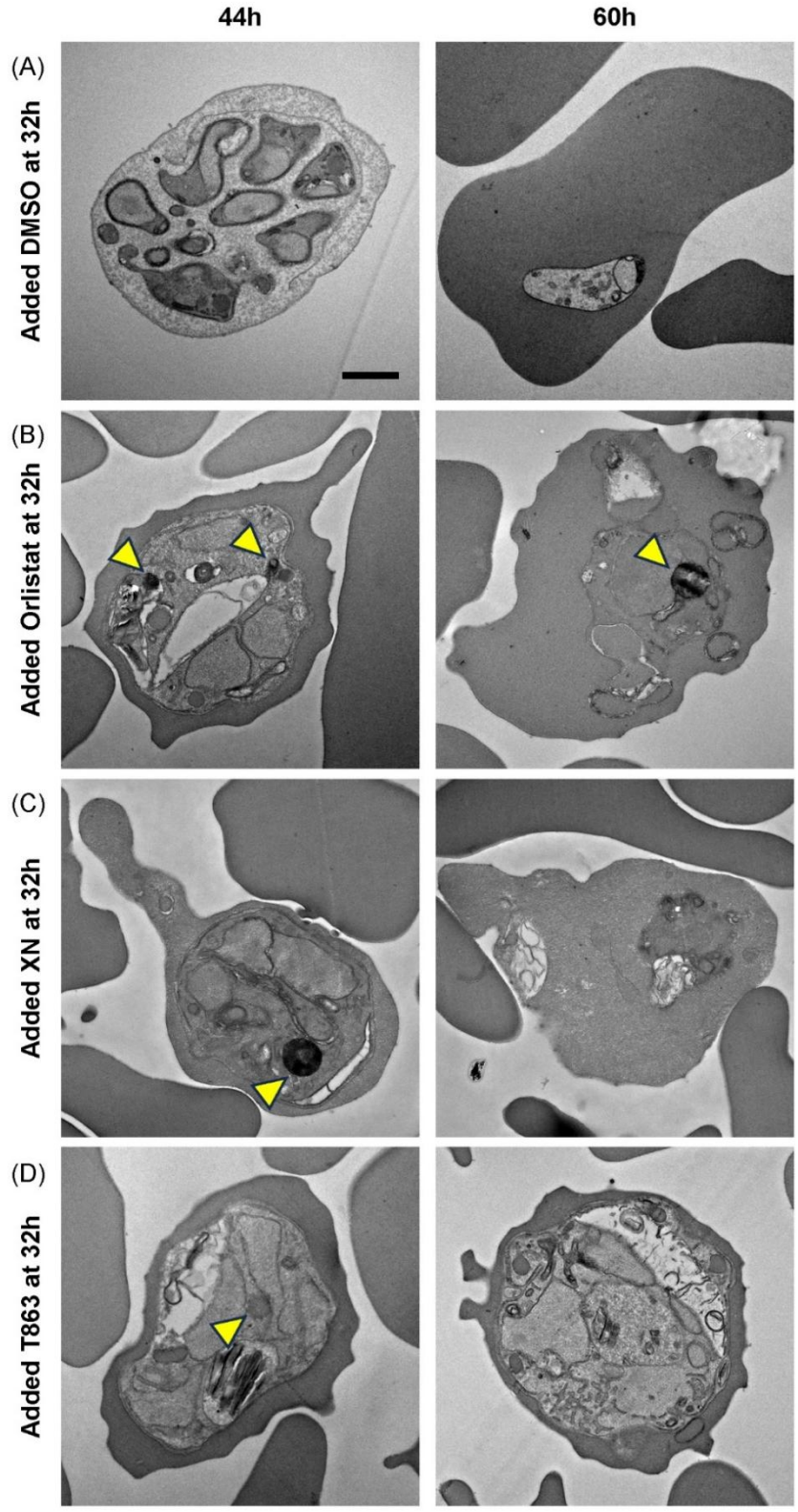

Figure 23. Ultrastructural analysis of *P. falciparum*-infected RBCs treated with inhibitors. Transmission Electron Microscopy (TEM) images of cells treated with (A) 0.1% DMSO (control), (B) 60 µM Orlistat, (C) 40 µM XN and (D) 200 µM T863 at 32 h post invasion. First row depicts cells prepared for TEM analysis at 44h post invasion while the second row shows cells prepared for TEM analysis at 60h post invasion. Yellow arrows indicate LDs. Scale bar: 1 µm.

Discussion

Lipid droplets change in number, size and content throughout the asexual stages

Applying two novel methodological approaches to the study of LDs in *P. falciparum* – namely emission splitting of the Nile red signal and 3D FIB SEM – together with the temporal resolution of different developmental stages, we were able to reveal the detailed dynamic of LD synthesis, growth and utilisation during the asexual replication cycle of the malaria parasite in the human host.

Neutral lipids accumulate in LDs until mid-schizont stage before these storage compartments are utilised to meet the demand for NLs during the formation of merozoites in segmenting schizonts. While a constant increase in neutral lipids from rings to late schizonts is implied in our data that utilised traditional Nile Red imaging conditions (excitation: 559 nm/emission: 636 nm) (**Figure 14**), the refined analysis using the split emission approach revealed a more differentiated picture: both LD numbers as well as NL content decreased at the late schizont stage, indicating that NLs such as acylglycerols and cholesterol esters are hydrolysed to provide building blocks for membrane formation. While the parasite accumulates lipids for later use from a nutrient-rich host environment, LDs prevent the cytosol from being overloaded by excess free lipids and hence avoid lipid toxicity.

In addition to using the emission splitting system that differentiates polar from non-polar lipids in the parasite cell, we employed 3D FIB SEM. In this protocol, LD content is intensely stained with heavy metals, making LDs easily distinguishable from other organelles in the cellular context. The ultrastructural data corroborated our light microscopy findings where number and volume of NL-enriched LDs increased as the parasites developed to the mid schizont stage. While the number of LDs decreased only slightly from

mid to late schizonts, the volume of LDs decreased dramatically to < 25% of the mid-schizont level. This result clearly demonstrates that LM analysis alone, due to its limited resolution, especially in a very small organism like *P. falciparum* (< 5µm), will not disclose the full picture of organellar dynamics. The detailed ultrastructural analysis also revealed that the small LDs remaining in late schizont stages were mainly associated with the residual body. This indicates that small remnants of LDs might be left over for disposal once the merozoites are released from the host cell to start a new intraerythrocytic cycle. The non-utilisation and surplus of lipids that are discarded in the DV might seem to be contradictory to nature's economy. However, these experiments are conducted under conditions where parasite access to lipids and lipid precursors is not limited and hence the possibility exists that fewer surplus lipids might be found in a more lipid restricted environment. In perspective, these techniques can now be applied to clinical samples, in order to study LD dynamics during human infections.

Taken together, split emission analysis of Nile Red-stained *P. falciparum*-iRBC in combination with analysing LDs at ultrastructural resolution in 3D revealed significant changes in the number and size of LDs in the parasite's asexual cycle.

LD contact with other organelles

Biogenesis and subsequent dynamics of LDs rely on close contact of LDs with various organelles. Interrogation of the 3D data revealed that most LDs were in close contact with various organelles throughout the asexual life cycle via membrane contact sites (MCS). These sites are regions where membranes of two organelles form contact sites that enable the transfer of lipids, metabolites and ions (Scorrano et al., 2019).

LD formation starts with synthesis of the molecules of the organelles' neutral lipid core,

which is mediated by enzymes located primarily on the ER (Watkins et al., 2007; Pol et al., 2014) . Unsurprisingly, the most abundant LD contact sites in this study were with the ER and the nucleus (the nuclear envelope being contiguous with the ER).

In mid schizont stages, I often observed an accumulation of LDs which were much bigger in size compared to LDs in earlier stages (**Figure 15**A, **Figure 16**C, **Figure 16**F). Interestingly, I observed potential LD budding sites from the ER in multiple parasite stages (**Figure 17** A, B and F), suggesting continuous LD biogenesis during the growth of the parasite. These might be able to fuse to form larger LDs in schizont stages (**Figure 17** D; green arrow).

I observed a drop in combined ER/nucleus-LD contact sites in late schizont stages, in line with the shift from accumulation to usage of LD lipids. In late stage schizonts, no LD interactions with nuclei were observed. In these stages, the nuclei are segregated to newly formed merozoites and hence spatially separated from the few remaining LDs that are found in the residual body (**Figure 19** E).

In *P. falciparum,* LDs have been implicated in the delivery of NL to the DV, where they are thought to play a role in haemozoin formation, a process that detoxifies haem that is released during haemoglobin digestion in the DV of the parasite (Jackson et al., 2004; Ambele and Egan, 2012). Hence, the high percentage of observed LD-DV contacts in this study supports the proclaimed role of neutral lipids in haem detoxification, a process that is essential for parasite survival.

I observed an increase in LD-mitochondria contact sites from early- to mid-schizonts. In many cell types, LDs deliver fatty acid containing NL to fuel the energy generating fatty acid oxidation of mitochondria (Rakotonirina-Ricquebourg et al., 2022). This is unlikely to be the case in *P. falciparum* since the parasite lacks a functional β-oxidation pathway in its mitochondria (van Dooren et al., 2006). However, delivery of energy in form of ATP from

mitochondria to LD was reported to fuel fatty acid activation in LDs of mammalian adipocytes. The high demand for energy to activate and access the lipids stored in LD might explain the increase in LD-mitochondria contact increase in mid-schizont stages.

The multifaceted interaction of LDs with various organelles underscores the versatile nature of LDs in orchestrating cellular functions. The quantification of contact points between organelles might indicate the relative importance of the LD-organelle interaction for a particular function, however, this can also be obscured by spatial constraints. Further investigations into proteins involved in the molecular mechanisms could reveal exciting new insights into specific functions associated with these contact sites.

LD composition dynamics

This study also provides more detailed insights into the composition of LDs. The LM data in this study represents for the first time a detailed quantitative analysis of neutral lipids throughout the asexual life cycle stages by employing a methodology that allows separation of lipid species due to their polarity (Greenspan, 1985; Greenspan and Fowler, 1985).

Traditional Nile Red analyses indicate a steady increase of neutral lipids throughout the development of the parasites (**Figure 14**). By separating the signal for polar lipids (magenta) and the signal for NL (yellow) we could show that NLs accumulate in LDs until the mid-schizont stage. In contrast, polar lipids continuously increase and are mostly associated with parasite membranes (**Figure 15**).

To distinguish between synthesis and utilisation of the lipids contained in LDs in the parasite, we combined the split emission approach with the use of specific inhibitors to disrupt lipid metabolism in LDs.

TAGs have been identified as one of the major neutral lipid classes in *P. falciparum* LDs

(Vielemeyer et al., 2004) and FAs released from TAG hydrolysis can serve as a source of fatty acids for various metabolic processes (Watt and Spriet, 2010). Using the TAG hydrolysis inhibitor Orlistat, I identified the contribution of LDs to meeting these demands during merozoite formation. When Orlistat was added between 20 and 32 hrs of development, the parasites continued to develop, but failed to produce proper merozoites which were also not released. The neutral lipid ratio profile clearly shows an accumulation of NL-containing LDs in late schizont stages which is not observed in the controls. These findings indicate that TAG is the major NL found in LD of *P. falciparum*, and highlight the importance of TAG utilisation during schizogony, where the development of organellar and plasma membranes of individual merozoites heavily relies on the availability of membrane building blocks. Furthermore, our results offer a plausible explanation for the severe growth phenotype associated with Orlistat exposure described by Gulati et al. (2015).

In addition to the dependence on free FAs for membrane biogenesis, the parasite relies on controlling DAG levels during the early development stages, with excess DAG being converted into TAG for storage, in order to maintain lipid homeostasis and to avoid lipotoxicity (Sheokand et al., 2023). DGATs are key enzymes which esterify DAGs with acyl-CoA to generate TAGs at the ER or on LDs (Yen et al., 2008). Exposing parasites to the DGAT inhibitors XN and T863 resulted in developmental arrests and death of the parasites even in early stages of the intraerythrocytic cycle, arguing that this phenotype is associated with lipid toxicity due to excess DAGs in the cytoplasm rather than a lack of TAGs in the LD. In addition, disruption of TAG synthesis might also lead to DAG accumulation in the ER which can cause severe defects in the endomembrane system, as has been shown in in other eukaryotic cells (Li et al., 2020).

The inhibitor assays in this study clearly demonstrate the functional duality and emphasise the indispensability of LDs in *P. falciparum* throughout the parasite's asexual

developmental stages (**Figure 24**): on the one hand, conversion of DAG to TAG and its storage provides a reservoir of FAs, which may be particularly important during periods of high demand for PL synthesis; and on the other hand, LD depletion along with TAG hydrolysis, which are crucial for parasite survival and highlight the vulnerability of these parasites when either of these metabolic functions is disturbed.

Disrupting the function of LDs has been implicated in many different human diseases, including type 2 diabetes, cancer, and neurological diseases like Alzheimer's and Parkinson's disease (Murphy, 2012). This chapter is an initial step toward understanding LD biology in *P. falciparum*, yet highlights its importance for parasite survival and potential as a therapeutic target.

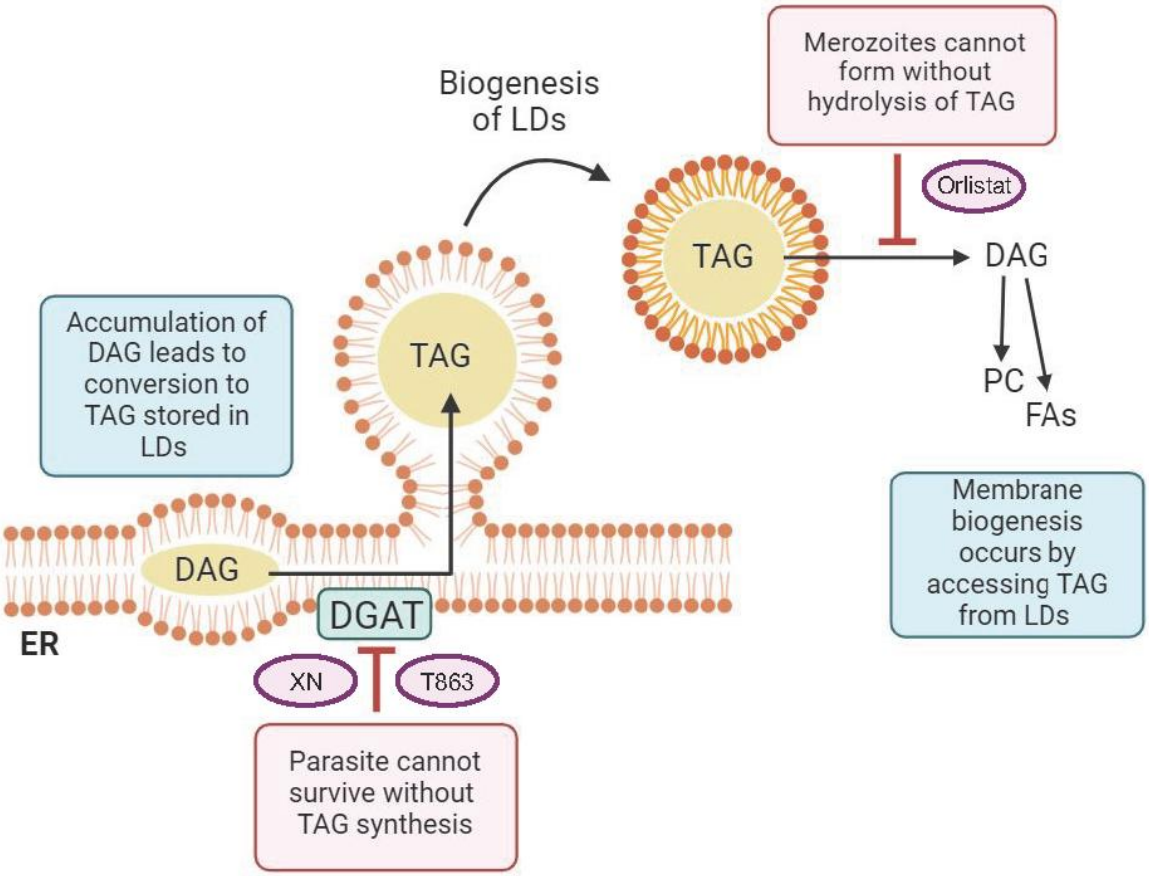

Figure 24. Model of lipid droplet (LD) dynamics in the *Plasmodium falciparum* asexual blood-stage cycle. At an early developmental stage (ring stage), the parasite synthesises DAG which accumulates in certain areas between the bilayer of the ER membrane. DAG is then converted to TAG, the storage form of neutral lipids, which coincides with the appearance of small LDs budding off the ER (blue box). When TAG synthesis is inhibited (*e.g.* by inhibitors like XN or T863), parasites fail to form LDs which leads to cell death due to lipotoxicity (red box). In the late schizont stage, parasites require access to LD-stored TAGs as an energy and FA resource to generate new membranes (blue box). When TAG hydrolysis is inhibited (*e.g.* by Orlistat), parasite development is arrested at the mid schizont stage, and no merozoites can be formed, breaking the parasite asexual cycle (red box). Created with BioRender.com.

Chapter 4. Systematic search for LD-associated proteins in *P. falciparum*

Introduction

LDs are functionally conserved, and highly dynamic organelles dedicated to the storage of metabolic energy and play a crucial role in cellular physiology. The identification of LD marker proteins has provided powerful tools for studying LD biology, enabling detailed investigations into their composition, function, and interactions. Over the past decades, LD isolation methods and proteomic technologies have significantly expanded our understanding of LD associated proteins across various cell types and organisms (Sato et al., 2006; Zhang et al., 2012; Horn et al., 2013; Khor et al., 2014; Brasaemle and Wolins, 2016).

Proteomic analyses have identified hundreds of LD-associated proteins, many of which have been further validated using biochemical, imaging, and functional approaches by knock out or overexpression studies (Bartz et al., 2007b; Gong et al., 2011; Jambunathan et al., 2011; Wang et al., 2011; Cartwright et al., 2014; Wilfling et al., 2014; Choudhary et al., 2015; Wang et al., 2016; Bersuker et al., 2018). While studies from various organisms report diverse protein profiles, certain groups of proteins consistently appear across species (Fujimoto et al., 2004; Kim et al., 2006; Wan et al., 2007; Bouchoux et al., 2011; Yang et al., 2012; Su et al., 2014).

The first group contains enzymes involved in lipid metabolism and synthesis include both neutral lipid synthesis (e.g., DGAT and ACAT) for LD cargo and phospholipid synthesis for monolayer of LD. These enzymes are among the most prevalent in proteomic data across diverse eukaryotic systems, including mammals, yeast, and unicellular eukaryotes (Lardizabal et al., 2001; Turkish and Sturley, 2007; Kim et al., 2011; Yoon et al., 2012). This consistency suggests their central role in generating and maintaining LDs.

The second group consists of proteins involved in LD biogenesis and dynamics such as Ras-super family of small GTPases (Rabs), Pelilipin (PLIN), RalA, and 14-3-3. These proteins

facilitate LD-organelle interactions, enabling lipid transfer between organelles, and also support the role of LDs in lipid-mediated signalling pathways (Maehama et al., 2008; Schuldiner and Bohnert, 2017; Pennington et al., 2018).

In *P. falciparum*, TAG-enriched LDs are predominantly formed during the asexual blood stages, where they play an essential role in parasite survival and intracellular lipid homeostasis (Lee et al., 2024). Ultrastructural studies have shown that LDs in asexual stages are closely associated with other cellular organelles, including the ER and mitochondria (Lee et al., 2024). These findings suggest active sites of lipid exchange and metabolic coordination. The electron microscopy data also indicate potential LD budding sites from the ER (Lee et al., 2024), implying that ER-localised proteins and neutral lipid synthetic enzymes may directly be involved in LD formation. Despite these observations, the molecular machinery that regulates LD-organelle contact in *Plasmodium* parasites remains largely unknown. Nonetheless, the structural association between LDs and other organelles in *P. falciparum* largely seems to resembles those seen in other eukaryotes, suggesting that the parasite may use similar mechanisms to form the contact sites and facilitate lipid trafficking. However, the identity and function of the proteins mediating these contacts in the parasite remain largely uncharacterised. To address this gap, this chapter first reviews widely conserved LD-associated proteins from mammalian systems. This provided a comparative framework for my homology searches and interpretation of stage-specific expression in *P. falciparum.*

Known LD-associated proteins in mammals

In mammalian cells, LDs are highly dynamic organelles that function not only as storage depots for neutral lipids but also as regulators of cellular lipid metabolism and signalling. The formation, maintenance, and turnover of LDs are tightly controlled by a specific population of LD-associated proteins. Because of many of these proteins have not been characterised in

Plasmodium, I reviewed their functions in other systems as a framework for identifying potential homologs in the parasite.

- ***Proteins involved in LD cargo synthesis***

During LD biogenesis, neutral lipids such as TAG and CE are synthesised by enzymes including DGAT and ACAT, which catalyse the final steps of TAG and CE formation, respectively. These neutral lipids accumulate between the leaflets of the ER bilayer to initiate LD formation.

Two different DGAT enzymes, DGAT1 and DGAT2, have been identified in mammals. Although both catalyse the final step of TAG synthesis, they evolved independently (Turchetto-Zolet et al., 2011). DGAT1, phylogenetically related to the ACAT family, localises exclusively to the ER and is responsible for general TAG synthesis and lipoprotein secretion (Cases et al., 1998b; Liang et al., 2004; Yamazaki et al., 2005; Shockey et al., 2006). In contrast, DGAT2 is found in both the ER and LDs and plays a crucial role in LD growth and expansion by acting at the ER and LD contact site (Cases et al., 2001; Stone et al., 2004; Shockey et al., 2006; Kuerschner et al., 2008).

Similarly, two forms of ACAT exist in mammals, ACAT1 and ACAT2 (Chang et al., 2009). ACAT1 is broadly expressed, with high levels in macrophages, steroidogenic tissues, sebaceous glands, and atherosclerotic lesions, and is localised to the cytoplasmic side of the ER (Chang et al., 1993; Meiner et al., 1996; Miyazaki et al., 1998; Joyce et al., 2000). By contrast, ACAT2 expression is largely restricted to the liver and small intestine and is localised to the luminal side of the ER (Anderson et al., 1998; Cases et al., 1998a; Joyce et al., 2000). This differential localisation suggests their distinct functions: ACAT1 regulates intracellular cholesterol homeostasis, whereas ACAT2 supports lipoprotein assembly by converting free

cholesterol into CEs for secretion (Klein and Rudel, 1983; Chang et al., 2001). DGAT1 is phylogenetically related to ACATs, highlighting the evolutionary relationship these enzymes (Turkish and Sturley, 2009).

Lecithin-cholesterol acyltransferase (LCAT), which transfers a fatty acid from phosphatidylcholine (lecitin) to free cholesterol, producing CE and lysolecithin (Sorci-Thomas et al., 1990). LCAT functions in the plasma membrane and plays a key role in lipoprotein maturation and cholesterol homeostasis (Dahlqvist et al., 2000). It facilitates cholesterol efflux from peripheral tissues by maintaining a gradient that drives cholesterol movement into high density lipoprotein (HDL) particles (Glomset, 1968; Czarnecka and Yokoyama, 1996). Once cholesterol released from membranes or LD via CE hydrolysis, free cholesterol can either be re-esterified by ACAT or efflux to extracellular acceptors such as HDL. This efflux process is mediated by ABC transporters, primarily ABCA1 and ABCG1 (Yvan-Charvet et al., 2007; Westerterp et al., 2013).

- ***Proteins involved in LD biogenesis and development/dynamics***

Several structural proteins regulate LD biogenesis and dynamics. Seipin facilitates the formation of LDs by stabilising nascent lipid lenses and regulating LD growth at ER-LD contact sites (Salo et al., 2019; Arlt et al., 2022). LDAF1 (lipid droplet assembly factor 1) forms a complex with Seipin to define LD nucleation sites in the ER, then later dissociates and relocates to the LD surface, where it promotes LD growth (Chung et al., 2019; Goodman, 2019). FIT (fat storage-inducing transmembrane) proteins also assist in early LD budding by potentially determining nucleation site and the direction of budding from the ER (Gross et al., 2011). Once formed, LDs are coated by specific surface proteins such as perilipins (PLIN1–PLIN5), which regulate LD formation and lipid homeostasis by controlling the storage and

mobilisation of intracellular lipids (Greenberg et al., 1991; Londos et al., 2005; Sztalryd and Kimmel, 2014). PLIN1 interacts with hormone-sensitive lipase to mediate TAG hydrolysis on LDs (Sztalryd et al., 2003). 14-3-3 protein complexes interact with PLIN1 and modulate lipolysis in adipocytes (Yang et al., 2023). PLIN5 function as a tether between LDs and mitochondria, allowing FA transfer for energy metabolism (Miner et al., 2023).

Trafficking proteins also shape LD dynamics. Rab proteins, Arf1, and RalA (Ras-related protein) facilitate LD movement, positioning, and membrane contact site formation.

Rab proteins are central regulators of vesicular traffic (Zerial and McBride, 2001), and only a subset - Rab1, Rab7, Rab8a, and Rab18 – show strong links to LD biology (Martin et al., 2005; Ozeki et al., 2005; Li and Yu, 2016). For instance, Rab18 is known to mediate tethering of LDs to the ER through interaction with the NRZ-SNARE complex and ZFYVE1, which facilitates lipid transfer and LD expansion (Xu et al., 2018).

Arf1 and COPI (Coat Protein Complex I) proteins localise to LDs and regulate surface composition. Cells lacking Arf1/COPI have increased phospholipid content on LDs, reducing surface tension of LD and impairing the formation of ER-LD bridges (Wilfling et al., 2014).

RalA facilitates TAG synthesis and promotes LD growth under nutrient stress. Loss of RalA leads to reduced TAG levels, indicating its critical role in LD growth during metabolic stress (Hussain et al., 2021).

Additional LD regulators include CIDE (cell death-inducing DNA fragmentation factor-like effector) proteins, particularly CIDEC/Fsp27 (fat-specific protein 27), mediate LD-LD fusion and lipid transfer (Xu et al., 2016; Gao et al., 2017). DFCP1 (Double FYVE domain containing protein 1), traditionally associated with autophagy initiation, has recently been implicated in LD degradation through lipophagy pathways (Li et al., 2019).

Together, these LD-associated proteins orchestrate the biogenesis, expansion, degradation, and metabolic integration of LDs. This allows cells to dynamically manage lipid storage and utilisation in response to metabolic needs. Based on these conserved proteins, homology searches were performed to identify putative LD-associated proteins in *Plasmodium falciparum*. Additionally, published stage-specific transcriptomic data were accessed to prioritise candidate proteins potentially involved in lipid droplet dynamics during different life cycle stages. The aims of this analysis were to:

1. Identify potential LD-associated proteins in *P. falciparum* through homology searches using known LD-associated proteins from other organisms, performed with BLASTP (https://blast.ncbi.nlm.nih.gov/).
2. Access transcriptomic data from PlasmoDB (https://plasmodb.org/plasmo/app/) to assess whether candidate proteins exhibit stage-specific expression, distinguishing those associated with asexual stages from those associated with sexual stages.

By compiling findings from lipidomic studies, comparative protein homology, and stage-specific transcriptomic profiles, this chapter proposes a list of potential LD-associated proteins in *P. falciparum*. These predictions provide preliminary insights into stage-specific neutral lipid storage strategies and lay the groundwork for future investigations into the mechanisms of lipid metabolism in malaria parasites.

Results

Identification of potential LD marker proteins in P. falciparum

To guide homology searches in *P. falciparum*, representative LD-associated proteins from mammalian systems were selected and performed a sequence similarity search. Protein sequences were obtained from UniProt (https://www.uniprot.org/), a comprehensive database of curated protein sequence and functional annotations. Homology searches were conducted using BLASTP (https://blast.ncbi.nlm.nih.gov/), comparing each reference sequence to the *P. falciparum* genome. In BLASTP, the expectation value (E value) is a statistical measure that quantifies the likelihood of obtaining a match by change (Pearson, 2013). A lower E value indicates a more significant, non-random match and thus values indicate a higher probability of true homology rather than random alignment. The E value was used to evaluate the significance of each match. For this study, only proteins with E-values below $1e^{-8}$ were considered significant homologs; all others were excluded from further investigation. These candidates were then organised into two functional categories based on established roles in LD biology: (1) cargo synthesis enzymes, and (2) biogenesis and dynamics regulators of proteins. In addition, I included *P. falciparum* proteins which are not classical LD proteins in mammals but with experimental evidence supporting roles in LD biology. The full list of candidates is summarised in **Table 4.1**.

- ***Proteins involved in LD cargo synthesis***

Homologs of enzymes involved in acyl-CoA dependent TAG / CE synthesis were identified though sequence similarity searches. These include PfDGAT (PF3D7_0322300) and PfACAT (PF3D7_1450900), which are predicted to catalyse the final steps of TAG and CE synthesis, respectively. Additionally, a homolog of LCAT, PfPL (PF3D7_0629300), was also identified.

Unlike ACAT, LCAT mediates cholesterol esterification using phospholipids as acyl donors. These enzymes likely contribute to the formation of the hydrophobic neutral lipid core of LDs and represent potential regulators of lipid storage in the parasite.

In addition, PfABCG2 (PF3D7_1426500), a member of the ATP-binding cassette (ABC) transporter of the G-subfamily, shares sequence similarity with human ABCG1 and ABCG2. PfABCG2 that has been studied for its involvement in neutral lipid storage in female gametocyte. Tran et al. (2014) demonstrated that PfABCG2 localises to neutral lipid-enriched foci in female gametocytes and that disruption of PfABCG2 leads to reduced neutral lipids level, indicating a potential role in lipid accumulation or regulation, possibly at a female-specific lipid storage site.

- ***Protein candidates potentially involved in LD biogenesis and development/dynamics***

No homologs were found for several core LD biogenesis and regulatory proteins that are well characterised in other eukaryotes (grey coloured entries in **Table 1**). However, several *P. falciparum* proteins were identified with homology to regulators of LD-organelle interactions and membrane dynamics, such as small GTPases Rab proteins, Arf1 (PF3D7_1020900), and 14-3-3 proteins (PF3D7_0818200). In mammalian cells, these proteins have been implicated in modulating LD formation, trafficking, and association with the ER. Their identification in *P. falciparum* suggests that although classical LD biogenesis pathways may be absent, the parasite may utilise alternative or simplified mechanisms to regulate LD development and dynamics.

- ***Non-classical LD-associated proteins in* P. falciparum**

In addition to homologs of mammalian LD proteins, *Plasmodium* expresses several proteins that have no known homologs in mammals but have been experimentally shown to play roles

in neutral lipid metabolism and may contribute to LD dynamics in *P. falciparum* (Asad et al., 2021; Sheokand et al., 2023). Two putative lysophospholipase have been implicated in neutral lipid metabolism. These proteins show no sequence similarity to mammalian proteins but are conserved across apicomplexans.

PfLPL1 (PF3D7_1476700) has been functionally characterised as lysophospholipase involved in neutral lipid generation during the asexual blood stage. Asad et al. (2021) demonstrated that PfLPL1 plays a critical role in hemozoin formation within the DV by supplying TAGs from phospholipid catabolism. Notably, PfLPL1 co-localise with LDs during the ABS and its disruption of results in impaired TAG accumulation and parasite growth (Asad et al., 2021).

PfLPL3 (PF3D7_1476800), another lysophospholipase homolog, also has been implicated in LD biogenesis. Shoekand et al. (2023) demonstrated that PfLPL3 plays a role in host lipid scavenging and re-esterification during asexual blood stage. Disruption of PfLPL3 was shown to decrease intracellular levels of TAG and DAG while simultaneously increasing free fatty acids (Sheokand et al., 2023). Although PfLPL3 localises to the PVM and tubulovesicular membrane (TVM) rather than LDs in asexual stage, these changes in lipid composition suggest a possible indirect role in LD biogenesis or lipid supply for LD formation.

Expression profile of candidate proteins in asexual and sexual stages

To assess stage-specific expression of candidate proteins potentially involved in LD dynamics, I examined publicly available transcriptomic data from PlasmoDB. These include: (1) illumine-based sequencing of seven sexual and asexual life stages (ring, early trophozoite, late trophozoite, schizont, gametocyte II, gametocyte V, and ookinete) from *P. falciparum* 3D7

mRNA (López-Barragán et al., 2011), (2) strand specific RNA-seq of four *P. falciparum* 3D7 life cycle stages: late trophozoite, schizont, gametocyte II and gametocyte V (López-Barragán et al., 2011), and (3) directional RNA-seq comparing male and female gametocyte transcriptomes from *P. falciparum* NF54 (Lasonder et al., 2016).

Neutral lipid synthesis enzymes such as PfDGAT and PfACAT were found to be highly expressed in mature asexual stages (late trophozoite and schizont stages) based on both the four and seven stage RNA-seq data (López-Barragán et al., 2011). Within the gametocyte-specific transcriptome, PfDGAT expression was enriched in male gametocytes, while PfACAT and PfPL showed higher transcript levels in female gametocytes (Lasonder et al., 2016).

Among the candidate LD-associated proteins, PfLPL1 and PfABCG2 were highly expressed in stage V gametocytes across 4 or 7 different life cycle stage datasets (López-Barragán et al., 2011) and were further enriched in female gametocytes in sex-specific transcriptome (Lasonder et al., 2016). In contrast, PfLPL3 showed peak expression in late trophozoite (4 different life cycle stage dataset) and stage II gametocytes (7 different life cycle stage dataset) and showed relatively higher expression in male gametocytes (López-Barragán et al., 2011; Lasonder et al., 2016).

Table 1. List of potential LD-associated proteins in *P. falciparum*, their potential functions, and stage-specific expression. List of proteins with sequence similarity to known LD-associated proteins in humans, along with their *P. falciparum* homologs (PlasmoDB ID), any functional characterisation available, and their expression profiles across different life cycle stages based on three transcriptome datasets (7-stage, 4stage, and gametocyte-specific RNA-seq). Functional annotations are based on published studies where available. Grey = no homologous protein found in *Plasmodium falciparum* (no significant sequence similarity). Transcriptomic expression patterns are colour-coded for visual clarity: Green = highly expressed in asexual stages; Yellow = highly expressed in gametocytes (unspecified sex); Blue = enriched in male gametocytes; Pink = enriched in female gametocytes.

Protein in Human	**Function in Human**	**Homology (PlasmoDB ID)**	**Functional studies in *P. falciparum***	**Transcriptome in 7 cycle**	**Transcriptome in 4 cycle**	**Transcriptome in gametocytes**
DGAT2	Synthesis TAG	No significant similarity found				
DGAT1	Synthesis TAG	PfDGAT (PF3D7_0322300) E value = $8e^{-46}$	Essential for intraerythrocytic proliferation. (Palacpac et al., 2004b)	Enriched in late trophozoite, gametocyte V	Enriched in Late trophozoite, Schizont	Enriched in Male
ACAT1	Synthesis CE	PfDGAT (PF3D7_0322300) E value = $1e^{-53}$				
ACAT2	Synthesis CE	PfACAT (PF3D7_1450900) E value = $8e^{-36}$	No functional studies found in *P. falciparum*	Enriched in Ring, Late trophozoite, Gametocyte V	Enriched in Late trophozoite	Enriched in Female

LCAT	Synthesis CE	PfPL (PF3D7_0629300) E value = $1e^{-21}$	Requires to facilitate efficient egress in asexual stages. (Ramaprasad et al., 2023)	Low through all	Low through all	Enriched in Female
Seipin	Promoting LD growth	No significant similarity found				
Arf1	Regulate LDs' surface composition	PfArf1 (PF3D7_1020900) E value = $3e^{-104}$	Localises adjacent to the ER and involves in export of non-PEXEL protein PfAK2 from the ER. (Taku et al., 2020)	Enriched in Ookinete, Schizont, Late trophozoite	Enriched in Late trophozoite	Enriched in Female
FIT	Assist LD budding	No significant similarity found				
PLIN	Regulate lipids storage and mobilisation of LD	No significant similarity found				
CIDE	Promote LD-LD fusion	No significant similarity found				
Rabs	Regulating LD dynamics (formation, mobilisation, fusion, vesicle budding) through	PfRab1A (PF3D7_0513800) E value = $5e^{-95}$	Localises to the rhoptries in schizonts and may involve in the trafficking of rhoptry proteins. (Morse et al., 2016)	Enriched in Gametocyte V	Enriched in Late trophozoite	Enriched in Female
		PfRab1B (PF3D7_0512600)	Localises near the ER and is involved in the trafficking of	Enriched in Gametocyte V	Enriched in Late trophozoite	Enriched in Female

	membrane trafficking	E value = $4e^{-93}$	the PEXEL-positive export protein Rifin. (Taku et al., 2020)			
		PfRab2 (PF3D7_1231100) E value = $1e^{-105}$	No functional studies found in *P. falciparum*.	Enriched in Ookinete	Enriched in Late trophozoite	Enriched in Male
		PfRab5B (PF3D7_1310600) E value = $7e^{-75}$	Essential for asexual blood stage development and is involved in the trafficking of proteins. (Ezougou et al., 2014; Ebine et al., 2016)	Enriched in Ookinete	Enriched in Schizont	Enriched in Male
		PfRab5C (PF3D7_0106800) E value = $7e^{-75}$	No functional study in *P. falciparum*.	Enriched in Gametocyte V, Ookinete	Enriched in Late trophozoite	Enriched in Female
		PfRab6 (PF3D7_1144900) E value = $6e^{-91}$	Associates with the nucleus of a forming daughter parasite. (de Castro et al., 1996)	Enriched in Ookinete	Enriched in Late trophozoite	Not much difference
		PfRab7 (PF3D7_0903200) E value = $3e^{-96}$	Involves in the parasite's retromer complex assembly near the digestive vacuole. (Siddiqui et al., 2020)	Enriched in Late trophozoite	Enriched in Late trophozoite	Enriched in Male

		PfRab18 (PF3D7_0807300) E value = $6e^{-62}$	No functional studies found in *P. falciparum*	Enriched in Ring, Gametocyte II	Enriched in Late trophozoite	Enriched in Male
		PfRab11A (PF3D7_1320600) E value = $5e^{-98}$	Plays a critical role in vesicular trafficking, particularly during the late stages of parasite development. Associates with rhoptries in late-stage schizonts. (Agop-Nersesian et al., 2009)	Enriched in Gametocyte V	Enriched in Late trophozoite	Not much difference
		PfRab11B (PF3D7_1340700) E value = $3e^{-96}$	No functional studies found in *P. falciparum*	Enriched in Gametocyte V	Enriched in Late trophozoite, Gametocyte II	Not much difference
14-3-3	Modulate lypolysis	Pf14-3-3 (PF3D7_0818200) E value = $2e^{-108}$	No functional studies found in *P. falciparum*	Enriched in Late trophozoite	Enriched in Late trophozoite	Enriched in Male
DFCP1 (FYVE)	Promoting LD degradation	PfDFCP (PF3D7_1460100) E value = $8e^{-13}$	No functional studies found in *P. falciparum*	Enriched in Ookinete, Gametocyte V	Enriched in Gametocyte II	Enriched in Female
Lysophosp holipase	Membrane remodelling by	PfLPL1 (PF3D7_1476700)	Localises to a neutral lipid enriched spot (LDs) during asexual blood stage.	Enriched in Gametocyte V	Enriched in Gametocyte V	Enriched in Female

	hydrolysing lysophospholipids	No significant similarity found	Contributes to TAG synthesis required for hemozoin formation within DV and essential for parasite survival during asexual stage. (Asad et al., 2021)			
Lysophospholipase	Membrane remodelling by hydrolysing lysophospholipids	PfLPL3 (PF3D7_1476800) No significant similarity found	Localises to PVM and TVM. Disruption of PfLPL3 results in reduced TAG and DAG levels while increased FAs. (Sheokand et al., 2023)	Enriched in Gametocyte V, Ookinete	Enriched in Late trophozoite	Enriched in Male
ABC transporter of the G-subfamily	Mediate sterol transport (ABCG1) and eliminate toxic substances from the organisms (ABCG2)	PfABCG2 (PF3D7_1426500) E value = $5e^{-57}$	Localises to a neutral lipid enriched spot in female gametocytes. Disruption of PfABCG2 results in reduced levels of neutral lipids. (Tran et al., 2014)	Enriched in Gametocyte V	Enriched in Gametocyte V	Enriched in Female

Discussion

In this chapter, I aimed to identify potential LD-associated proteins in *P. falciparum* by conducting sequence homology searches against well-characterised LD proteins in human. Given the minimal understanding of LD biology in *Plasmodium*, this approach provided a foundational dataset that can guide future experimental studies. Combined with stage-specific transcriptomic analysis, the findings presented here offer insights into how *P. falciparum* might regulate neutral lipid storage in a developmental and sex-specific manner.

Proteins involved in LD cargo synthesis

Three candidate enzymes involved in LD cargo synthesis were identified: PfDGAT, PfACAT, and PfPL.

PfDGAT (PF3D7_0322300) represents the sole member of the DGAT family in *P. falciparum* and exhibits strong homology to human DGAT1 and ACAT1, with no detectable similarity to the human DGAT2. Since DGAT1 is phylogenetically related to ACAT family members while DGAT2 has similarities with MGAT (Turchetto-Zolet et al., 2011), PfDGAT appears closer to DGAT1 and ACAT1. PfDGAT is therefore the most likely enzyme responsible for catalysing the terminal step in TAG synthesis and may also contribute to CE production.

Transcriptomic data show PfDGAT is weakly transcribed in ring stages and becomes strongly upregulated at late trophozoite stage (López-Barragán et al., 2011), closely mirroring the stage-specific accumulation of TAG and LD biogenesis (Palacpac et al., 2004a; Vielemeyer et al., 2004; Gulati et al., 2015; Lee et al., 2024). The inability to genetically disrupt PfDGAT further indicates its essential role in the parasite proliferation during the asexual stage (Palacpac et al., 2004a; Vielemeyer et al., 2004; Lee et al., 2024). These observations strongly suggest that

PfDGAT is a major contributor to TAG synthesis and LD formation in asexual stages. Genetically tagging PfDGAT and determining its subcellular localisation would be a valuable next step to validate its involvement in LD biology. This approach could also make it possible to isolate LDs and carry out proteomic analysis to determine their molecular composition.

Although CEs represent only 0-1% of total neutral lipids during asexual stages, substantial CE accumulation is observed during gametocytogenesis - particularly in female gametocytes, where CEs account for up to 86% of total neutral lipids compared to 52% in male gametocytes (Tran et al., 2016; Ridgway et al., 2022). This pattern suggests that CE synthesis is regulated in stage-specific manner, with the related enzymatic activity likely elevated in female gametocytes. Notably, both putative CE synthesis enzymes, PfPL and PfACAT, show relatively high transcript levels in female gametocytes (López-Barragán et al., 2011; Lasonder et al., 2016).

PfPL shares homology with human LCAT and plant PDAT1, with greater similarity to LCAT based on sequence and phylogenetic analyses (Nawabi et al., 2003). In mammals, LCAT catalyses CE formation by transferring a fatty acid from phosphatidylcholine to cholesterol and plays a key role in cholesterol homeostasis and lipoprotein maturation. For example, LCAT is responsible for up to 70% of CE production in human plasma (Yamamuro et al., 2020). In *P. falciparum*, PfPL transcript levels are generally low across most intraerythrocytic stages (López-Barragán et al., 2011), but show enriched expression in female gametocytes compare to males (Lasonder et al., 2016), aligning with the marked CE accumulation at this stage (Tran et al., 2016; Ridgway et al., 2022).

Although the role of PfPL in CE synthesis has not been directly validated, it has been implicated in parasite egress during asexual stages (Ramaprasad et al., 2023). Ramaprasad et al. (2023) showed that PfPL-null parasites exhibit altered lipid profiles, including increased levels of phospholipids such as phosphatidylserine and acylphosphatidylglycerol upon egress.

These changes may reflect a compensatory response to regulate cholesterol levels in the membrane. Given that cholesterol is required for successful egress (Maier and van Ooij, 2022), these observations suggest a potential role for PfPL in regulating cholesterol homeostasis in the parasite.

PfACAT (PF3D7_1450900) shows sequence similarity to human ACAT2 and is broadly expressed across ring, late trophozoite, and mature gametocyte stages, with particularly high expression in female gametocytes (López-Barragán et al., 2011; Lasonder et al., 2016). The functional relevance of ACAT activity in *P. falciparum* has been explored using known ACAT inhibitors. Sandoz 58-035, a selective inhibitor of ACAT1 (Ross et al., 1984; Veldhuis et al., 1985; To et al., 2024), and Glibenclamide, an anti-diabetic drug that inhibit both ACAT1 and ACAT2 (Ohgami et al., 2000), were tested for their effects on parasite growth. In asexual stages, Sandoz 58-035 has no significant impact on parasite growth (Nawabi et al., 2003; Vielemeyer et al., 2004), consistent with lipidomic data showing very low CE abundance during these stags. Surprisingly, both Sandoz 58-035 and Glibenclamide also failed to affect female gametocyte viability, despite the notable accumulation of CE in this stage (Ridgway et al., 2022). This may indicate that gametocytes preferentially synthesise CE via an LCAT-like enzymatic pathway (potentially mediated by PfPL) rather than relying on PfACAT. Alternatively, CE storage may not be essential for gametocyte maturation but could play a critical role following transmission.

Taken together, these findings highlight PfDGAT as a strong candidate for studying LD biology during asexual stages, whereas PfPL appears to be the most promising candidate for investigating CE enrichment in female gametocytes.

Protein candidates potentially involved in LD biogenesis and development/dynamics

It is notable that no homologs were found for a core LD biogenesis regulator that are known to be essential for LD nucleation, growth, and fusion in mammalian cells (grey coloured entries in **Table 1**). The absence of these conserved proteins suggests that *P. falciparum* may employ minimal or alternative mechanisms for LD formation, which could involve novel combinations of known trafficking proteins, or alternatively, parasite-specific strategies involving proteins with no clear homologs in other organisms.

Nonetheless, homologs of proteins potentially involved in LD-organelle interactions were identified, including Rab proteins, Arf1, and 14-3-3 proteins (**Table 1**).

In mammalian systems, some of Rab proteins have been reported to be functionally linked with LDs (Martin et al., 2005; Ozeki et al., 2005; Li and Yu, 2016). Rab1 localises on LDs and may acts as molecular switch priming LDs for fusion with the ER (Bersuker et al., 2018; Song et al., 2022). Rab5 localises to LD surfaces and facilitates endosome-LD tethering, potentially linking LDs to early endosomal and / or multivesicular body compartments (Liu et al., 2007). Rab7 drives LD degradation via lipophagy by targeting LDs to lysosomes and autophagosomes (Schroeder et al., 2015). Rab8a assemble with PLIN5 to transfer lipids from LDs into mitochondria for β-oxidation (Ouyang et al., 2023). Rab18 localises to the surface of LDs and mediates their close association with the ER (Martin et al., 2005; Ozeki et al., 2005).

The *P. falciparum* family of Rabs is estimated to comprise 11 genes - PfRab1a, PfRab1b, PfRab2, PfRab5a, PfRab5b, PfRab5c, PfRab6, PfRab7, PfRab11a, PfRab11b, PfRab17 – 10 of which are expressed in infected erythrocytes (Quevillon et al., 2003). Among these, PfRab1 and PfArf1 co-localise with PfRab5b near the ER and are involved in cargo transport and cargo selection during the asexual blood stage (Taku et al., 2020). PfRab5b localises to a compartment close to the ER and plays an essential role in parasite growth and replication during asexual blood stage (Ezougou et al., 2014; Ebine et al., 2016). Although no functional

studies of PfRab5c have been reported in *P. falciparum,* study in *P. berghei* suggest that PbRab5c appears to have a non-overlapping role with PbRab5b as PbRab5c could not compensate for the loss of PbRab5b function (Ezougou et al., 2014). In contrast to mammalian Rab5, which regulates early endosomal trafficking (Bucci et al., 1992), Rab5b in apicomplexan parasites has evolved to mediate protein trafficking to the PVM, suggesting divergence towards parasite-specific secretory pathway (Ebine et al., 2011; Ebine et al., 2012; Kremer et al., 2013).

While the previous studies show the functions of several PfRabs in vesicular trafficking pathways within the parasite and to the host cell (like ER-Golgi transport, endosomal pathways, trafficking to the PVM/TVN and food vacuole), they do not explicitly state that any identified *P. falciparum* Rab protein is directly located on LDs in the parasite (Ward et al., 1997).

Evidence from mammalian studies indicates that Arf1, Rab, and 14-3-3 proteins localise to or are strongly associated with LD-ER contact sites, where they contribute to lipid exchange, LD maturation, and inter-organelle communication (Martin et al., 2005; Ozeki et al., 2005; Wilfling et al., 2014; Bersuker et al., 2018; Song et al., 2022; Yang et al., 2023). In *P. falciparum*, homologs of these proteins - PfArf1, PfRabs, and Pf14-3-3 – were identified in this study as putative LD-associated proteins. The identification of homologs in *P. falciparum* to LD-tethering proteins in other organisms suggests the possibility that similar LD-organelle contact mechanisms may exist in the parasite. Given the conserved functional roles of their orthologs in other organisms, it is plausible that these *P. falciparum* protein*s* also act at ER-LD contact sties. Also, I observed consistent strong association between LD and various organelles through asexual stage in Chapter 3. However, to date, none of these homologous proteins have been experimentally validated for direct LD-association in *Plasmodium,* and their functional roles in LD biology remain speculative.

Interestingly, PfArf1, five Rab proteins (PfRab1b, PfRab6, PfRab7, PfRab11a, and PfRab18), and Pf14-3-3 proteins were also previously detected as DRM proteins in late trophozoite / early schizont-infected RBCs (Yam et al., 2013).

DRM fractions are biochemically isolated membrane domains that remain insoluble in non-ionic detergents at low temperatures and are commonly used as biochemical proxies for lipid rafts**.** Lipid rafts are typically defined as dynamic microdomains within cellular membranes that are enriched in saturated phospholipids, sphingolipids, cholesterol, and certain types of proteins include GPI-anchored and transmembrane proteins (Denny et al., 2001; Saha et al., 2016). These raft-like domains thought to support membrane sorting, trafficking, and cell signalling (Sezgin et al., 2017; Ouweneel et al., 2020). In the ER, such raft like microdomains have been proposed to provide favourable environments for selective recruitment of LD regulatory proteins (van Meer, 2001). Several raft-associated proteins, such as caveolins and flotillins, have been implicated in regulating LD formation and trafficking in other eukaryotes (Cohen et al., 2004; Rajendran et al., 2007; Patel and Insel, 2008).

Although *P. falciparum* lacks caveolins and flotillins, the localisation of potential LD-associated candidate proteins to DRM fractions in *P. falciparum* raises the possibility that LD formation in the parasite may occur at or near lipid raft-like ER subdomains.

Together, these observations suggest that PfRabs, PfArf1, and Pf14-3-3 are plausible candidates for contributing LD biogenesis or related trafficking processes in P. falciaprum. However, their precise roles remain unclear, and they may not function as constitutive LD regulators. Further experimental validation is required to establish whether these proteisn act directly at LDs or influence LD biology indirectly through broader membrane trafficking pathways.

Promising candidate proteins for sexual stage-specific LD markers

LDs are dynamic organelles whose size, composition, and function are tightly linked to metabolic demands of the cell. In *P. falciparum*, the metabolic requirements differ markedly between asexual and sexual stages. Identifying stage-specific LD marker proteins is therefore key to understand how the parasite regulates lipid storage and utilisation across different development stages.

Transcriptomic patterns support the notion that *P. falciparum* regulates neutral lipid metabolism and LD dynamics in a stage and sex-specific manner. The high expression of PfACAT and PfPL in female gametocytes aligns with the observed enrichment of CE at this stage, suggesting a tailored mechanism for CE storage. Additionally, female-enriched expression of PfABCG2 and PfLPL1 supports their potential involvement in the formation or maintenance of a female-specific LD. In contrast, male-enriched expression of PfDGAT and PfLPL3 implies that different lipid metabolic pathways may be active in male gametocytes, potentially supporting different metabolic or structural needs.

To date, conventional LD structures have not been clearly observed in *P. falciparum* gametocytes in microscopy studies. However, previous lipidomic studies have shown that female gametocytes contain neutral lipids enriched in CE, while asexual stages are enriched in TAG (Ridgeway et al., 2022). These observations suggest that the LD structures in gametocytes may differ from the LDs observed during asexual stages, as characterised in Chapter 3. This discrepancy underscores the need for advanced imaging, lipid tracking, and functional validation to further characterise these structures in sexual stages.

This systemic search in this chapter identified several putative LD-associated proteins with elevated expression in particular life cycle stage, some of which may serve as valuable markers for LD biology in *P. falciparum*.

PfDGAT, the sole DGAT homolog, is upregulated during asexual development and appears essential for TAG synthesis and LD formation (Palacpac et al., 2004a; Vielemeyer et al., 2004) making it a strong candidate for studying LD biology in asexual stages. PfLPL1 has been shown to localise to LDs during asexual stages (Asad et al., 2021) and is also highly enriched in female gametocytes, providing a versatile marker that could be used for studying LDs in both asexual and female gametocyte stages. PfPL, a putative LCAT-like enzyme, is a promising candidate for studying CE synthesis and CE-enriched lipid storage in gametocytes. Finally, PfABCG2, already validated to localise to neutral lipid–rich spot in female gametocytes (Tran et al., 2014), positioning it as a particularly attractive marker for exploring female-specific LD biology.

Taken together, these findings point to PfDGAT as the strongest candidate for studying LD biology in asexual stages, PfLPL1 as a bridge between asexual and sexual stages, and PfPL and PfABCG2 as promising candidates for investigating CE enrichment and lipid storage in female gametocytes (**Table 2**). While transcriptomic and homology-based data provide a valuable starting point, further experimental validation will be essential to confirm their functional roles. These candidates open new avenues for exploring stage-specific lipid storage strategies in *P. falciparum*.

In particular, PfABCG2 will be further explored as a potential female gametocyte-specific LD marker in Chapter 5, helping to clarify the biological role and identity of lipid storage structures in female gametocytes.

Table 2. Candidate proteins for LD analysis in *P. falciparum*. This table summarises the most promising proteins for investigating LD biology in *P. falciparum*, based on sequence homology, transcriptomic expression, and available experimental evidence. Gene essentiality is indicated as the mutagenesis index score (MIS; phenotype), based on PiggyBac phenotypic data from PlasmoDB (https://plasmodb.org/). MIS values close to 0 indicate essential genes, whereas values close to 1 indicate dispensable genes.

PlasmoDB ID	Functional category	Stage	Notes	MIS (phenotype)
PfDGAT (PF3D7_0322300)	LD cargo synthesis (neutral lipid enzymes)	Asexual stage	Predicted role in TAG synthesis and LD cargo accumulation	0.199
PfLPL1 (PF3D7_1476700)	LD biogenesis and dynamics (lipid remodelling)	Asexual stage / Female gametocytes	Predicted role in shaping LD monolayer curvature and TAG accumulation	0.999
PfPL (PF3D7_0629300)	LD cargo synthesis (neutral lipid enzymes)	Female gametocytes	Predicted role in cholesterol esterification using phospholipids, contributing to CE enrichment	0.425
PfABCG2 (PF3D7_1426500)	LD trafficking	Female gametocytes	Predicted role in neutral lipid transport and storage	1

Chapter 5. Neutral lipid storage and dynamics in *P. falciparum* female gametocyte

Introduction

Malaria transmission between human and mosquitoes depends on gametocytes, the sexual stages of *P. falciparum*, which are taken up by mosquitoes during a blood meal and develop into infectious forms in mosquito midgut. Mosquitos lack desaturase enzymes and are also incapable of *de novo* cholesterol synthesis (Clayton, 1964; Turunen, 1979). As a result, once inside the mosquito, the parasite encounters limited access to essential lipids such as cholesterol. Unlike asexual blood stages, which complete a 48-hour replication cycle, gametocytes spend 10–12 days maturing inside the erythrocyte. During this extended growth phase, they must not only sustain their slow development but also stockpile lipids in preparation for the nutrient-poor conditions of the mosquito midgut. While the direct role of neutral lipids (NLs) in transmission remains to be clarified, studying their dynamics during gametocytogenesis provides valuable insight into how the parasite allocates resources in anticipation of this transition.

A previous study has shown that the lipid composition of parasite-infected RBCs significantly alters during the sexual development of *P. falciparum* (Tran et al., 2016). NLs are the main contributor to the substantial increase in overall lipids upon parasite infection and gametocyte maturation. Compared to uninfected RBCs, the proportion of NLs compared to total lipids increases from 3% in uRBCs to 18% in trophozoite-infected RBCs and to 27% in mature gametocyte-infected RBCs (Tran et al., 2016). Among the three major NLs (TAG, DAG, CE), CE and DAG dominate the NLs profile of gametocytes while DAG and TAG are the predominant NLs in asexual stages (Tran et al., 2016). Additionally, NLs accumulation is sex specific, with female gametocyte accumulating significantly more CE than male gametocytes (Ridgway et al., 2022). This distinction in lipid profiles reflects the differing biological roles of female gametocytes. This sex-specific lipid profile likely reflects the differing biological

roles of male and female gametocytes. Female gametes contribute virtually all cellular material to the newly formed zygote and, subsequently, the ookinete in the mosquito host, whereas the male gamete contributes primarily genetic material (Dash et al., 2022). As a result, the lipids present in the fertilised zygote are exclusively derived from the female gametocyte. In particular, the marked enrichment of CE in females may support the formation of specialised lipid storage compartments tailored to their function. Despite these clear differences, the morphology and precise role of neutral lipid storage in female gametocytes remain poorly understood.

Lipid synthesis in gametocytes likely follows a general eukaryotic framework (**Figure 8**). FAs, either scavenged or synthesised *de novo*, are activated to acyl-CoA by ACS, which are essential for downstream lipid synthesis. *De novo* synthesis of DAG begins with glucose and proceeds through the sequential acylation of G3P to LPA, PA a, and finally DAG (grey box, **Figure 25**). DAG functions as a key intermediate in lipid metabolism, serving as a substrate for both TAG synthesis via PfDGAT and phospholipid biosynthesis.

Cholesterol is scavenged from the external environment, possibly via the parasite transporter PfNCR1, as *P. falciparum* lacks the enzymes for *de novo* cholesterol synthesis (Istvan et al., 2019). Cholesterol is converted to its storage form of CE via two routes. The acyl-CoA–dependent esterification of cholesterol is catalysed by PfACAT (PF3D7_1450900), while an alternative, acyl-CoA independent route may involve PfPL (PF3D7_0629300), a putative LCAT-like enzyme that uses phospholipids as acyl donors. Interestingly, despite the significant accumulation of CE in female gametocytes, inhibitions of ACAT did not impair gametocyte viability (Ridgway et al., 2022). This suggests that *P. falciparum* gametocytes may rely more heavily on LCAT-mediated CE synthase, PfPL.

Phospholipid synthesis is required for membrane formation and also LD expansion. Phospholipids such as PC and PE are a primarily synthesised via the Kennedy pathway (yellow box, **Figure 25**). This involves the conversion of choline or ethanolamine to CDP-choline or CDP-ethanolamine, which are then conjugated with DAG to form PC or PE, respectively. Additional phospholipid remodelling is supported by the Land cycle, which enables the dynamic turnover between phospholipids (PL) and lysophospholipids (LPL) (orange box, **Figure 25**).

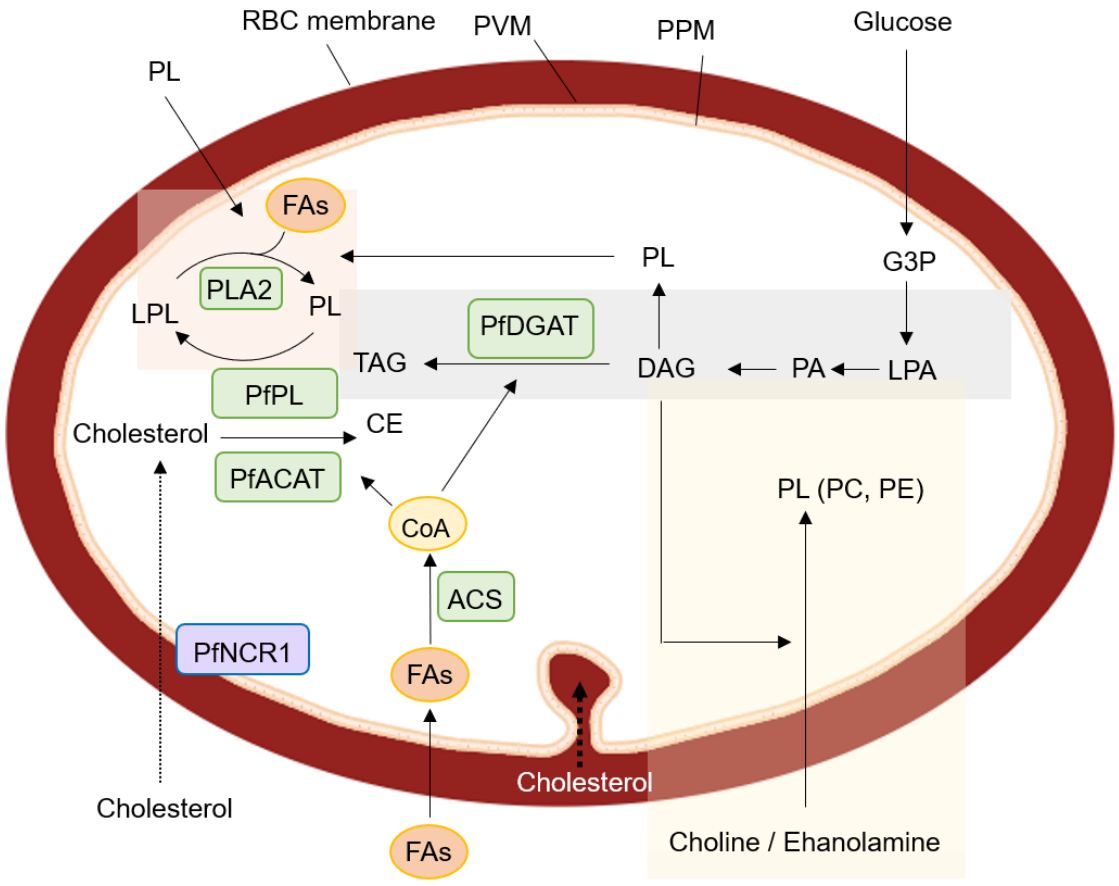

Figure 25. **Proposed lipid synthetic pathways in *P. falciparum* gametocytes**. FAs, obtained through scavenging or PLA_2 mediated PL recycling, are converted into CoA via ACS and channeled into multiple lipid synthetic pathways. TAG synthesis begins with G3P, which is converted to PA and subsequently to DAG (grey box). DAG serves as a key intermediate for TAG synthesis via PfDGAT and for PL synthesis via the Kennedy pathway (yellow box). PLA_2 also supports PL turnover (orange box). Cholesterol, imported PfNCR1, is esterified to CE

either through an acyl-CoA-dependent route (PfACAT) or an acyl-CoA-independent route (PfPL).

ACS, acyl-CoA synthetase; CE, cholesteryl ester; CoA, fatty acyl-CoA; DAG, diacylglycerol; FAs, fatty acids; G3P, glycerol-3-phosphate; LPA, lysophosphatidic acid; LPL, lysophospholipid; PA, phosphatidic acid; PC, phosphatidylcholine; PE, phosphatidylethanolamine; PfACAT, *P. falciparum* acyl-CoA:cholesterol acyltransferase; PfDGAT, *P. falciparum* diacylglycerol acyltransferase; PfNCR1, *P. falciparum* Niemann–Pick C1-related protein; PfPL, *P. falciparum* lecithin:cholesterol acyltransferase-like enzyme; PL, phospholipid; PLA_2, phospholipase A_2; TAG, triacylglycerol.

While these biosynthetic pathways provide the enzymatic framework for NL production in gametocytes, how these NLs are stored in gametocytes remain poorly understood.

In mammalian cells, ABC transporters play a fundamental role in cellular lipid trafficking. Three members of the human G subfamily have been shown to play a significant role in cellular cholesterol biology: ABCG1 mediates cellular cholesterol and other sterol transport (Wang et al., 2013; Skarda et al., 2021); and ABCG5 and ABCG8 restrict intestinal absorption and promote biliary excretion of sterols (Graf et al., 2003; Lee et al., 2016). Unlike these, ABCG2 has been characterised as an important part of self-defense systems in organisms by eliminating potentially toxic substances from the organisms (Nakanishi and Ross, 2012).

In *P. falciparum*, a single ABC transporter of the G subfamily, PfABCG2 (PlasmoDB ID: PF3D7_1426500), has been identified as a strong candidate involved in female-specific NL storage (Tran et al., 2014), with its expression largely restricted to the female gametocyte stage (López-Barragán et al., 2011; Pelle et al., 2015; Lasonder et al., 2016). PfABCG2 shares strong sequence similarity with human ABCG2 and ABCG1 (Edaye and Georges, 2015), and also shows significant homology to the six ABCG members in *Toxoplasma gondii*, which have been suggested as sterol regulators in the parasite (Ehrenman et al., 2010; Edaye and Georges, 2015). Since PfABCG2 gene disruption leads to a reduction in NLs, the molecule with a potential role in NLs storage in female gametocyte has been proposed (Tran et al., 2014). Taken together,

these findings raise the possibility that PfABCG2 may function in NL transport or regulation in *P. falciparum*. Despite these observations, the ultrastructure of the PfABCG2 associated NL-enriched region has not been fully explored. Given that mature *P. falciparum* gametocytes lack classical LDs, PfABCG2 may serve as a marker for a previously unrecognised lipid storage compartment in female gametocytes. This study aims to characterise the PfABCG2 associated morphological structure and provide new insights into how NLs are stored and regulated in female gametocytes.

This chapter aims to:

1) Characterise female specific, NL enriched structure using Nile Red spectral imaging in combination with the female specific marker PfABCG2.
2) Identify the ultrastructure of the PfABCG2 associated NL enriched spot (referred to here as the female lipid body, femLB) by using correlative light and electron microscopy (CLEM)
3) Define ultrastructure and subcellular localisation of the femLB through 3D volume imaging.
4) Assess the impact of lipid metabolic inhibitors on neutral lipid storage and PfABCG2-associated femLBs in PfABCG2-GFP and ΔPfABCG2 gametocytes, in order to evaluate the functional significance of this compartment during gametocyte maturation.
5) Explore a possible connection between the femLB and lipid raft using detergent resistant membrane (DRM) isolation and western blot analysis.

Together, these approaches provide a comprehensive characterisation of the femLB and offer insights into its potential role.

Results

Female gametocytes contain an additional NL enriched structure

To investigate the distribution of NLs in gametocytes, I stained gametocytes with the neutral lipid dye (Nile Red) and analysed spectral shift using a radiometric imaging approach as described in Chapter 3. In asexual stage, LDs appear as distinct, very low polarity structures which indicates high NL content (Lee et al., 2024). In contrast, gametocytes did not exhibit discrete LDs detectable by this method. Instead, both male and female gametocytes displayed various lipid-rich structures, each containing comparable levels of NLs and phospholipids.

Using a PfABCG2-GFP expressing cell line (Tran et al., 2014), clear differences between male and female gametocytes were observable, with females displaying a distinct GFP-positive structure absent in males. Nile red staining revealed clear differences in lipid distribution between male and female, although both showed relatively high NL content throughout the parasite membrane (**Figure 26**). In male gametocytes, NLs were primarily concentrated within the DV that contains hemozoin crystals. On the other hand, female gametocytes exhibited several membrane-like structures contains high NLs compare to rest of the parasite's cytoplasm (depicted in yellow, **Figure 26**). Among these, the most notable was a spot located near one end of the parasite (white arrows, **Figure 26**). This region showed the lowest polarity within the parasite's cytoplasm on the ratio map (indicated in green to sky blue in ratio image, **Figure 26**), and it co-localised with the PfABCG2-GFP signal. Given that lipidomic analyses have shown greater CE enrichment in female compared to male gametocytes (Tran et al., 2016; Ridgway et al., 2022), this PfABCG2 associated NL-enriched structure drew my attention as a strong candidate for a female-specific lipid storage organelle. Throughout this chapter, I refer to this structure as the female lipid body (femLB).

In WT gametocytes, multiple Nile Red stained regions were observed with relatively low polarity which indicates NL enrichment. Among these, one region consistently localised near one end of the parasite exhibited relatively high NL as appeared sky blue in the ratio map which indicate a low polarity domain (white arrowheads, **Figure 27**). This result shows a similar pattern to the femLB spot observed in PfABCG2-GFP expressing female gametocytes (**Figure 26**).

To address the possibility that the strong NL signal observed in PfABCG2-GFP expressing cell line may arise from fluorescence bleed though from the GFP channel, spectral spillover was assessed (**Figure 10C**). This analysis showed minimal GFP contribution to the non-polar detection channels, indicating that bleed through is unlikely to account for the enhanced NL signal observed in the femLB. Instead, the increased NL signal within the femLB region likely reflects stabilisation of the femLB structure in PfABCG2-GFP expressing gametocytes.

In ΔPfABCG2 gametocytes, one of the most obvious changes from WT gametocytes is the parasite membrane. The ratio map showed a reduce NL signal with most of the parasite membrane displaying blue to light blue colours (**Figure 27**). Most of relatively NL enriched signalss within the parasite were not directly co-localised with the DV but were localised nearby. These regions appeared as sky blue in the ratio map which indicate moderately low polarity (**Figure 27**). Faint spots at one polar end of the parasite were observed in ΔPfABCG2 gametocytes, similar to the region identified in WT gametocytes, but appeared less distinct. These spots appeared predominantly blue with a small patch of sky blue in the ratio map (grey arrows, **Figure 27**), suggesting it may represent a residual femLB structure with lower level of NLs.

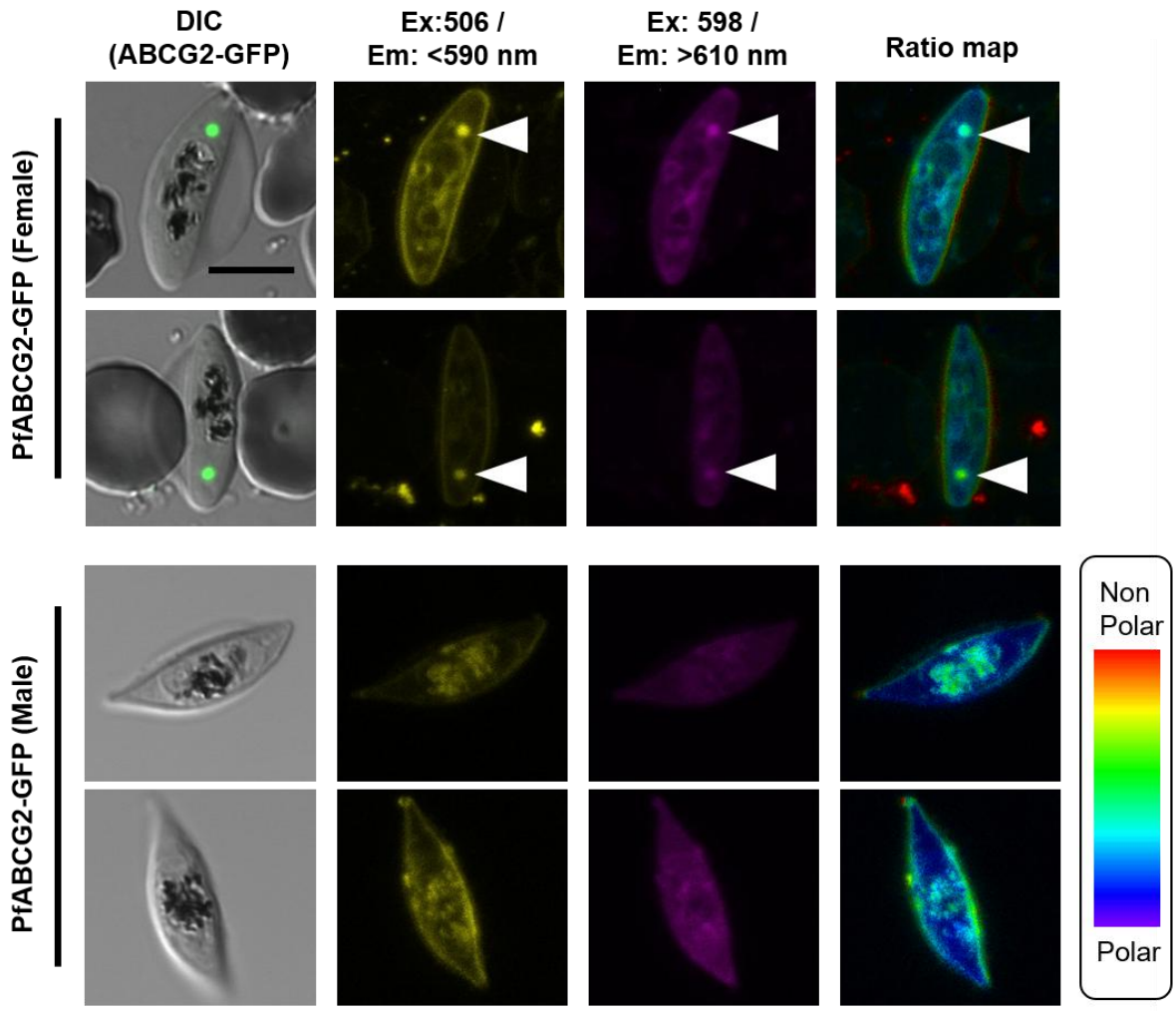

Figure 26. **Differentiating polar and non-polar lipids in Nile Red stained *P. falciparum* female and male gametocytes.** Representative confocal images of Nile red stained mature female and male gametocytes (Stage IV), employing different excitation and emission settings on PfABCG2-GFP expressing cell line. Differential Interference Contrast (DIC) images with GFP merged images are depicted in the first column, non-polar lipid-enriched features are depicted in yellow (excitation: 506 nm/emission: 520-590 nm; second row), polar lipids are depicted in magenta (excitation: 598 nm /emission: 610-75 0nm, third row) and a ratio map is depicted in the far right column. The ratio images, regions closer to the blue end of the spectrum indicate higher polarity, whereas those shifted towards the red end signify lower polarity. All images, except DIC, are maximum intensity projections. White arrowheads: PfABCG2 associated spot (femLB). Scale bar = 5 µm

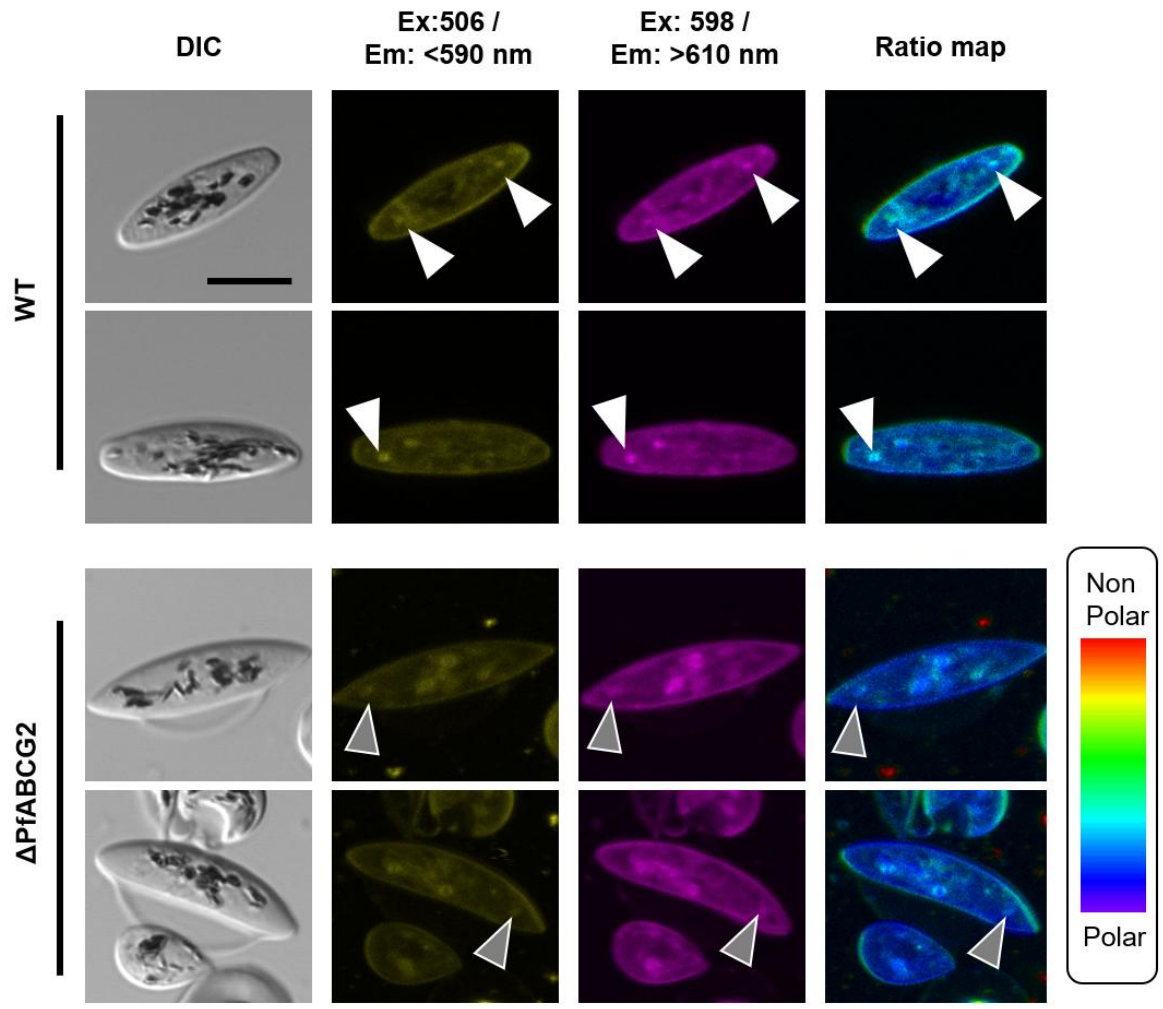

Figure 27. **Differentiating polar and non-polar lipids in Nile Red stained *P. falciparum* gametocytes.** Representative confocal images of Nile red stained mature gametocytes (stage IV), employing different excitation and emission settings on WT and ΔPfABCG2 cell line. Differential Interference Contrast (DIC) images are depicted in the first column, non-polar lipid-enriched features are depicted in yellow (excitation: 506 nm/emission: 520-590 nm; second row), polar lipids are depicted in magenta (excitation: 598 nm /emission: 610-750 nm, third row) and a ratio map is depicted in the far right column. The ratio images, regions closer to the blue end of the spectrum indicate higher polarity, whereas those shifted towards the red end signify lower polarity. All images, except DIC, are maximum intensity projections. White arrowheads: femLB, grey arrowheads: residual femLB. Scale bar = 5 µm

PfABCG2 localises to a distinct membrane compartment

Given that the femLB structure appears relatively more hydrophobic than the surrounding cytosol in both WT and PfABCG2-GFP expressing gametocytes, but is absent in male gametocytes, it likely represents a female specific lipids storage compartment. Correlative light and electron microscopy (CLEM) was performed using the PfABCG2-GFP expressing cell line to identify the cellular structure of the femLB. A total of 95 female gametocytes were selected based on PfABCG2-GFP fluorescence using confocal microscope. Of these, the detailed ultrastructure of the femLB was examined in 20 randomly selected gametocytes. CLEM analysis revealed that PfABCG2 consistently co-localises with a region which has a honeycomb-like arrangement of multi membrane stacks that closely associated with membranes resembling ER morphology (**Figure 28**). TEM analysis showed that the entire structure (honeycomb-like structure with the surrounded ER structure) had an average diameter of 1 µm (standard deviation (SD) = 0.19 µm, n = 20, range: 0.8-1.3 µm), while the densely packed central honeycomb-like structure measured approximately 0.5 µm (SD = 0.11 µm, n = 20, range: 0.3-0.6 µm).

To further investigate the cellular structure of the femLB, PfABCG2-GFP expressing gametocytes were processed using OTO (osmium-thiocarbohydrazide-osmium) method. High resolution section images revealed that although some of femLBs appeared as vesicle-like, most were tightly interconnected, forming a honeycomb-like arrangement (**Figure 29**). The femLB region exhibited slightly higher electron density than the surrounding membranes resembling ER morphology, suggesting a higher unsaturated lipids content (**Figure 29**).

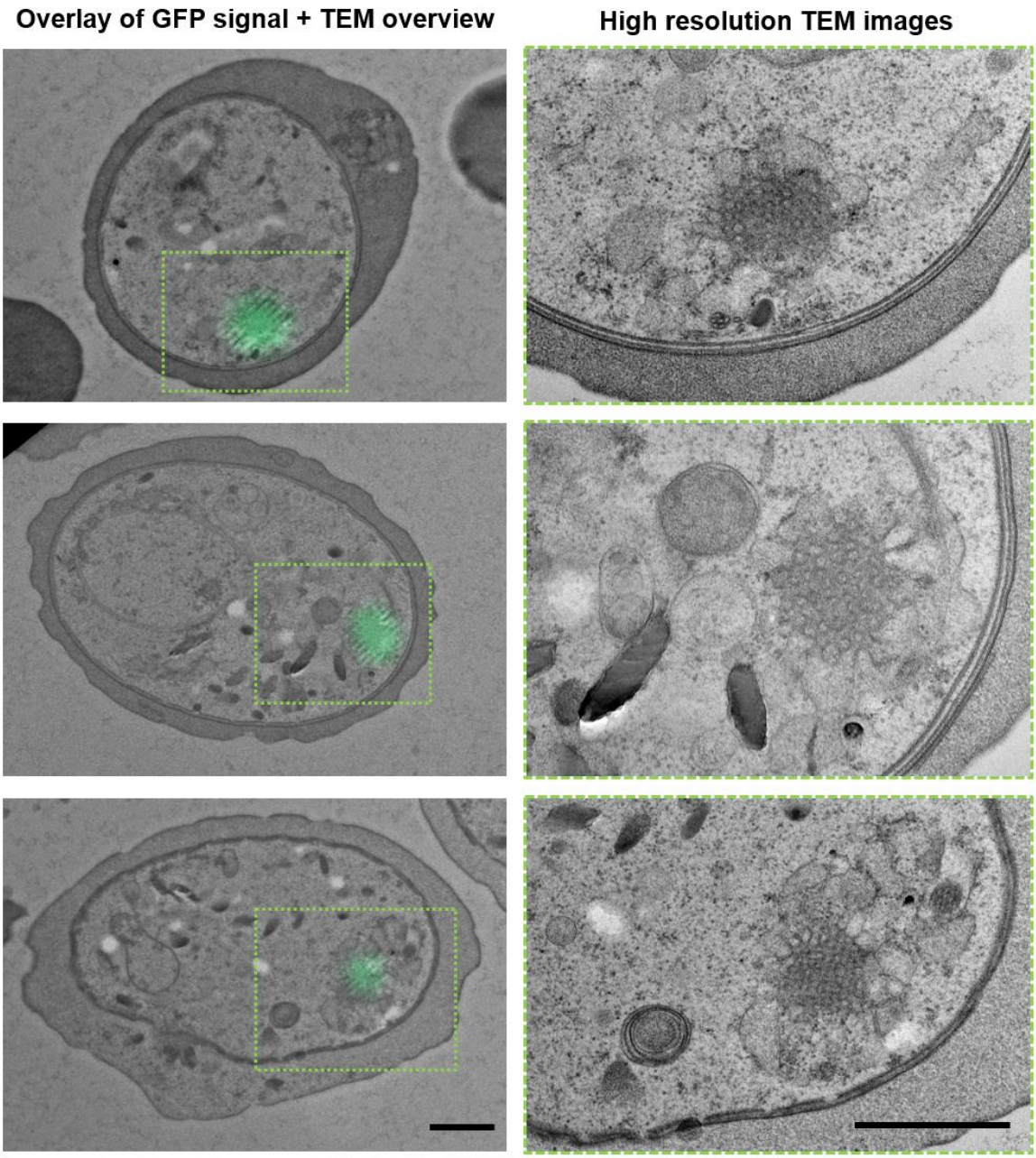

Figure 28. **Correlative light and electron microscopy (CLEM) images of PfABCG2-GFP expressing mature gametocytes.** Female gametocytes were selected based on strong GFP signal observed via confocal microscopy and the same cells were subsequently imaged by TEM. Overlay images of fluorescence (GFP) and TEM (left panels) show the localisation of PfABCG2-GFP signal in *P. falciparum* gametocytes and higher resolution TEM images of the boxed area are shown on the right. Scale bar = 1 µm

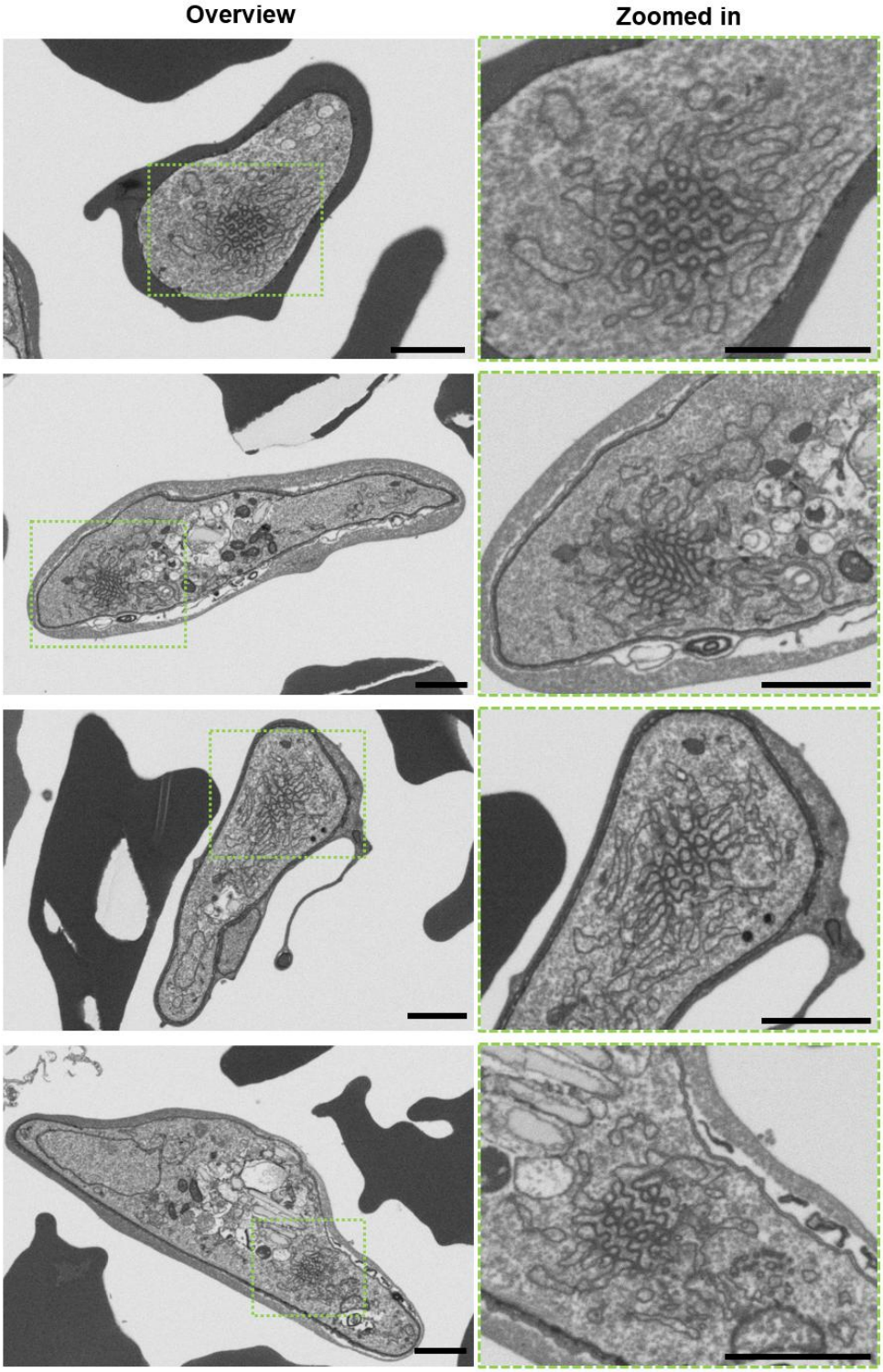

Figure 29. **Ultrastructure of PfABCG2-associated compartment (femLB) in PfABCG2-GFP expressing gametocytes.** Representative SEM images of mature female gametocytes (stage IV) prepared using the OTO method, sectioned at ~100 nm, and imaged using a Zeiss CrossBeam SEM with a backscattered electron (BSE) detector. Overview of whole parasites showing the femLB region (green boxed area) in left column and corresponding zoomed in views of the boxed region highlighting the densely packed, curved membrane structures characteristic of the femLB. Scale bar = 1 μm

Absence of PfABCG2 effects the ultrastructure of female specific lipid body

To determine whether the absence of PfABCG2 affects the morphology of femLB, I conducted ultrastructural analyses using TEM and 3D volume EM imaging (FIB-SEM) on PfABCG2-GFP expressing, WT and ΔPfABCG2 gametocytes (Stage IV). Samples were processed either by high pressure freezing followed by freeze substitution (as used in CLEM experiments) or by the OTO method. Based on ultrastructural features, female and male gametocytes could be readily distinguished. Female gametocytes were identified by their distinctly higher numbers of osmiophilic bodies compared to male gametocytes.

Using high pressure freezing and freeze substitution, I consistently observed a densely packed vesicle-like structure surrounded by the loosely arranged membranes (most likely the ER) in PfABCG2-GFP expressing female gametocytes (**Figure 30**). However, this exact structural arrangement was not observed in WT or ΔPfABCG2 gametocytes. In WT female gametocytes, a similar structure consisting of densely packed vesicle-like elements were observed, surrounded by membranes with morphology resembling ER (**Figure 30**). In contrast, the vesicle-like clusters in ΔPfABCG2 gametocytes showed little or no obvious association with such ER-like membranes (**Figure 30**).

Interestingly, femLBs in WT gametocytes were less interconnected compared to those in PfABCG2-GFP expressing gametocytes (**Figure 30**). My Nile Red analysis also showed that femLBs in PfABCG2-GFP expressing gametocytes showed a more pronounced NL spectral signal compared to those in WT gametocytes (**Figure 26** and **27**). This observation prompted further investigation to using 3D FIB-SEM to determine whether the compartments observed across all three cell lines were equivalent.

Absence of PfABCG2 alters femLB–ER structural organisation

In order to investigate the 3D organisation of FemLB and how it is affected by the absence of PfABCG2, I performed volume EM using FIB-SEM on stage IV gametocytes of PfABCG2-GFP expressing, WT, and ΔPfABCG2 cell lines. Samples were prepared using the OTO method.

When compared to high pressure frozen and freeze substituted samples (**Figure 30**), OTO-processed gametocytes showed broadly consistent femLB morphologies but with some differences (**Figure 29 & 31**). In PfABCG2-GFP expressing gametocytes, the stacked membranes of the femLB appeared even more interconnected with the ER under OTO preparation, making them difficult to separate from the ER (**Figure 29**). Similarly, in WT gametocytes, femLBs observed by OTO processing closely resembled those in cryo-fixed samples (**Figure 30**), appearing as clusters of densely packed vesicle-like structures, often encased by loosely arranged ER membranes (**Figure 31 & 32**). These consistencies across preparation methods support the interpretation that the femLB is a robust structural feature rather than a fixation artefact.

Across cell lines, PfABCG2-GFP expressing and WT gametocytes displayed femLBs with comparable organisation, consistently localised near one end of the parasite and associated with the ER (**Figures 29 & 31**). However, GFP tagging appeared to stabilise or promote aggregation of the core femLB membranes. In contrast, ΔPfABCG2 gametocytes displayed more dispersed, less densely packed vesicle-like elements. These structures were positioned near the ER but showed little or no direct contact with it (**Figure 31 & 33**).

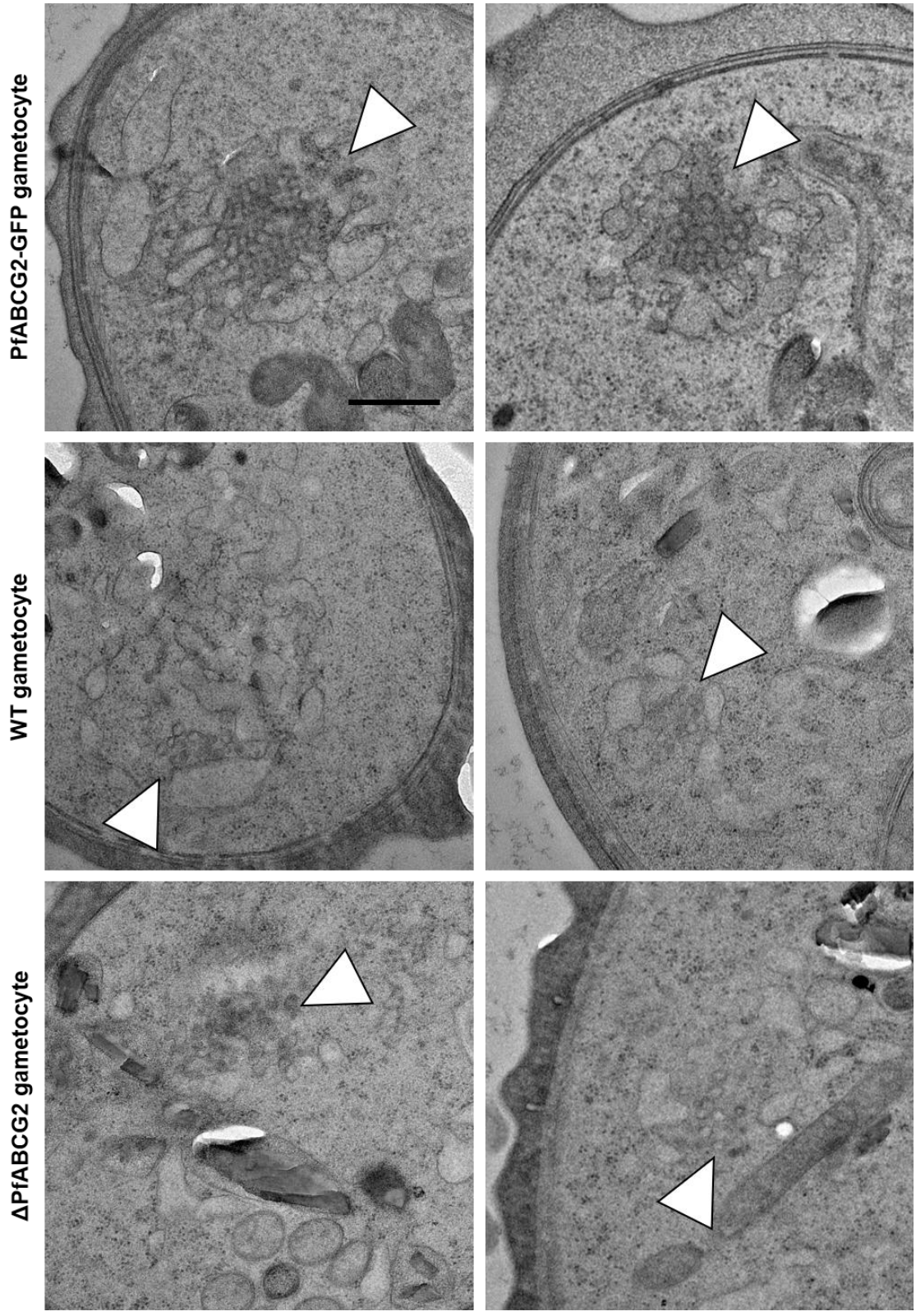

Figure 30. Ultrastructural comparison of femLB morphology in PfABCG2-GFP–expressing, WT, and ΔPfABCG2 gametocytes. TEM images of mature female gametocytes (stage IV) showing putative femLB structures (white arrowheads). Samples were processed by high-pressure freezing, freeze substitution, and embedded in HM20 resin. Ultrathin sections (~70 nm) were imaged using a JEOL F200 TEM. Scale bar = 1 µm.

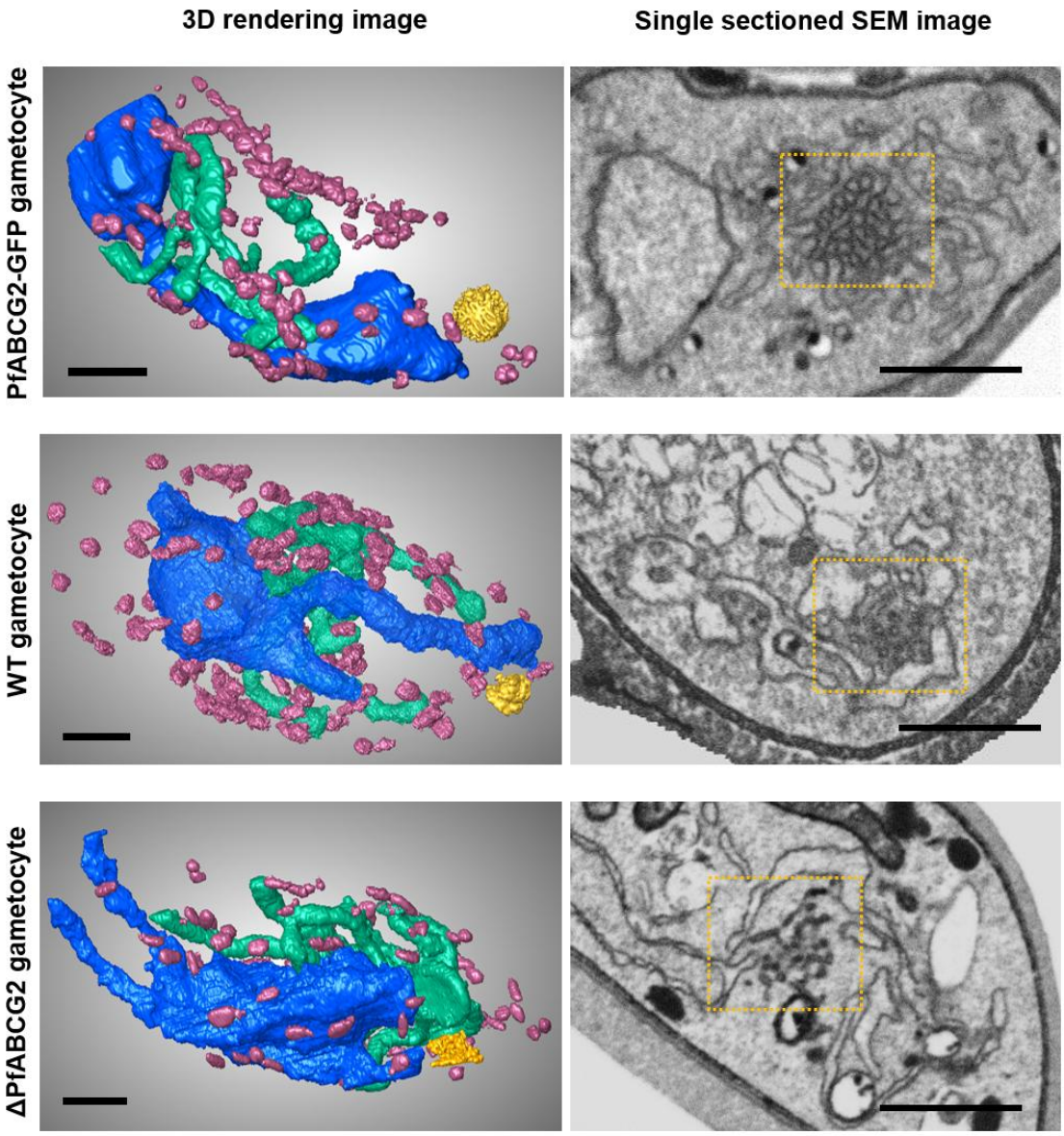

Figure 31. 3D rendering and ultrastructure of femLB and its association with other organelles in PfABCG2-GFP expressing, WT, and ΔPfABCG2 female gametocytes (stage IV). femLBs (yellow), nucleus (blue), mitochondrion (green), and osmiophilic bodies (pink) were segmented and visualised in 3D rendered models (left). Corresponding single-section SEM images show femLB structure (highlighted by yellow boxes, right). Scale bar = 1 μm

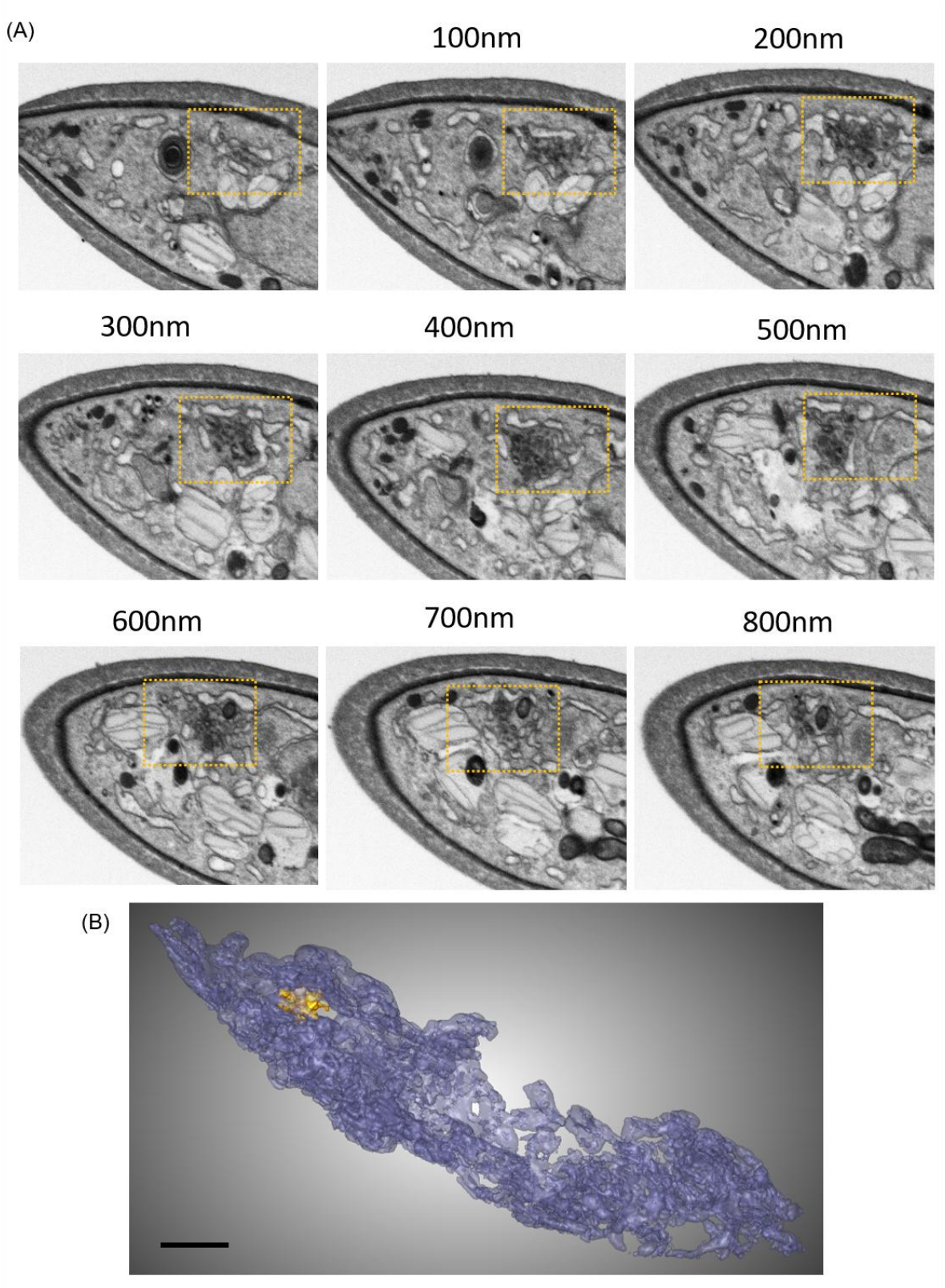

Figure 32. **Serial SEM images and 3D rendered model of the femLB and ER in WT female gametocyte (stage IV).** (A) Serial BSE images show a femLB (highlighted by yellow boxes). Each subsequent image is taken at an additional 100 nm depth. (B) 3D rendering of the same cell shows the femLB (yellow) tightly surrounded within the ER (purple). Scale bar = 1 μm

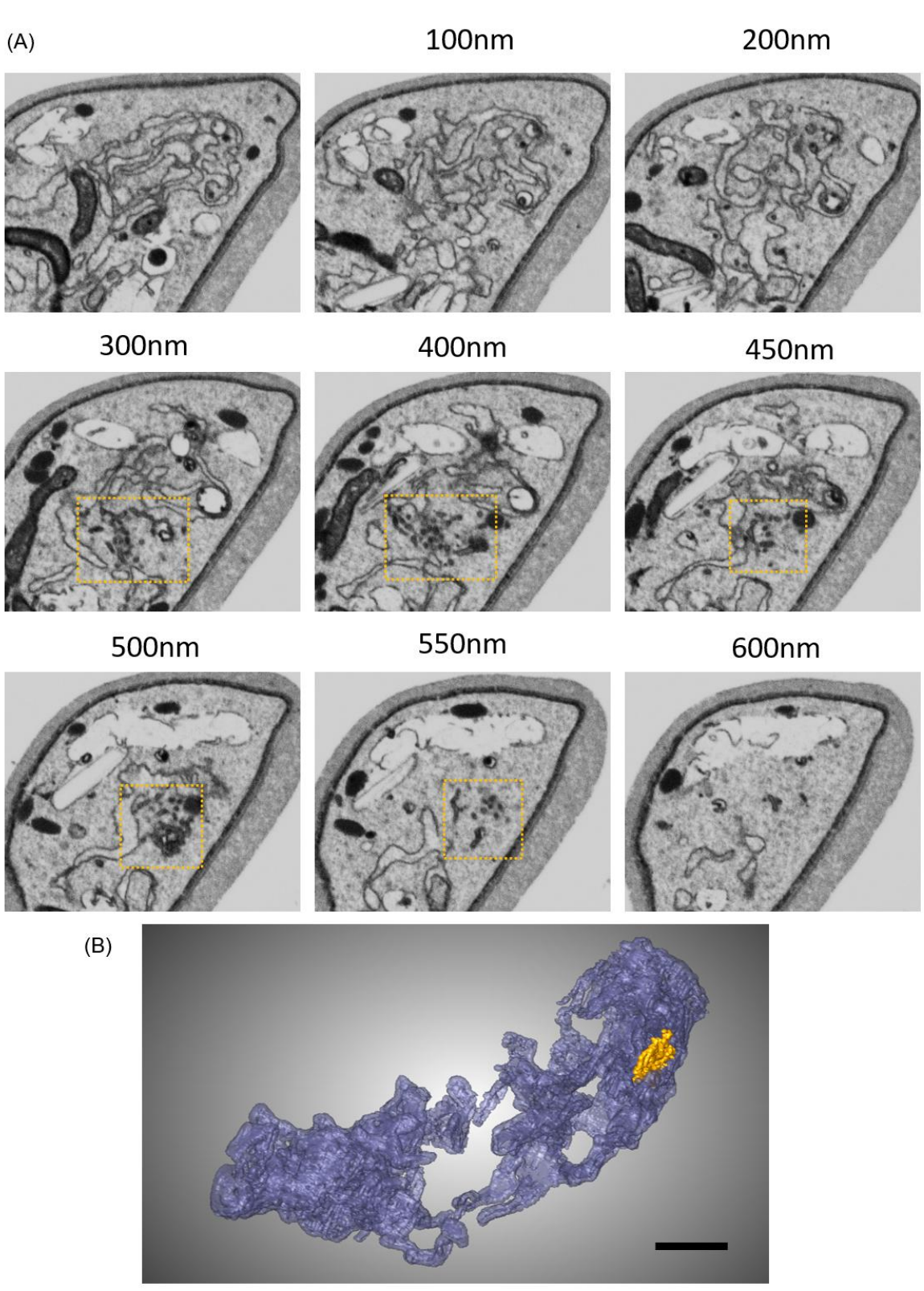

Figure 33. Serial SEM images and 3D rendered model of the femLB and ER in ΔPfABCG2 female gametocyte (stage IV). (A) Serial BSE images show a femLB (highlighted by yellow boxes) and (B) 3D rendering of the same cell shows the femLB (yellow) and the ER (purple). Scale bar = 1 µm

Effect of NL inhibitors on gametocyte viability

To investigate the role of NL metabolism in gametocytes, inhibitors targeting pathways involved in TAG and CE metabolism were selected. These inhibitors have previously been used to study LD dynamics during the asexual stages of *P. falciparum* (see Chapter 3), were chosen for their ability to disrupt NL metabolism in gametocyte.

Orlistat is a lipase inhibitor that blocks TAG hydrolysis, preventing TAG breakdown and leading to TAG accumulation (**Figure 34**A). Previous study has shown that Orlistat increases TAG levels in late schizont stages (Gulati et al., 2015). XN and T863 inhibit a key enzyme in TAG biosynthesis, DGAT, which blocking the final step of TAG synthesis DGAT (Tabata et al., 1997; Inokoshi et al., 2009; Cao et al., 2011). Ezetimibe is a cholesterol transport inhibitor that blocks Niemann-Pick C1 like 1 (NPC1L1)-mediated cholesterol uptake (Xie et al., 2012) (**Figure 34**A). In *P. falciparum*, Ezetimibe treatment significantly reduces cholesterol levels in both asexual and sexual stages of iRBCs which indicate the parasite relies on cholesterol uptake from the host cytosol and/or extracellular environment (Hayakawa et al., 2020; Hayakawa et al., 2021). Because the major pathway of CE synthesis in *P. falciparum* remains undefined, Ezetimibe was used to reduce cholesterol availability for esterification, thereby potentially indirectly affecting CE production.

To assess the importance of NL metabolism in gametocyte viability, inhibitor assays were performed on PfABCG2-GFP expressing gametocytes over a 72 hours period (from Day 7 to Day10; Stage IV to Stage V). Compared to the asexual stages, gametocytes showed significantly reduced sensitivity to Orlistat as requiring nearly 20-fold higher concentrations (IC_{50} values shifting from 7.8 μM to 120 μM) to achieve the same level of inhibition (**Figure 34B**). XN and Ezetimibe also required higher doses in gametocytes, with IC_{50} values approximately 6-fold (IC_{50} values shifting from 5.5 μM to 30 μM) (**Figure 34C**) and 4-fold

higher (IC_{50} values shifting from 26 μM to 110 μM) (**Figure 34D**), respectively, than in asexual parasites. In contrast, T863 had no measurable effect on gametocyte viability, even at concentrations up to 200μM (the maximum dose tested without DMSO-related toxicity), indicating that the IC_{50} value in gametocytes is > 200 μM compared to 30 μM in asexual stags. These results indicate that the mobilisation of stored lipids (TAG breakdown) plays a lesser role in gametocyte maturation compared to NL synthesis and storage.

ΔPfABCG2 gametocytes show unchanged sensitivity to the lipid metabolic inhibitors tested

To determine the importance of NLs during gametogenesis, inhibitor assays were performed on ΔPfABCG2 gametocytes using Orlistat, XN, and Ezetimibe. These compounds, which target different aspects of NL metabolism (**Figure 34A**), were applied to mature gametocytes over a 72 hours period (from Day 7 to Day10; Stage IV to Stage V). Given that previous study has shown significant reduced levels of CE, TAG and DAG in ΔPfABCG2 gametocytes (Tran et al., 2014), these inhibitors were expected to strongly affect viability if NLs are essential during gametocyte maturation.

However, the IC_{50} value of all three inhibitors remained relatively unchanged between PfABCG2-GFP expressing and ΔPfABCG2 gametocytes, with Orlistat at 123 μM vs. 139.7 μM (**Figure 34B**), XN at 31.4 μM vs. 24.3 μM (**Figure 34C**), and Ezetimibe at 111.6 μM vs. 98 μM (**Figure 34D**), respectively (**Figure 34F**). These results suggest that absence of PfABCG2 does not alter gametocyte sensitivity to the lipid metabolic inhibitors tested. The absence of such an effect suggests that, despite altered lipid composition, ΔPfABCG2 gametocytes retain sufficient metabolic flexibility to maintain viability.

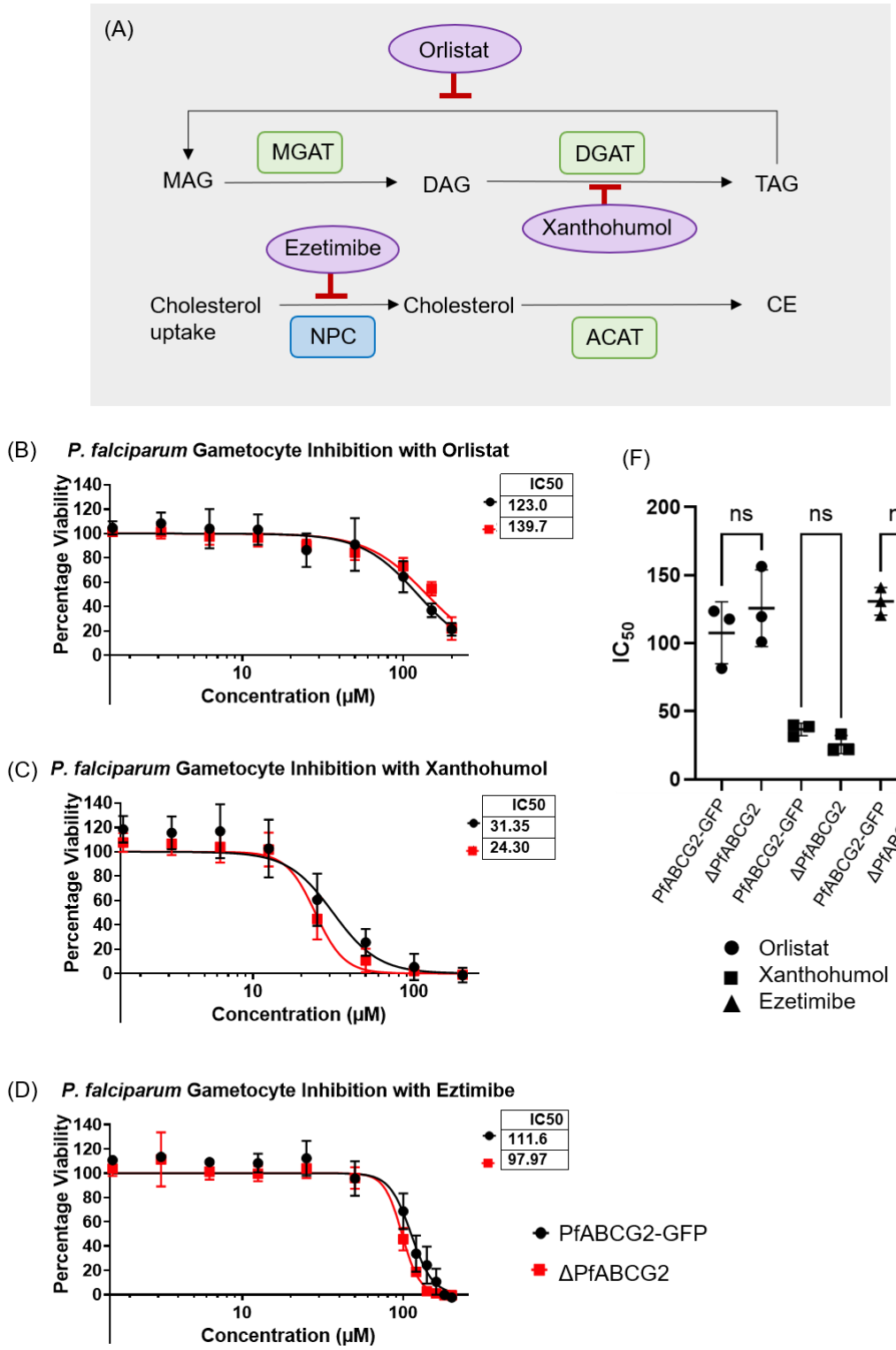

Figure 34. Drug sensitivity of PfABCG2-GFP expressing and ΔPfABCG2 *P. falciparum* gametocytes. (A) Schematic overview of TAG and CE synthesis pathway and action of selected inhibitors. (B-D) Dose-response curves showing the effects of 72 hours treatment (from stage IV to V) on gametocyte viability for (B) Orlistat, (C) Xanthohumol, and (D) Ezetimibe. Mean ± SD. n = 3 (F) Comparison of IC_{50} values between PfABCG2-GFP expressing and Δ PfABCG2 gametocytes. Individual points represent the IC_{50} values from independent experiments; bars represent mean ± SD. NS, not significant.

Disruption of NLs metabolism alter femLB properties

To investigate which metabolic pathways contribute to NLs accumulation in the femLB, PfABCG2-GFP expressing gametocytes (Stage IV) were treated with inhibitors targeting TAG hydryolysis (Orlistat), DGAT-mediated TAG synthesis (XN), and cholesterol uptake (Ezetimibe). NL content and PfABCG2-GFP expression were assessed 24 hours later (Stage V). Controls included 0.1% DMSO (maximum DMSO concentration in inhibitor treatments) and Primaquine. DMSO control was included to account for any potential toxicity from the solvent present in each inhibitor treatment. Primaquine, an established antimalarial for *P. falciparum* gametocyte (Graves et al., 2012), was includes as a positive control since it does not interfere with NL metabolism. All treatments were applied at their respective IC_{50} concentrations determined from the 72 hours gametocyte viability assay (**Figure 34B-D**) for 24 hours. Nile Red spectral imaging was used to assess lipid polarity (**Figure 35A**), and PfABCG2-GFP intensity and perimeter were quantified (**Figure 35B**).

In DMSO and Primaquine treated controls, polarity level of femLB remained consistent with that observed in untreated gametocytes (green in ratio maps; white arrowheads, **Figure 35A**).

Orlistat treated gametocytes showed a shift toward lower polarity (more red in the ratio map; blue arrow, **Figure 35A**), as expected since Orlistat blocks TAG breakdown, leading to TAG accumulation and consequently reduced polarity. However, PfABCG2-GFP intensity and perimeter were unchanged (**Figure 35B**).

XN treated gametocytes showed a modest polarity shift (green arrow, **Figure 35A**) and a significant reduction in PfABCG2-GFP intensity (**Figure 35B**). These results suggest that PfABCG2 expression in the femLB changed, even though the overall NL polarity remained relatively unchanged.

Ezetimibe treated gametocytes exhibited the most pronounced changes, with the femLB appearing blue in ratio map (yellow arrows, **Figure 35A**), indicates decreased NL content. Additionally, the PfABCG2-GFP signal was strongly diminished compared to controls, and the GFP signal perimeter varied widely between cells as some exhibited diffuse or greatly reduced GFP signal (**Figure 35A&B**).

(A)

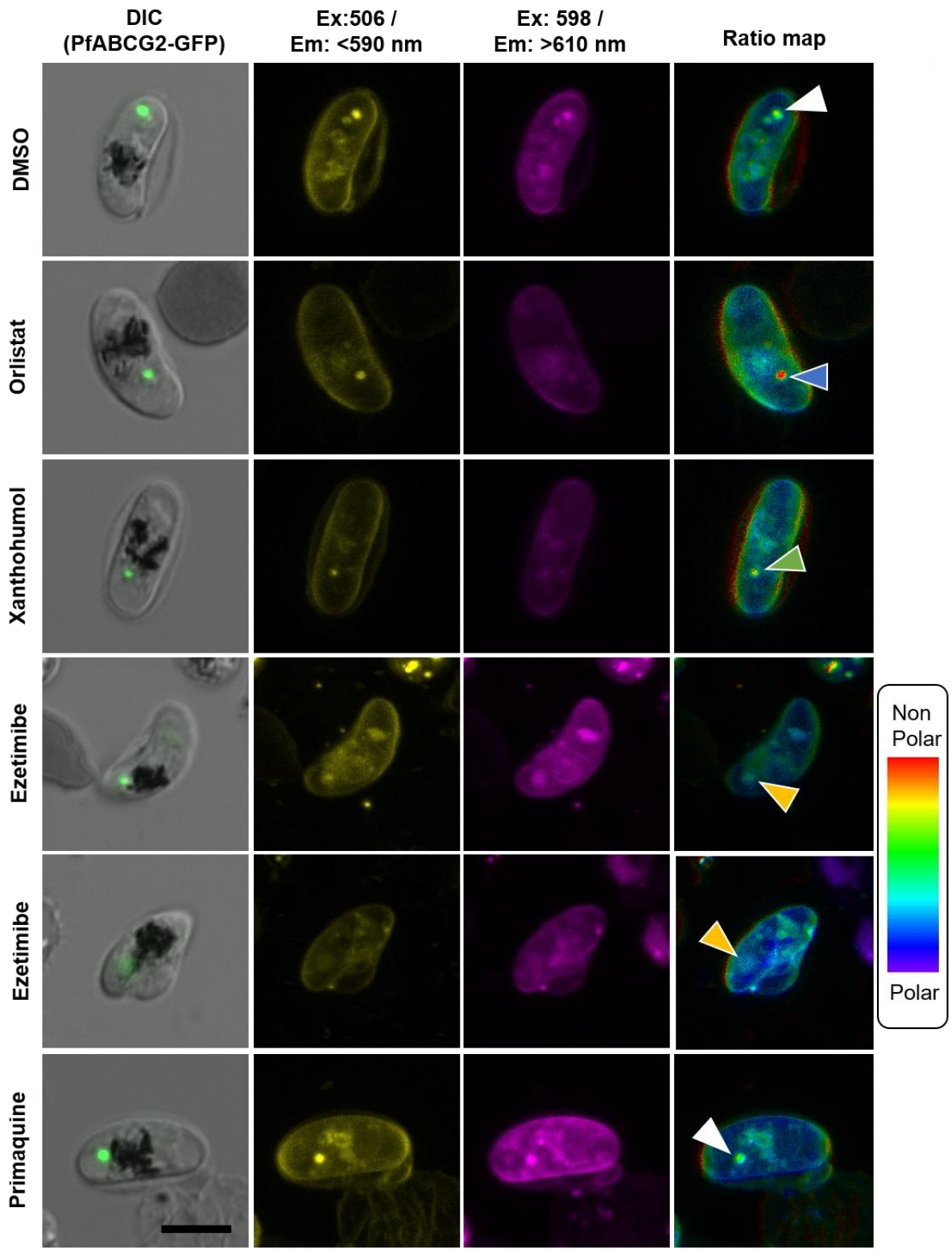
DIC
(PfABCG2-GFP)
Ex:506 /
Em: <590 nm
Ex: 598 /
Em: >610 nm
Ratio map
DMSO
Orlistat
Xanthohumol
Ezetimibe
Ezetimibe
Primaquine
Non
Polar
Polar

(B)

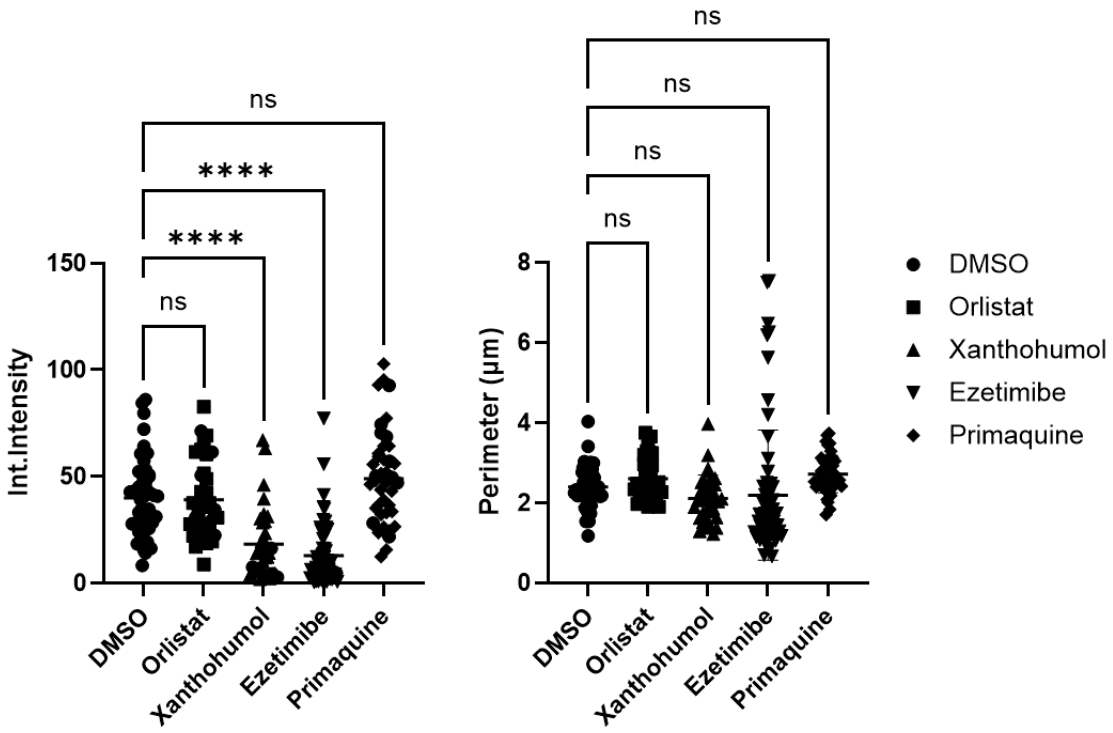

Figure 35 (A) Effect of inhibitors on lipid composition of PfABCG2 associated structure. Each inhibitors (1xIC_{50}) were added into mature gametocytes (stageIV) for 24 hours and stained with Nile Red. 0.1% DMSO was added for control, 120µM of Orlistat, 30 µM of xanthohunol, 110 µM of Ezetimibe, and 20 µM of Primaquine was added. Except DIC image, all depict representative images of maximum intensity projection of cells captured through z-stack imaging. Scale bar = 5µm (**B**) **Analysis GFP signal intensity and perimeter in ABCG2-GFP expressing gametocytes treated with inhibitors for 24 hours.** Gametocytes were treated with Control (0.1% DMSO), Orlistat (120 µM), Xanthohumol (30 µM), Ezetimibe (110 µM), or Primaquine (20 µM). The average integrated intensity and perimeter of GFP signals were quantified using maximum intensity projection images from z-stack. Total sample sizes for each treatment group: DMSO (n= 48), Orlistat (n= 34), Xanthohumol (n = 34), Ezitimibe (n = 64), Primaquine (n= 43). Mean ± SEM. An ordinary one-way ANOVA was performed, **** = p <0.0001, ns; not significant.

PfABCG2 is not localised in lipid rafts

Following the observation that PfAGBC2 expression is disrupted by reducing cholesterol levels in the parasite (Ezetimibe treatment), it was investigated whether PfABCG2 localises to lipid rafts. Cholesterol is a key structural component of lipid rafts, where it stabilises ordered membrane microdomains together with sphingolipids; thus, perturbing cholesterol levels can directly affect raft formation (Ouweneel et al., 2020). Given that gametocytes lack LDs yet still accumulate high level of NLs, it is possible that these lipids are organised through alternative membrane microdomains such as lipid rafts. Human ABCG2 has been reported to partition into raft-like membrane domains (Storch et al., 2007). On this basis, I hypothesised that PfABCG2 may associate with such structures within the femLB.

To test this, DRM extraction was performed with ice-cold Triton X-100, followed by Western blot analysis to determine whether PfABCG2 is localised in lipid rafts. One biochemical characteristic of lipid rafts is their insolubility in non-ionic detergents such as Triton X-100 (London and Brown, 2000).

PfEMP1 (*P. falciparum* erythrocyte membrane protein 1), a raft-associated protein, was used as a positive control (Frankland et al., 2006; Maier et al., 2006). As expected, PfEMP1 was detected in the Triton X-100-insoluble, SDS-soluble fraction (DRM fraction), verifying that this fraction corresponds to lipid raft associated proteins.

In contrast, a protein of the expected size (~92kDa, including the GFP tag: 65kDa for PfABCG2 and 26kDa for GFP) (Tran, 2014; Edaye and Georges, 2015) was not detected in DRM fraction. Instead, a protein around the expected molecular mass was detected in the Triton X-100-insluble, SDS-insoluble fraction (**Figure 36**). This indicates that PfABCG2 is not associated with lipid rafts. Rather, its detergent insolubility may reflect incorporation into tightly packed membrane domains or other specialised membrane regions, such as membrane

contact sites, where lipid transfer and organisation frequently occur (Jain and Holthuis, 2017). This localisation would be consistent with a potential role for PfABCG2 in lipid transfer at specilised membrane interfaces, although this remains to be directly tested.

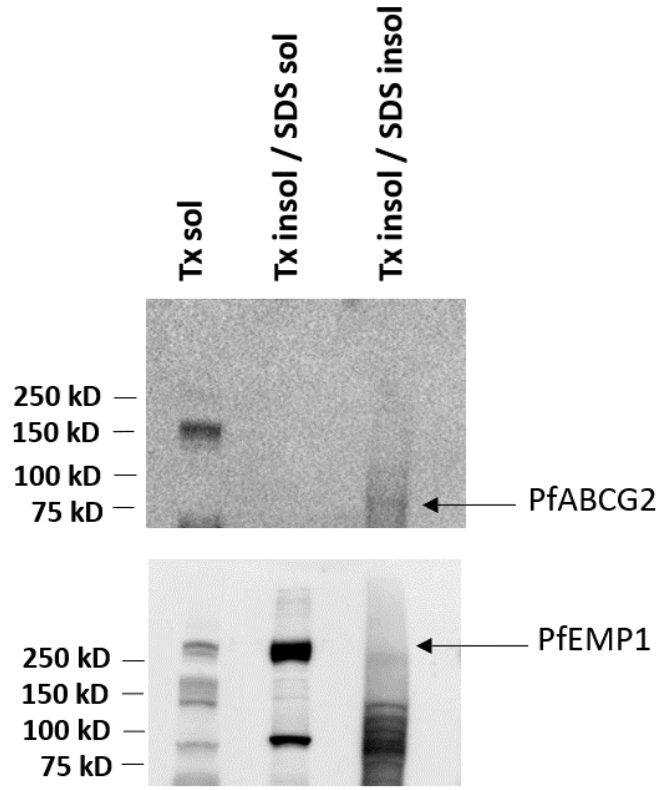

Figure 36. **SDS-PAGE and immunoblot analysis of PfABCG2 with Trion X-100 treatment.** Triton X-100, SDS soluble, and insoluble fractions of mature gametocytes were analysed by western blotting with anti-GFP to detect PfABCG2 and mouse monoclonal anti-ATS 1B/ 98-6H1-1(1:200) to detect PfEMP1(Maier et al., 2006). Horseradish peroxidase-coupled anti-mouse Ig (1:1000) were used as secondary antibodies. Tx sol = Triton X- 100 soluble fraction, Tx insol / SDS sol = Triton X-100 insoluble and SDS soluble fraction, Tx insol / SDS insol = Triton X-100 insoluble and SDS insoluble fraction.

Discussion

PfABCG2-associated NL compartment in female gametocytes, femLB

Using Nile Red spectral imaging on PfABCG2-GFP expressing gametocytes, a NL-enriched spot was consistently observed near one end of the parasite, co-localising with PfABCG2 (**Figure 26**). Given its absence in male gametocytes and previous study suggesting a potential role for PfABCG2 in NL storage (Tran et al., 2014), this structure was considered a candidate for a female-specific lipid storage organelle and is referred to here as the femLB.

Ultrastructural analyses of PfABCG2-GFP expressing gametocytes revealed that PfABCG2 localises to a densely packed, membrane structure closely associated with the ER (**Figure 28 & 29)**. A similar membrane compartment was also identified in WT female gametocytes, displaying comparable morphology, size, subcellular localization (**Figure 28 & 32**). These observations suggest that the femLB is a consistent structural feature of female gametocytes, independent of PfABCG2-GFP tagging.

The honeycomb-like organisation of the femLB may reflect a structural adaptation that maximises the surface area for lipid packing and exchange with surrounding membranes, while maintaining a compact form within the parasite. Its consistent proximity to the ER suggests that the compartment may rely on ER membranes for lipid supply or protein trafficking. The presence of a single femLB per gametocyte could indicate a centralised lipid storage strategy, concentrating neutral lipids into one defined organelle rather than distributing them across multiple smaller droplets, perhaps to effectively facilitate regulated mobilisation whenever it required.

Interestingly, a recent FIB-SEM study described similar densely packed vesicle-like structure in the polar regions of the mature female gametocytes, which was interpreted as Golgi based

on its morphology (Evers et al., 2025). However, previous immunofluorescence analysis showed no co-localisation between PfABCG2 and a Golgi marker (Tran et al., 2014), arguing against this interpretation. Together, these features suggest that the femLB likely represents a highly specialised, female-specific solution to the challenge of storing and mobilising neutral lipids.

PfABCG2 supports femLB morphology and ER association

In ΔPfABCG2 female gametocytes, the femLB like structure was still detectable but showed marked alterations in morphology and lipid polarity (**Figure 27, 30 & 33**). Three-dimensional ultrastructural analysis revealed a femLB-like compartment at a similar subcellular location to that seen in WT and PfABCG2-GFP expressing gametocytes, consistent with Nile Red spectral imaging. However, the organisation of this structure was notably altered in the absence of PfABCG2. The vesicle-like elements appeared more dispersed, and the association with surrounding ER membranes was reduced (**Figure 33**). These morphological changes may reflect altered lipid composition or membrane dynamics at the femLB, potentially affecting its stability or capacity to accumulate neutral lipids.

As previously reported, absence of PfABCG2 led to a significant reduction in NLs (CE, DAG, and TAG) accompanied by an increase in phospholipids (Tran et al.,2014). This shift in lipid composition suggests that PfABCG2 may help maintain lipid homeostasis, possibly by modulating the balance between NL storage and phospholipid synthesis. Given that DAG is a shared precursor for both TAG synthesis and phospholipid production, PfABCG2 may act at the femLB–ER interface to influence how DAG is utilised. One possibility is that PfABCG2 regulates the distribution or accessibility of DAG, thereby determining whether it is channelled into TAG storage within the femLB or diverted into phospholipid biosynthesis for membrane

expansion. In the absence of PfABCG2, DAG may be preferentially directed into phospholipid production at the expense of NL storage, accounting for the observed reduction in DAG, TAG, and CE levels, alongside a relative increase in phospholipids.

NL biosynthesis and gametocyte viability

IC_{50} assays for Orlistat (TAG hydrolysis inhibitor), XN (DGAT inhibitor), and Ezetimibe (Cholesterol uptake inhibitor) showed no statistically significant changes between PfABCG2-GFP expressing and ΔPfABCG2 gametocytes (**Figure 35**). Thus, despite the significantly reduced NL levels in ΔPfABCG2 gametocytes, similar inhibitor concentrations were required to impair viability. These results suggest that PfABCG2-associated NL stores may be dispensable for gametocyte viability under the conditions tested.

However, there are some important limitation to consider. First, the assays were conducted on mixed-sex cultures. Previously study has shown that neither deletion nor GFP-tagging of PfABCG2 alters the gametocyte sex ratio, which remains approximately 3:1 (female: male), consistent with WT parasites (Tran et al., 2014). Although this consistent and strong female bias makes it unlikely that male gametocytes substantially diluted the results, their presence may still have introduced some variability. Second, ΔPfABCG2 gametocytes still display a femLB-like structure that is less distinct (**Figure 27, 30 & 33**) but retains some morphological similarity to the normal femLB, albeit with reduced NL content. This means that the assays test a reduced rather than complete loss of NL stores.

TAG hydrolysis, but not synthesis, affects femLB NL accumulation

Inhibition of TAG hydrolysis with Orlistat led to increased NL accumulation within femLBs (**Figure 35**), supporting the idea that this compartment functions as a NL storage site. This

result also suggests that femLBs are sites of active TAG turnover, where hydrolysis contributes to lipid mobilisation during gametocyte maturation.

In contrast, inhibition of DGAT-mediated TAG synthesis using XN did not significantly reduce NL levels in femLBs (**Figure 35**). This suggests that additional pathways such as CE synthesis may partially compensate for reduced TAG production. However, since TAG and CE serve distinct biological functions, it is unlikely that CE alone can fully substitute for the loss of TAG.

In asexual stages, *P. falciparum* forms TAG-enriched LDs serve as energy reservoirs and support membrane biogenesis during schizogony. In contrast, the femLB may rely on a defined TAG:CE ratio to fulfil a female-specific role - potentially balancing energy storage (via TAG) and cholesterol management or signalling (via CE). In mammalian cells, ongoing TAG synthesis requires to facilitates the condensation of CE and other neutral lipids, acting as a thermodynamic pump to extract them from the ER bilayer (Dumesnil et al., 2023). This strategy allows efficient sequestration of neutral lipids, even when TAG is not the primary storage form, by maintaining a baseline level of TAG production to promote droplet nucleation.

Disruption of TAG synthesis may therefore alter the femLB lipid profile without reducing the overall NL level. Instead, such a shift might affect the compartment's protein composition or structural integrity, potentially explaining the observed reduction in PfABCG2-GFP signal intensity following XN treatment. Moreover, if the femLB stores an altered profile of NLs, these changes could be critical for parasite development in the mosquito, raising the possibility that the functional consequences may become more pronounced during the mosquito stage.

Cholesterol availability influences femLB properties

Inhibition of cholesterol uptake using Ezetimibe resulted in a marked reduction in NL accumulation within the femLB (**Figure 35**). Compared to controls, femLBs in Ezetimibe treated gametocytes appeared morphologically variable, with both smaller and enlarged forms observed. These changes suggest that cholesterol availability influences femLB composition and alters its structural organisation.

Since *P. falciparum* lacks the ability to synthesis cholesterol *de novo*, it depends entirely on uptake from the host and extracellular environment. Therefore, blocking cholesterol uptake may impair the parasite's ability to maintain CE levels. The observed shift in lipid polarity within the femLB following Ezetimibe treatment suggests that CEs may be a major component of the stored lipids in this compartment.

Notably, Ezetimibe treatment led to a significant reduction in the GFP signal intensity, similar to the effect of XN treatment. This suggests that disruption of the TAG:CE balance within the femLB may affect PfABCG2 localisation or stability in the compartment. Given that *P. falciparum* gametocytes likely favour PfPL-mediated CE synthesis which consumes PC as an acyl donor, this reaction not only contributes to CE production but may also influence the local phospholipid profile. The resulting shifts in the PC:PE balance could in turn affect membrane curvature and packing, thereby shaping the femLB structure (Parks et al., 2000; Hamai et al., 2006; Jarsch et al., 2016). Together with the TAG: CE balance, this interplay between neutral and phospholipids may be critical for maintaining the biophysical environment required for femLB formation and stability.

femLB is not raft-associated but forms part of a distinct membrane compartment

Biological membranes are often organised into domains enriched in specific lipids and

proteins. These specialised domains are believed to act as platforms for membrane signalling by concentrating certain lipids and proteins. Multiple studies have provided evidence that some of ABC transporter associated with membrane lipid homeostasis and might regulate plasma membrane organisation (Wu et al., 2020). In human cancer cells, ABCG2 is localised to highly-ordered, cholesterol-rich lipid raft microdomains and change the location to non-raft structure under altered cholesterol condition (Storch et al., 2007; Szilagyi et al., 2017).

In *P. falciparum*, however, PfABCG2 was not detected in lipid rafts, but instead was detected in the Triton X-100 and SDS-insoluble fraction (**Figure 36**). Ultrastructural analyses further showed that the PfABCG2-associated compartment, femLB, is an interwoven, densely packed membrane compartment. Together, these observations support the interpretation that femLB is not a cholesterol enriched raft-like domain, but rather the NL enrichment in the femB is achieved through processes other than classical raft organisation.

One possible explanation lies in phospholipid-driven membrane curvature. Membrane curvature is influenced by lipid composition, particularly the PE:PC ratio, which plays role in controlling membrane fluidity and stability in higher eukaryotes (Chakraborty et al., 2020; Pohnl et al., 2023). PE is a cone-shaped lipid that promotes membrane bending whereas PC is more cylindrical and maintains bilayer stability (McMahon and Boucrot, 2015; Kunduri et al., 2022). In ΔPfABCG2 gametocytes, PE became the most abundant phospholipids, whereas PC predominates in WT gametocytes (Tran et al., 2014). Although whole cell lipidomic study cannot directly describe the femLB microenvironment, this overall shift in PE:PC ratio suggests altered curvature properties that may contribute to the disrupted femLB morphology observed in the absence of PfABCG2 (**Figure 30 & 33**). Such altered curvature may in turn influence how NLs are packaged and retained within the femLB.

A second possibility is that PfABCG2 directly influences membrane organisation through phospholipid transport. In eukaryotic system, ABCG2 has been shown to transport PS and PC

analogues in vitro upon over expression (Woehlecke et al., 2003). This activity resembles that of phospholipid flippase, which translocate phospholipids from one leaflet of the bilayer to the other, thereby modulating membrane asymmetry (van Meer et al., 2006; Coleman et al., 2013). Although flippase activity among ABC transporters is poorly conserved across the eukaryotic kingdom, if PfABCG2 plays a similar function it could locally remodel phospholipid asymmetry at the membranes in femLB structure, thereby promoting curvature of membrane and lipid packing that stabilise the compartment.this stabilisation would provide the structural environment needed to concentrate and retain NLs.

This hypothesis is particularly relevant given the dynamic nature of the ER. The ER membrane is highly fluid and allows rapid phospholipid movement across the bilayer (van Meer et al., 2008). While the femLB appears more tightly packed and compositionally distinct from the ER membranes. The transition from a fluid to an ordered femLB membranes may therefore require active lipid remodelling. In this context, PfABCG2 may play a dual role: not only contributing to neutral lipid storage, but also shaping and compartmentalising the femLB through phospholipid remodelling. Such a mechanism would help explain how female gametocytes establish a dedicated, ultrastructurally distinct NL storage.

Overall, the observations in this chapter suggest that NL storage in female gametocytes involves a more complex mechanism than LDs in asexual stage. Although the morphology of the femLB does not change with altered NL composition, and PfABCG2 is not essential for gametocytogenesis, these observations do not rule out an important role for the femLB in later stages of the parasite's sexual life cycle. The femLB may act as a pre-assembled lipid reservoir, providing membranes and energy to support parasite development in the nutrient limited mosquito midgut. A possible link may also exist between the femLB and the crystalloid organelle described in various *Plasmodium* species, including *P. falciparum* ookinetes (Meis and Ponnudurai, 1987), and shown to be essential for sporogony and transmission in *P. berghei*

(Dessens et al., 2011; Dessens et al., 2021). Crystalloids are characterised by clusters of tightly packed membrane units that adopt a honeycomb-like symmetry. The femLB shares several features with these crystalloids, including a close association with the ER, a tightly packed membrane-rich ultrastructure, and spatial localisation near one end of the parasite. While this comparison remains speculative, it raises the possibility that female gametocytes may pre-assemble specialised membrane domains for swift mosquito-stage development.

While many questions remain, this chapter provides structural framework for understanding how female gametocytes establish a specialised lipid storage strategy, which may be particularly well-suited for survival across two distinct host environments.

Chapter 6. General Discussion and Conclusion

Summary of key findings

Plasmodium falciparum parasites have a complex life cycle that includes development in the human host as well as the *Anopheles* vector. Throughout its life cycle, *P. falciparum* undergoes dramatic metabolic shifts and morphological changes, each requiring specific lipid compositions and quantities. While neutral lipid storage in other eukaryotes is primarily mediated by LDs, the mechanisms used by *P. falciparum* have remained largely unexplored. This thesis investigated how *P. falciparum* parasites store and traffic neutral lipids across different stages in the intraerythrocytic cycle.

In Chapter 3, it was shown that neutral lipids are primarily stored in LD, with LD formation and degradation tightly linked to parasite development during the asexual blood stages. Spectral shift imaging with Nile Red stain, FIB-SEM volume imaging, and inhibitor assays were used to show that TAG-rich LDs accumulate progressively during the asexual blood stages and are essential for parasite development. Moreover, functional inhibition of TAG hydrolysis impaired merozoite formation while inhibition of TAG synthesis disrupted LD formation and blocked parasite maturation. These findings establish that LD formation and turnover are not incidental but essential for lipid homeostasis and membrane biosynthesis for parasite replication.

In Chapter 4, a list of potential LD-associated proteins in *P. falciparum* was compiled using homology-based searches. Although *P. falciparum* lacks homologs of several structural LD-associated proteins described in other eukaryotic systems, several neutral lipid synthesis enzymes (PfDGAT, PfACAT, PfPL) and trafficking regulators (homologs of Rab GTPases, Arf1, 14-3-3 proteins) were identified. This suggests that *P. falciparum* may use simplified or alternative mechanisms for LD formation and regulation. Expression profiling of these proteins showed distinct patterns between asexual and sexual stages, with TAG synthesis related

enzymes like PfDGAT enriched in mature asexual stage and male gametocytes, while CE synthesis related enzymes like PfACAT and PfPL were more prominent in female gametocytes. PfLPL1 and PfABCG2 which previously showed their functional relevance into lipid storage in the parasite were highly expressed in female gametocytes which makes them promising LD-associated protein candidates for studying LD biology in female gametocytes.

In Chapter 5, one of the neutral lipid-enriched compartments in female gametocytes, which we now termed the femLB, was ultrastructurally characterised. The ATP-binding cassette transporter PfABCG2 was previously found to be localised to the femLB and it was now characterised as a tightly packed membrane compartment that is ultrastructurally distinct from LDs observed in asexual stages. Inhibitor assays further revealed that neutral lipid metabolism – particularly CE accumulation – affects femLB lipid composition and influences PfABCG2 localisation. These findings suggest that the femLB maintains a defined TAG:CE balance to preserve its membrane organisation, and that PfABCG2 localisation is sensitive to changes in this ratio.

Together, these results reveal a stage- and sex-specific regulation of neutral lipid storage in *P. falciparum*.

LD biogenesis models in *P. falciparum*

Ultrastructural observations in asexual stages support the ER budding model of LD formation, which is widely accepted in other eukaryotic systems. In this model, neutral lipids accumulate between the ER membrane leaflets, forming a lens that buds outward toward the cytosol. In *P. falciparum,* LDs observed during asexual development appear to originate directly from the ER, consistent with this model. PfDGAT, a putative TAG synthesis enzyme, likely catalyses TAG formation at the ER membrane, facilitating LD formation.

While the ER budding model appears to explain LD formation during asexual development, other molecular evidence suggests that additional mechanisms may also be at play. For example, several putative LD-associated proteins - such as PfArf1, PfRab1, PfRab7, PfRab18, and Pf14-3-3 - have been previously identified in DRM fractions (Yam et al., 2013). Although the absence of classical lipid raft markers like caveolin makes it difficult to interpret these findings as direct evidence for raft involvement in LD biogenesis, the enrichment of potential LD regulators in DRM fractions raises possibility that microdomain-based organisation could assist lipid packaging.

Thus, these observations suggest that *P. falciparum* employs more than one mechanism for LD biogenesis. ER budding appears to predominate in asexual stages, while alternative mechanisms such as vesicle efflux or microdomain-mediated organisation may become more relevant under specific developmental requirements.

In gametocytes, no LD structures are observed based on ultrastructural studies; they do not exhibit the typical spherical, highly electron dense appearance after preparation with OTO method. Instead, female gametocytes contain a neutral lipid-rich compartment in tightly packed membranes (femLB). This architecture suggests a possible resemblance to the vesicle efflux model, in which neutral lipids are incorporated into small ER derived vesicles. The distinct membrane organisation of the femLB may be shaped by local phospholipid composition. While this study focused on characterising the femLB, it is important to note that additional lipid-rich compartments may exist in gametocytes, as suggested by Nile Red staining, and remain to be defined.

Although both asexual stages and gametocytes store neutral lipids, the structural and functional context differs markedly between these life cycle stages. In asexual parasites, LDs are small, spherical organelles that support rapid membrane biosynthesis and energy demands

during schizogony. In contrast, gametocytes develop more slowly and must accumulate neutral lipids in preparation for transmission, where resources in the mosquito midgut are scarce. The femLB represents a female-specific solution to this challenge: a tightly packed, membrane-bound reservoir that may allow lipids to be stored in a more stable, protected form. Thus, stage-specific lipid storage strategies likely reflect the differing physiological requirements of a parasite that alternates between proliferation in human red blood cells and survival through transmission to the mosquito.

Composition dependent lipid storage in *P. falciparum*

The structural characteristics of LDs in eukaryotic cells are highly influenced by the relative abundance of TAG and CE. TAG-rich LDs typically form spherical, fluid droplets due to TAG's low melting point (~4 ºC) and high miscibility with phospholipids (Dumesnil et al., 2023). In contrast, CE-rich LDs become more ordered and rigid, particularly when the CE:TAG ratio exceeds 9:1 at physiological temperatures (~37 °C), forming solid-like structures known as liquid-crystalline phases (Dumesnil et al., 2023). These CE-rich droplets are harder to form on their own, but a small amount of TAG can help "seed" their formation by making it easier for CEs to condense into a stable droplet. Without TAG, CE condensation is inefficient, underscoring the importance of TAG as a nucleation facilitator even when it is not the dominant stored lipid.

A key biological distinction between asexual and sexual stages of *P. falciparum* is their exposure to different host environments. Asexual stages remain within human red blood cells at a constant ~37 °C, while mature female gametocytes are transmitted to the mosquito midgut, where ambient temperatures range from 20 to 28 °C. This thermal shift imposes constraints on lipid storage. TAG-rich LDs, while well-suited for rapid turnover and membrane synthesis at

body temperature, may be less stable or more fluid in cooler environments. In contrast, CE-rich structures become more ordered and compact as temperature drops, making them potentially more robust during transmission. Therefore, the enrichment of either TAG or CE in different stages may reflect the parasite's adaptive response to the temperature and metabolic conditions it faces in each host.

The requirement for a different TAG:CE ratio in forming and maintaining neutral lipid storage across different blood stage forms highlights the importance of tightly regulated lipid synthesis in preparing the parasite for successful progression through its complex life cycle.

Future directions

Lipid biosynthesis and trafficking pathways have been shown to be essential for the development of many protozoan parasites and represent promising targets for therapeutic intervention (Mitamura and Palacpac, 2003; Coppens and Vielemeyer, 2005; Vial and Ben Mamoun, 2005). As *P. falciparum* reside within RBCs, which lack organelles and biosynthetic capacity, the parasite must establish its own lipid storage and trafficking systems without the help of the host cell. Disrupting these processes could therefore be detrimental to parasite survival.

This thesis highlights the remarkable adaptability of *P. falciparum* in managing neutral lipids across its life cycle. The discovery of distinct lipid storage strategies - transitioning from TAG-rich LDs in asexual stages to likely CE-rich membrane bound compartments (femLB) in female gametocytes - suggests tightly regulated, stage and sex specific lipid storage and trafficking. These strategies likely reflect the divergent biological demands of replication versus transmission preparation.

While this work provides new insights into neutral lipid biology in *P. falciparum*, several important questions remain:

- **Are there additional lipid storage structures in gametocytes?** Nile Red fluorescence microscopy revealed multiple neutral lipid-enriched spots in both female and male gametocytes, yet 3D-EM imaging showed no classical LDs in either. This suggests that gametocytes may store neutral lipids in non-conservative compartments.
- **What proteins are associated with lipid storage and trafficking?** Although this study identified putative LD-associated proteins through homology search, the actual proteome of LDs and femLBs remains undefined. Proteomic analysis of biochemically isolated lipid storage compartments will be essential to determine whether these structures are functionally distinct and to define their regulatory protein machinery.
- **How are femLBs formed and maintained?** The close association of femLB with the ER suggests a potential ER-derived origin. However, its distinct membrane organisation implies that it may form through a specialised mechanism. One possibility is that the femLB is generated and stabilised by membrane curvature driven by local phospholipid composition, providing an structural environment that favours the storage of neutral lipids. However, the precise role of PfABCG2 and the molecular steps involved in femLB formation remain unresolved.
- **What is the role of femLBs after transmission?** Neutral lipid storage appears dispensable for gametocyte maturation, suggesting that femLBs may serve a function after transmission to the mosquito. Investigating whether femLBs contribute to zygote development, ookinete maturation, or midgut invasion in the mosquito may uncover new targets for transmission-blocking strategies.

Although these questions remain unresolved, the findings presented here offer new insights into stage-specific neutral lipid storage in *P. falciparum* and provide a foundation for future investigations of parasite lipid biology

Conclusion

Together, the findings presented in this thesis expand our understanding of how *P. falciparum* regulates and uses lipid storage throughout its complex life cycle. By combining imaging, inhibitor studies, and bioinformatic approaches, this work reveals that the parasite adapts its lipid storage strategies to meet the distinct physiological demands in different intraerythrocytic stages of the parasite's life cycle. While classical LDs rich in TAGs support rapid replication in asexual stages, female gametocytes appear to store neutral lipids in a structurally distinct compartment, the femLB, potentially to fuel development after transmission to the mosquito. These observations lay the foundation for future studies aimed at characterising the molecular composition and functional roles of lipid storage in *P. falciparum*, with the potential to uncover new targets for stage-specific or transmission-blocking antimalarial strategies.

References

Adams, C. W. M., Abdulla, Y. H. and Bayliss, O. B. (1967). Osmium tetroxide as a histochemical and histological reagent. *Histochemistry & Cell Biology* 9, 68-77.

Adeyo, O., Horn, P. J., Lee, S., Binns, D. D., Chandrahas, A., Chapman, K. D. and Goodman, J. M. (2011). The yeast lipin orthologue Pah1p is important for biogenesis of lipid droplets. *Journal of Cell Biology* 192, 1043-55.

Agop-Nersesian, C., Naissant, B., Ben Rached, F., Rauch, M., Kretzschmar, A., Thiberge, S., Menard, R., Ferguson, D. J. P., Meissner, M. and Langsley, G. (2009). Rab11A-controlled assembly of the inner membrane complex is required for completion of apicomplexan cytokinesis. *PLOS Pathogens* 5, e1000270.

Altmann, R. (1894). Die Elementarorganismen und ihre Beziehungen zu den Zellen.*Berlin, Boston: De Gruyter*

Ambele, M. A. and Egan, T. J. (2012). Neutral lipids associated with haemozoin mediate efficient and rapid β-haematin formation at physiological pH, temperature and ionic composition. *Malaria Journal* 11, 337.

Ancelin, M. L. and Vial, H. J. (1989). Regulation of phosphatidylcholine biosynthesis in *Plasmodium*-infected erythrocytes. *Biochimica et Biophysica Acta (BBA) - Lipids and Lipid Metabolism* 1001, 82-89.

Anderson, R. A., Joyce, C., Davis, M., Reagan, J. W., Clark, M., Shelness, G. S. and Rudel, L. L. (1998). Identification of a form of Acyl-CoA:cholesterol acyltransferase specific to liver and intestine in nonhuman primates. *Journal of Biological Chemistry* 273, 26747-26754.

Arlt, H., Sui, X., Folger, B., Adams, C., Chen, X., Remme, R., Hamprecht, F. A., DiMaio, F., Liao, M., Goodman, J. M. et al. (2022). Seipin forms a flexible cage at lipid droplet formation sites. *Nature Structural & Molecular Biology* 29, 194-202.

Asad, M., Yamaryo-Botte, Y., Hossain, M. E., Thakur, V., Jain, S., Datta, G., Botte, C. Y. and Mohmmed, A. (2021). An essential vesicular-trafficking phospholipase mediates neutral lipid synthesis and contributes to hemozoin formation in *Plasmodium falciparum*. *BMC Biology* 19, 159.

Bartz, R., Li, W. H., Venables, B., Zehmer, J. K., Roth, M. R., Welti, R., Anderson, R. G. W., Liu, P. and Chapman, K. D. (2007a). Lipidomics reveals that adiposomes store ether lipids and mediate phospholipid traffic. *Journal of Lipid Research* 48, 837-847.

Bartz, R., Zehmer, J. K., Zhu, M., Chen, Y., Serrero, G., Zhao, Y. and Liu, P. (2007b). Dynamic activity of lipid droplets: protein phosphorylation and GTP-mediated protein translocation. *Journal of Proteome Research* 6, 3256-3265.

Belevich, I., Joensuu, M., Kumar, D., Vihinen, H. and Jokitalo, E. (2016). Microscopy Image Browser: A platform for segmentation and analysis of multidimensional datasets. *PLOS Biology* 14, e1002340.

Bell, R. M. and Coleman, R. A. (1980). Enzymes of glycerolipid synthesis in eukaryotes. *Annual Review of Biochemistry* 49, 459-487.

Benador, I. Y., Veliova, M., Liesa, M. and Shirihai, O. S. (2019). Mitochondria bound to lipid droplets: where mitochondrial dynamics regulate lipid storage and utilization. *Cell Metabolism* 29, 827-835.

Benador, I. Y., Veliova, M., Mahdaviani, K., Petcherski, A., Wikstrom, J. D., Assali, E. A., Acín-Pérez, R., Shum, M., Oliveira, M. F., Cinti, S. et al. (2018). Mitochondria bound to lipid droplets have unique bioenergetics, composition, and dynamics that support lipid droplet expansion. *Cell Metabolism* 27, 869-885.e6.

Bersuker, K., Peterson, C. W. H., To, M., Sahl, S. J., Savikhin, V., Grossman, E. A., Nomura, D. K. and Olzmann, J. A. (2018). A proximity labeling strategy provides insights into the composition and dynamics of lipid droplet proteomes. *Developmental Cell* 44, 97-112.e7.

Bethke, L. L., Zilversmit, M., Nielsen, K., Daily, J., Volkman, S. K., Ndiaye, D., Lozovsky, E. R., Hartl, D. L. and Wirth, D. F. (2006). Duplication, gene conversion, and genetic diversity in the species-specific acyl-CoA synthetase gene family of *Plasmodium falciparum*. *Molecular and Biochemical Parasitology* 150, 10-24.

Binns, D., Januszewski, T., Chen, Y., Hill, J., Markin, V. S., Zhao, Y., Gilpin, C., Chapman, K. D., Anderson, R. G. W. and Goodman, J. M. (2006). An intimate collaboration between peroxisomes and lipid bodies. *Journal of Cell Biology* 173, 719-731.

Bopp, S., Pasaje, C. F. A., Summers, R. L., Magistrado-Coxen, P., Schindler, K. A., Corpas-Lopez, V., Yeo, T., Mok, S., Dey, S., Smick, S., Nasamu, A. S., Demas, A. R., Milne, R., Wiedemar, N., Corey, V., Gomez-Lorenzo, M. G., Franco, V., Early, A. M., Lukens, A. K., Milner, D., Furtado, J., Gamo, F. J., Winzeler, E. A., Volkman, S. K., Duffey, M., Laleu, B., Fidock, D. A., Wyllie, S., Niles, J. C. and Wirth, D. F. (2023). Potent acyl-CoA synthetase 10 inhibitors kill *Plasmodium falciparum* by disrupting triglyceride formation. *Nature Communications* 14, 1455.

Bouchoux, J., Beilstein, F., Pauquai, T., Guerrera, I. C., Chateau, D., Ly, N., Alqub, M., Klein, C., Chambaz, J., Rousset, M., Lacorte, J. M., Morel, E. and Demignot, S. (2011). The proteome of cytosolic lipid droplets isolated from differentiated Caco-2/TC7 enterocytes reveals cell-specific characteristics. *Biology of the Cell* 103, 499-517.

Brasaemle, D. L. and Wolins, N. E. (2016). Isolation of lipid droplets from cells by density gradient centrifugation. *Current Protocols in Cell Biology* 72, 3 15 1-3 15 13.

Bucci, C., Parton, R. G., Mather, I. H., Stunnenberg, H., Simons, K., Hoflack, B. and Zerial, M. (1992). The small GTPase rab5 functions as a regulatory factor in the early endocytic pathway. *Cell* 70, 715-728.

Cao, J., Zhou, Y., Peng, H., Huang, X., Stahler, S., Suri, V., Qadri, A., Gareski, T., Jones, J., Hahm, S., Perreault, M., McKew, J., Shi, M., Xu, X., Tobin, J. F. and Gimeno, R. E. (2011). Targeting Acyl-CoA:diacylglycerol acyltransferase 1 (DGAT1) with small molecule inhibitors for the treatment of metabolic diseases. *Journal of Biological Chemistry* 286, 41838-41851.

Cartwright, B. R., Binns, D. D., Hilton, C. L., Han, S., Gao, Q. and Goodman, J. M. (2014). Seipin performs dissectible functions in promoting lipid droplet biogenesis and regulating droplet morphology. *Molecular Biology of the Cell* 26, 726-739.

Cases, S., Novak, S., Zheng, Y.-W., Myers, H. M., Lear, S. R., Sande, E., Welch, C. B., Lusis, A. J., Spencer, T. A., Krause, B. R., Erickson, S. K. and Farese, R. V. Jr. (1998a). ACAT-2, a second mammalian acyl-CoA:Cholesterol Acyltransferase: Its cloning, expression, and characterization. *Journal of Biological Chemistry* 273, 26755-26764.

Cases, S., Smith, S. J., Zheng, Y.-W., Myers, H. M., Lear, S. R., Sande, E., Novak, S., Collins, C., Welch, C. B., Lusis, A. J., Erickson, S. K. and Farese, R. V. Jr. (1998b). Identification of a gene encoding an acyl CoA:diacylglycerol acyltransferase, a key enzyme in triacylglycerol synthesis. *Proceedings of the National Academy of Sciences* 95, 13018-13023.

Cases, S., Stone, S. J., Zhou, P., Yen, E., Tow, B., Lardizabal, K. D., Voelker, T. and Farese, R. V. (2001). Cloning of DGAT2, a second mammalian diacylglycerol acyltransferase, and related family members. *Journal of Biological Chemistry* 276, 38870-38876.

Chakraborty, S., Doktorova, M., Molugu, T. R., Heberle, F. A., Scott, H. L., Dzikovski, B., Nagao, M., Stingaciu, L. R., Standaert, R. F., Barrera, F. N., Katsaras, J., Khelashvili, G., Brown, M. F. and Ashkar, R. (2020). How cholesterol stiffens unsaturated lipid membranes. *PNAS Biophysics & Computational Biology* 117, 21896-21905.

Chang, C., Huh, H. Y., Cadigan, K. M. and Chang, T. Y. (1993). Molecular cloning and functional expression of human acyl-coenzyme A: cholesterol acyltransferase cDNA in mutant Chinese hamster ovary cells. *Journal of Biological Chemistry* 268, 20747-20755.

Chang, T.Y., Li, B.L., Chang, C. C. Y. and Urano, Y. (2009). Acyl-coenzyme A:cholesterol acyltransferases. *American Journal of Physiology-Endocrinology and Metabolism* 297, E1-E9.

Chang, T. Y., Chang, C. C. Y., Lu, X. and Lin, S. (2001). Catalysis of ACAT may be completed within the plane of the membrane: a working hypothesis. *Journal of Lipid Research* 42, 1933-1938.

Cheng, J., Fujita, A., Ohsaki, Y., Suzuki, M., Shinohara, Y. and Fujimoto, T. (2009). Quantitative electron microscopy shows uniform incorporation of triglycerides into existing lipid droplets. *Histochemistry & Cell Biology*132, 281-91.

Choudhary, V., Ojha, N., Golden, A. and Prinz, W. A. (2015). A conserved family of proteins facilitates nascent lipid droplet budding from the ER. *Journal of Cell Biology* 211, 261-271.

Choudhary, V. and Schneiter, R. (2021). A unique junctional interface at contact sites between the endoplasmic reticulum and lipid droplets. *Frontiers in Cell & Developmental Biology* 9, 650186.

Chung, J., Wu, X., Lambert, T. J., Lai, Z. W., Walther, T. C. and Farese, R. V. (2019). LDAF1 and Seipin form a lipid droplet assembly complex. *Developmental Cell* 51, 551-563.e7.

Clausen, M. K., Christiansen, K., Jensen, P. K. and Behnke, O. (1974). Isolation of lipid particles from baker's yeast. *FEBS Letters* 43, 176-179.

Clayton, R. B. (1964). The utilization of sterols by insects. *Journal of Lipid Research* 5, 3-19.

Cohen, A. W., Razani, B., Schubert, W., Williams, T. M., Wang, X. B., Iyengar, P., Brasaemle, D. L., Scherer, P. E. and Lisanti, M. P. (2004). Role of Caveolin-1 in the modulation of lipolysis and lipid droplet formation. *Diabetes* 53, 1261-1270.

Coleman, J. A., Quazi, F. and Molday, R. S. (2013). Mammalian P4-ATPases and ABC transporters and their role in phospholipid transport. *Biochimica et Biophysica Acta (BBA) - Molecular and Cell Biology of Lipids* 1831, 555-574.

Coleman, R. A. (2020). The “discovery” of lipid droplets: A brief history of organelles hidden in plain sight. *Biochimica et Biophysica Acta (BBA) - Molecular and Cell Biology of Lipids* 1865, 158762.

Coleman, R. A. and Lee, D. P. (2004). Enzymes of triacylglycerol synthesis and their regulation. *Progress in Lipid Research* 43, 134-76.

Coppens, I. and Vielemeyer, O. (2005). Insights into unique physiological features of neutral lipids in Apicomplexa: from storage to potential mediation in parasite metabolic activities. *International Journal for Parasitology* 35, 597-615.

Czarnecka, H. and Yokoyama, S. (1996). Regulation of cellular cholesterol efflux by Lecithin:Cholesterol Acyltransferase reaction through nonspecific lipid exchange. *Journal of Biological Chemistry* 271, 2023-2028.

Dahlqvist, A., Ståhl, U., Lenman, M., Banas, A., Lee, M., Sandager, L., Ronne, H. and Stymne, S. (2000). Phospholipid:diacylglycerol acyltransferase: An enzyme that catalyzes the acyl-CoA-independent formation of triacylglycerol in yeast and plants. *Proceedings of the National Academy of Sciences* 97, 6487-6492.

Dash, M., Sachdeva, S., Bansal, A. and Sinha, A. (2022). Gametogenesis in *Plasmodium*: delving deeper to connect the dots. *Frontiers in Cellular and Infection Microbiology* 12, 877907.

de Castro, F. A., Ward, G. E., Jambou, R., Attal, G., Mayau, V., Jaureguiberry, G., Braun-Breton, C., Chakrabarti, D. and Langsley, G. (1996). Identification of a family of Rab G-proteins in *Plasmodium falciparum* and a detailed characterisation of pfrab6. *Molecular and Biochemical Parasitology* 80, 77-88.

Denny, P. W., Field, M. C. and Smith, D. F. (2001). GPI-anchored proteins and glycoconjugates segregate into lipid rafts in Kinetoplastida. *FEBS Letters* 491, 148-153.

Dessens, J. T., Saeed, S., Tremp, A. Z. and Carter, V. (2011). Malaria crystalloids: specialized structures for parasite transmission? *Trends in Parasitology* 27(3), 106-110.

Dessens, J. T., Tremp, A. Z. and Saeed, S. (2021). Crystalloids: Fascinating parasite organelles essential for Malaria transmission. *Trends in parasitology*, *37*(7), 581–584.

Diaz, G., Melis, M., Batetta, B., Angius, F. and Falchi, A. M. (2008). Hydrophobic characterization of intracellular lipids in situ by Nile Red red/yellow emission ratio. *Micron* 39, 819-24.

Dudka, W., Salo, V. T. and Mahamid, J. (2024). Zooming into lipid droplet biology through the lens of electron microscopy. *FEBS Letters* 598, 1127-1142.

Dumesnil, C., Vanharanta, L., Prasanna, X., Omrane, M., Carpentier, M., Bhapkar, A., Enkavi, G., Salo, V. T., Vattulainen, I., Ikonen, E. and Thiam, A. R. (2023). Cholesterol esters form supercooled lipid droplets whose nucleation is facilitated by triacylglycerols. *Nature Communications* 14, 915.

Ebine, K., Fujimoto, M., Okatani, Y., Nishiyama, T., Goh, T., Ito, E., Dainobu, T., Nishitani, A., Uemura, T., Sato, M. H., Thordal-Christensen, H., Tsutsumi, N., Nakano, A. and Ueda, T. A. (2011). A membrane trafficking pathway regulated by the plant-specific RAB GTPase ARA6. *Nature Cell Biology* 13, 853-859.

Ebine, K., Hirai, M., Sakaguchi, M., Yahata, K., Kaneko, O. and Saito-Nakano, Y. (2016). *Plasmodium* Rab5b is secreted to the cytoplasmic face of the tubovesicular network in infected red blood cells together with N-acylated adenylate kinase 2. *Malaria Journal* 15, 323.

Ebine, K., Naoto, M., Masaru, F., Tomohiro, U., Akihiko, N. and and Ueda, T. (2012). Endosomal trafficking pathway regulated by ARA6, a RAB5 GTPase unique to plants. *Small GTPases* 3, 23-27.

Edaye, S. and Georges, E. (2015). Characterization of native PfABCG protein in *Plasmodium falciparum*. *Biochemical Pharmacology* 97, 137-46.

Ehrenman, K., Sehgal, A., Lige, B., Stedman, T. T., Joiner, K. A. and Coppens, I. (2010). Novel roles for ATP-binding cassette G transporters in lipid redistribution in *Toxoplasma*. *Molecular Microbiology* 76, 1232-49.

Elliott, D. A., McIntosh, M. T., Hosgood, H. D., 3rd, Chen, S., Zhang, G., Baevova, P. and Joiner, K. A. (2008). Four distinct pathways of hemoglobin uptake in the malaria parasite *Plasmodium falciparum*. *PNAS Cell Biology* 105, 2463-8.

Evers, F., Roverts, R., Boshoven, C., Kea-te Lindert, M., Verhoef, J. M. J., Sommerdijk, N., Sinden, R. E., Akiva, A. and Kooij, T. W. A. (2025). Comparative 3D ultrastructure of *Plasmodium falciparum* gametocytes. *Nature Communications* 16, 69.

Ezougou, C. N., Ben-Rached, F., Moss, D. K., Lin, J. W., Black, S., Knuepfer, E., Green, J. L., Khan, S. M., Mukhopadhyay, A., Janse, C. J., Coppens, I., Year, H., Holder, A. A. and Langsley, G. (2014). *Plasmodium falciparum* Rab5B is an N-terminally myristoylated Rab GTPase that is targeted to the parasite's plasma and food vacuole membranes. *PLOS One* 9, e87695.

Farese, R. V., Jr. and Walther, T. C. (2009). Lipid droplets finally get a little R-E-S-P-E-C-T. *Cell* 139, 855-60.

Fivelman, Q. L., McRobert, L., Sharp, S., Taylor, C. J., Saeed, M., Swales, C. A., Sutherland, C. J. and Baker, D. A. (2007). Improved synchronous production of *Plasmodium falciparum* gametocytes in vitro. *Molecular and Biochemical Parasitology* 154(1), 119-123.

Flammersfeld, A., Panyot, A., Yamaryo-Botté, Y., Aurass, P., Przyborski, J. M., Flieger, A., Botté, C. and Pradel, G. (2020). A patatin-like phospholipase functions during gametocyte induction in the malaria parasite *Plasmodium falciparum*. *Cellular Microbiology* 22, e13146.

Francia, M. E. and Striepen, B. (2014). Cell division in apicomplexan parasites. *Nature Reviews Microbiology* 12, 125-36.

Frankland, S., Adisa, A., Horrocks, P., Taraschi, T. F., Schneider, T., Elliott, S. R., Rogerson, S. J., Knuepfer, E., Cowman, A. F., Newbold, C. I. and Tilley, L. (2006). Delivery of the malaria virulence protein PfEMP1 to the erythrocyte surface requires cholesterol-rich domains. *Eukaryotic Cell* 5, 849-60.

Frölich, S., Schubert, C., Bienzle, U. and Jenett-Siems, K. (2005). In vitro antiplasmodial activity of prenylated chalcone derivatives of hops (*Humulus lupulus*) and their interaction with haemin. *Journal of Antimicrobial Chemotherapy* 55, 883-887.

Fujimoto, T. and Ohsaki, Y. (2006). Cytoplasmic lipid droplets: rediscovery of an old structure as a unique platform. *ANNALS of the New York Academy of Sciences* 1086, 104-15.

Fujimoto, T., Ohsaki, Y., Suzuki, M. and Cheng, J. (2013). Imaging lipid droplets by electron microscopy. *Methods in Cell Biology* 116, 227-51.

Fujimoto, T. and Parton, R. G. (2011). Not just fat: the structure and function of the lipid droplet. *Cold Spring Harbor Perspectives in Biology* 3(3), a004838.

Fujimoto, Y., Itabe, H., Sakai, J., Makita, M., Noda, J., Mori, M., Higashi, Y., Kojima, S. and Takano, T. (2004). Identification of major proteins in the lipid droplet-enriched fraction isolated from the human hepatocyte cell line HuH7. *Biochimica et Biophysica Acta (BBA) - Molecular Cell Research* 1644, 47-59.

Gao, G., Chen, F.-J., Zhou, L., Su, L., Xu, D., Xu, L. and Li, P. (2017). Control of lipid droplet fusion and growth by CIDE family proteins. *Biochimica et Biophysica Acta (BBA)-Molecular & Cell Biology of Lipids* 1862, 1197-1204.

Gao, Y., Chen, G. and Weselake, R. J. (2014). A rapid nile red fluorescence-based method for triacylglycerol content in microspore-derived cell suspension cultures of Brassica napus. *Lipids* 49, 1161-8.

Garten, M., Beck, J. R., Roth, R., Tenkova-Heuser, T., Heuser, J., Istvan, E. S., Bleck, C. K. E., Goldberg, D. E. and Zimmerberg, J. (2020). Contacting domains segregate a lipid transporter from a solute transporter in the malarial host–parasite interface. *Nature Communications* 11, 3825.

Gatton Michelle, L., Martin Laura, B. and Cheng, Q. (2004). Evolution of resistance to sulfadoxine-pyrimethamine in *Plasmodium falciparum*. *Antimicrobial Agents and Chemotherapy* 48, 2116-2123.

Gibellini, F. and Smith, T. K. (2010). The Kennedy pathway—De novo synthesis of phosphatidylethanolamine and phosphatidylcholine. *IUBMB Life* 62, 414-428.

Glomset, J. A. (1968). The plasma lecithin:cholesterol acyltransferase reaction. *Journal of Lipid Research* 9, 155-167.

Gong, J., Sun, Z., Wu, L., Xu, W., Schieber, N., Xu, D., Shui, G., Yang, H., Parton, R. G. and Li, P. (2011). Fsp27 promotes lipid droplet growth by lipid exchange and transfer at lipid droplet contact sites. *Journal of Cell Biology* 195, 953-963.

Goodman, J. M. (2019). LDAF1 holds the key to Seipin function. *Developmental Cell* 51, 544-545.

Graf, G. A., Yu, L., Li, W. P., Gerard, R., Tuma, P. L., Cohen, J. C. and Hobbs, H. H. (2003). ABCG5 and ABCG8 are obligate heterodimers for protein trafficking and biliary cholesterol excretion. *Journal of Biological Chemistry* 278, 48275-82.

Graves, P. M., Gelband, H. and Garner, P. (2012). Primaquine for reducing *Plasmodium falciparum* transmission. *Cochrane Database of Systematic Reviews*, Cd008152.

Greenberg, A. S., Egan J. J., Wek, S. A., Garty, N. B., Blanchette-Mackie, E. J. and Londos, C. (1991). Perilipin, a major hormonally regulated adipocyte-specific phosphoprotein associated with the periphery of lipid storage droplets. *Journal of Biological Chemistry* 266(17), 11341–11346.

Greenspan, P., Eugene P. Mayer, and Stanley D. Fowler. (1985). Nile Red: A selective fluorescent stain for intracellular lipid droplets. *Journal of Cell Biology* 100, 965-973.

Greenspan, P. and Fowler, S. D. (1985). Spectrofluorometric studies of the lipid probe, nile red. *Journal of Lipid Research* 26, 781-9.

Gross, D. A., Zhan, C. and Silver, D. L. (2011). Direct binding of triglyceride to fat storage-inducing transmembrane proteins 1 and 2 is important for lipid droplet formation. *Proceedings of the National Academy of Sciences* 108, 19581-19586.

Gruenberg, J., Allred, D. R. and Sherman, I. W. (1983). Scanning electron microscope-analysis of the protrusions (knobs) present on the surface of *Plasmodium falciparum*-infected erythrocytes. *Journal of Cell Biology* 97, 795-802.

Gubern, A., Casas, J., Barceló-Torns, M., Barneda, D., de la Rosa, X., Masgrau, R., Picatoste, F., Balsinde, J., Balboa, M. A. and Claro, E. (2008). Group IVA phospholipase A2 is necessary for the biogenesis of lipid droplets. *Journal of Biological Chemistry* 283, 27369-27382.

Gulati, S., Ekland, E. H., Ruggles, K. V., Chan, R. B., Jayabalasingham, B., Zhou, B., Mantel, P. Y., Lee, M. C., Spottiswoode, N., Coburn-Flynn, O., Hjelmqvist, D., Worgall, T. S., Marti, M., Di Paolo, G. and Fidock, D. A. (2015). Profiling the essential nature of lipid metabolism in asexual blood and gametocyte stages of *Plasmodium falciparum*. *Cell Host & Microbe* 18, 371-81.

Gupta, S. K., Schulman, S. and Vanderberg, J. P. (1985). Stage-dependent toxicity of N-acetyl-glucosamine to Plasmodium falciparum. *The Journal of protozoology*, *32*(1), 91–95.

Hamai, C., Yang, T., Kataoka, S., Cremer, P. S. and Musser, S. M. (2006). Effect of average phospholipid curvature on supported bilayer formation on glass by vesicle fusion. *Biophysical Journal* 90, 1241-1248.

Hayakawa, E. H., Kato, H., Nardone, G. A. and Usukura, J. (2021). A prospective mechanism and source of cholesterol uptake by *Plasmodium falciparum*-infected erythrocytes co-cultured with HepG2 cells. *Parasitology International* 80, 102179.

Hayakawa, E. H., Yamaguchi, K., Mori, M. and Nardone, G. (2020). Real-time cholesterol sorting in *Plasmodium falciparum*-erythrocytes as revealed by 3D label-free imaging. *Nature Scientific Reports* 10, 2794.

Hayat, M. A. (1973). Principles and techniques of electron microscopy. Biological applications, volume 3.

Hayes, T. L., Lindgren, F. T. and Gofman, J. W. (1963). A quantitative determination of the osmium tetroxide-lipoprotein interaction. *Journal of Cell Biology* 19, 251-255.

Hoang, A. N., Sandlin, R. D., Omar, A., Egan, T. J. and Wright, D. W. (2010). The neutral lipid composition present in the digestive vacuole of *Plasmodium falciparum* concentrates heme and mediates beta-hematin formation with an unusually low activation energy. *Biochemistry* 49, 10107-16.

Horn, P. J., James, C. N., Gidda, S. K., Kilaru, A., Dyer, J. M., Mullen, R. T., Ohlrogge, J. B. and Chapman, K. D. (2013). Identification of a new class of lipid droplet-associated proteins in plants. *Plant Physiology* 162, 1926-1936.

Hugenroth, M. and Bohnert, M. (2020). Come a little bit closer! Lipid droplet-ER contact sites are getting crowded. *Biochimica et Biophysica Acta (BBA) – Moecular Cell Research* 1867(2), 118603.

Hussain, S. S., Tran, T.-M., Ware, T. B., Luse, M. A., Prevost, C. T., Ferguson, A. N., Kashatus, J. A., Hsu, K.-L. and Kashatus, D. F. (2021). RalA and PLD1 promote lipid droplet growth in response to nutrient withdrawal. *Cell Reports* 36.

Inokoshi, J., Kawamoto, K., Takagi, Y., Matsuhama, M., Omura, S. and Tomoda, H. (2009). Expression of two human acyl-CoA:diacylglycerol acyltransferase isozymes in yeast and selectivity of microbial inhibitors toward the isozymes. *The Journal of Antibiotics* 62, 51-54.

Istvan, E. S., Das, S., Bhatnagar, S., Beck, J. R., Owen, E., Llinas, M., Ganesan, S. M., Niles, J. C., Winzeler, E., Vaidya, A. B. and Goldberg, D. E. (2019). *Plasmodium* Niemann-Pick type C1-related protein is a druggable target required for parasite membrane homeostasis. *eLife* 8, e40529.

Jackson, K. E., Klonis, N., Ferguson, D. J., Adisa, A., Dogovski, C. and Tilley, L. (2004). Food vacuole-associated lipid bodies and heterogeneous lipid environments in the malaria parasite, *Plasmodium falciparum*. *Molecular Microbiology* 54, 109-22.

Jacquier, N., Choudhary, V., Mari, M., Toulmay, A., Reggiori, F. and Schneiter, R. (2011). Lipid droplets are functionally connected to the endoplasmic reticulum in Saccharomyces cerevisiae. *Journal of Cell Science* 124, 2424-37.

Jain, A., and Holthuis, J. C. M. (2017). Membrane contact sites, ancient and central hubs of cellular lipid logistics. *Biochimica et biophysica acta. Molecular cell research*, *1864*(9), 1450–1458.

Jambunathan, S., Yin, J., Khan, W., Tamori, Y. and Puri, V. (2011). FSP27 promotes lipid droplet clustering and then fusion to regulate triglyceride accumulation. *PLOS One* 6, e28614.

Jarsch, I. K., Daste, F. and Gallop, J. L. (2016). Membrane curvature in cell biology: An integration of molecular mechanisms. *Journal of Cell Biology* 214, 375-387.

Josling, G. A. and Llinas, M. (2015). Sexual development in *Plasmodium* parasites: knowing when it's time to commit. *Nature Reviews Microbiology* 13, 573-587.

Joyce, C. W., Shelness, G. S., Davis, M. A., Lee, R. G., Skinner, K., Anderson, R. A. and Rudel, L. L. (2000). ACAT1 and ACAT2 membrane topology segregates a serine residue essential for activity to opposite sides of the endoplasmic reticulum membrane. *Molecular Biology of the Cell* 11, 3675-3687.

Khor, V. K., Ahrends, R., Lin, Y., Shen, W. J., Adams, C. M., Roseman, A. N., Cortez, Y., Teruel, M. N., Azhar, S. and Kraemer, F. B. (2014). The proteome of cholesteryl-ester-enriched versus triacylglycerol-enriched lipid droplets. *PLOS One* 9, e105047.

Kim, H. U., Lee, K. R., Go, Y. S., Jung, J. H., Suh, M. C. and Kim, J. B. (2011). Endoplasmic reticulum-located PDAT1-2 from castor bean enhances hydroxy fatty acid accumulation in transgenic plants. *Plant and Cell Physiology* 52, 983-993.

Kim, S. C., Chen, Y., Mirza, S., Xu, Y., Lee, J., Liu, P. and Zhao, Y. (2006). A clean, more efficient method for in-solution digestion of protein mixtures without detergent or urea. *Journal of Proteome Research* 5, 3446-3452.

Klein, R. L. and Rudel, L. L. (1983). Effect of dietary cholesterol level on the composition of thoracic duct lymph lipoproteins isolated from nonhuman primates. *Journal of Lipid Research* 24, 357-367.

Koivuniemi, A., Heikelä, M., Kovanen, P. T., Vattulainen, I. and Hyvönen, M. T. (2009). Atomistic simulations of phosphatidylcholines and cholesteryl esters in high-density lipoprotein-sized lipid droplet and trilayer: clues to cholesteryl ester transport and storage. *Biophysical Journal* 96, 4099-4108.

Krahmer, N., Guo, Y., Wilfling, F., Hilger, M., Lingrell, S., Heger, K., Newman, Heather W., Schmidt-Supprian, M., Vance, Dennis E., Mann, M., Farese, R. V. Jr. and Walther, T. C. (2011). Phosphatidylcholine synthesis for lipid droplet expansion is mediated by localized activation of CTP:Phosphocholine Cytidylyltransferase. *Cell Metabolism* 14, 504-515.

Kremer, K., Kamin, D., Rittweger, E., Wilkes, J., Flammer, H., Mahler, S., Heng, J., Tonkin, C. J., Langsley, G., Hell, S. W., Carruthers, V. B., Ferguson, D. J. and Meissner, M. (2013). An overexpression screen of toxoplasma gondii Rab-GTPases reveals distinct transport routes to the micronemes. *PLOS Pathogens* 9, e1003213.

Kuerschner, L., Moessinger, C. and Thiele, C. (2008). Imaging of lipid biosynthesis: How a neutral lipid enters lipid droplets. *Traffic* 9, 338-352.

Kunduri, G., Acharya, U. and Acharya, J. K. (2022). Lipid polarization during cytokinesis. *Cells* 11(24), 3977.

Ladinsky, M. S., Mardones, G. A., Orlicky, D. J., Howell, K. E. and McManaman, J. L. (2019). Electron tomography revels that milk lipids originate from endoplasmic reticulum domains with novel structural features. *Journal of Mammary Gland Biology and Neoplasia* 24, 293-304.

Lambros, C. and Vanderberg, J. P. (1979). Synchronization of *Plasmodium falciparum* erythrocytic stages in culture. *The Journal of Parasitology* 65(3), 418-420.

Lardizabal, K. D., Mai, J. T., Wagner, N. W., Wyrick, A., Voelker, T. and Hawkins, D. J. (2001). DGAT2 is a new diacylglycerol acyltransferase gene family: purification, cloning, and expression in insect cells of two polypeptides from *Mortierella ramanniana* with diacylglycerol acyltransferase activity. *Journal of Biological Chemistry* 276, 38862-38869.

Lasonder, E., Rijpma, S. R., van Schaijk, Ben C. L., Hoeijmakers, Wieteke A. M., Kensche, P. R., Gresnigt, M. S., Italiaander, A., Vos, M. W., Woestenenk, R., Bousema, T., Mair, G. R., Khan, S. M., Janse, C. J., Bártfai, R. and Sauerwein, R. W. (2016). Integrated transcriptomic and proteomic analyses of *P. falciparum* gametocytes: molecular insight into sex-specific processes and translational repression. *Nucleic Acids Research* 44, 6087-6101.

Leber, R., Zinser, E., Paltauf, F., Daum, G. and Zellnig, G. (1994). Characterization of lipid particles of the yeast, *Saccharomyces cerevisiae*. *Yeast* 10, 1421-1428.

Lee, J., Matuschewski, K., van Dooren, G., Maier, A. G. and Rug, M. (2024). Lipid droplet dynamics are essential for the development of the malaria parasite *Plasmodium falciparum*. *Journal of Cell Science* 137(20):jcs262162.

Lee, J. Y., Kinch, L. N., Borek, D. M., Wang, J., Wang, J., Urbatsch, I. L., Xie, X. S., Grishin, N. V., Cohen, J. C., Otwinowski, Z., Hobbs, H. H. and Rosenbaum, D. M. (2016). Crystal structure of the human sterol transporter ABCG5/ABCG8. *Nature* 533, 561-4.

Lehner, R. and Kuksis, A. (1996). Biosynthesis of triacylglycerols. *Progress in Lipid Research* 35, 169-201.

Li, C. and Yu, S. S. (2016). Rab proteins as regulators of lipid droplet formation and lipolysis. *Cell Biology International* 40, 1026-32.

Li, D., Yang, S. G., He, C. W., Zhang, Z. T., Liang, Y., Li, H., Zhu, J., Su, X., Gong, Q. and Xie, Z. (2020). Excess diacylglycerol at the endoplasmic reticulum disrupts endomembrane homeostasis and autophagy. *BMC Biology* 18, 107.

Li, D., Zhao, Y. G., Li, D., Zhao, H., Huang, J., Miao, G., Feng, D., Liu, P., Li, D. and Zhang, H. (2019). The ER-localized protein DFCP1 modulates ER-lipid droplet contact formation. *Cell Reports* 27(2), 343-358.

Liang, J. J., Oelkers, P., Guo, C., Chu, P. C., Dixon, J. L., Ginsberg, H. N. and Sturley, S. L. (2004). Overexpression of human diacylglycerol acyltransferase 1, acyl-coa:cholesterol acyltransferase 1, or acyl-CoA:cholesterol acyltransferase 2 stimulates secretion of apolipoprotein B-containing lipoproteins in McA-RH7777 cells. *Journal of Biological Chemistry* 279(43), 44938-44944.

Listenberger, L. L., Han, X., Lewis, S. E., Cases, S., Farese, R. V., Ory, D. S. and Schaffer, J. E. (2003). Triglyceride accumulation protects against fatty acid-induced lipotoxicity. *Proceedings of the National Academy of Sciences* 100, 3077-3082.

Liu, P., Bartz, R., Zehmer, J. K., Ying, Y.-s., Zhu, M., Serrero, G. and Anderson, R. G. W. (2007). Rab-regulated interaction of early endosomes with lipid droplets. *Biochimica et Biophysica Acta (BBA) - Molecular Cell Research* 1773, 784-793.

London, E. and Brown, D. A. (2000). Insolubility of lipids in triton X-100: physical origin and relationship to sphingolipid/cholesterol membrane domains (rafts). *Biochimica et Biophysica Acta (BBA) - Biomembranes* 1508(1-2), 182-195.

Londos, C., Sztalryd, C., Tansey, J. T. and Kimmel, A. R. (2005). Role of PAT proteins in lipid metabolism. *Biochimie* 87(1), 45-49.

López-Barragán, M. J., Lemieux, J., Quiñones, M., Williamson, K. C., Molina-Cruz, A., Cui, K., Barillas-Mury, C., Zhao, K. and Su, X.-z. (2011). Directional gene expression and antisense transcripts in sexual and asexual stages of *Plasmodium falciparum*. *BMC Genomics* 12, 587.

Luo, J., Yang, H. and Song, B. L. (2020). Mechanisms and regulation of cholesterol homeostasis. *Nature Reviews Molecular Cell Biology* 21, 225-245.

Ma, X., Qian, H., Chen, A., Ni, H. M. and Ding, W. X. (2021). Perspectives on mitochondria–ER and mitochondria–lipid droplet contact in hepatocytes and hepatic lipid metabolism. *Cells*, 10(9), 2273.

Maehama, T., Tanaka, M., Nishina, H., Murakami, M., Kanaho, Y. and Hanada, K. (2008). RalA functions as an indispensable signal mediator for the nutrient-sensing system. *Journal of Biological Chemistry* 283, 35053-35059.

Maguire, P. A. and Sherman, I. W. (1990). Phospholipid composition, cholesterol content and cholesterol exchange in *Plasmodium falciparum*-infected red cells. *Molecular and Biochemical Parasitology* 38, 105-112.

Maier, A. G., Matuschewski, K., Zhang, M. and Rug, M. (2019). *Plasmodium falciparum*. *Trends in Parasitology* 35(6), 481-482.

Maier, A. G. and Rug, M. (2013). In vitro culturing *Plasmodium falciparum* erythrocytic stages. *Methods in Molecular Biology* 923, 3-15.

Maier, A. G., Rug, M., O'Neill, M. T., Beeson, J. G., Marti, M., Reeder, J. and Cowman, A. F. (2006). Skeleton-binding protein 1 functions at the parasitophorous vacuole membrane to traffic PfEMP1 to the *Plasmodium falciparum*–infected erythrocyte surface. *Blood* 109, 1289-1297.

Maier, A. G. and van Ooij, C. (2022). The role of cholesterol in invasion and growth of malaria parasites. *Frontiers in Cellular & Infecttion Microbiology* 12, 984049.

Malhotra, V. and Campelo, F. (2011). PKD regulates membrane fission to generate TGN to cell surface transport carriers. *Cold Spring Harbor Perspectives in Biology* 3(2), a005280.

Martin, S., Driessen, K., Nixon, S. J., Zerial, M. and Parton, R. G. (2005). Regulated localization of Rab18 to lipid droplets: effects of lipolytic stimulation and inhibition of lipid droplet catabolism. *Journal of Biological Chemistry* 280(51), 42325-42335.

McMahon, H. T. and Boucrot, E. (2015). Membrane curvature at a glance. *Journal of Cell Science* 128, 1065-1070.

Meiner, V. L., Cases, S., Myers, H. M., Sande, E. R., Bellosta, S., Schambelan, M., Pitas, R. E., McGuire, J., Herz, J. and Farese Jr, R. V. (1996). Disruption of the acyl-CoA: cholesterol acyltransferase gene in mice: evidence suggesting multiple cholesterol esterification enzymes in mammals. *Proceedings of the National Academy of Sciences* 93, 14041-14046.

Meis, J. F. and Ponnudurai, T. (1987). Ultrastructural studies on the interaction of Plasmodium falciparum ookinetes with the midgut epithelium of Anopheles stephensi mosquitoes. *Parasitology research 73*(6), 500–506.

Michelis, S., Danglot, L., Vauchelles, R., Klymchenko, A. S. and Collot, M. (2022). Imaging and measuring vesicular acidification with a plasma membrane-targeted ratiometric pH probe. *Analytical Chemistry* 94(15), 5996-6003.

Miner, G. E., So, C. M., Edwards, W., Ragusa, J. V., Wine, J. T., Wong Gutierrez, D., Airola, M. V., Herring, L. E., Coleman, R. A., Klett, E. L. and Cohen, S. (2023). PLIN5 interacts with FATP4 at membrane contact sites to promote lipid droplet-to-mitochondria fatty acid transport. *Developmental Cell* 58(14), 1250-1265.e6.

Mitamura, T. and Palacpac, N. M. (2003). Lipid metabolism in *Plasmodium falciparum*-infected erythrocytes: possible new targets for malaria chemotherapy. *Microbes & Infection* 5(6), 545-552.

Miyazaki, A., Sakashita, N., Lee, O., Takahashi, K., Horiuchi, S., Hakamata, H., Morganelli, P. M., Chang, C. C. and Chang, T.-Y. (1998). Expression of ACAT-1 protein in human atherosclerotic lesions and cultured human monocytes-macrophages. *Arteriosclerosis, Thrombosis, and Vascular Biology* 18, 1568-1574.

Morse, D., Webster, W., Kalanon, M., Langsley, G. and McFadden, G. I. (2016). *Plasmodium falciparum* Rab1A localizes to rhoptries in schizonts. *PLOS One* 11, e0158174.

Murphy, D. J. (2012). The dynamic roles of intracellular lipid droplets: from archaea to mammals. *Protoplasma* 249, 541-585.

Murphy, D. J. and Vance, J. (1999). Mechanisms of lipid-body formation. *Trends in Biochemical Sciences* 24, 109-115.

Murphy, S., Martin, S. and Parton, R. G. (2009). Lipid droplet-organelle interactions; sharing the fats. *Biochimica et Biophysica Acta (BBA) – Molecular & Cell Biology of Lipids* 1791(6), 441-447.

Nakanishi, T. and Ross, D. D. (2012). Breast cancer resistance protein (BCRP/ABCG2): its role in multidrug resistance and regulation of its gene expression. *Chinese Journal of Cancer* 31(2),73-99

Nawabi, P., Lykidis, A., Ji, D. and Haldar, K. (2003). Neutral-lipid analysis reveals elevation of acylglycerols and lack of cholesterol esters in *Plasmodium falciparum*-infected erythrocytes. *Eukaryotic Cell* 2, 1128-1131.

Ngotho, P., Soares, A. B., Hentzschel, F., Achcar, F., Bertuccini, L. and Marti, M. (2019). Revisiting gametocyte biology in malaria parasites. *FEMS microbiology reviews*, *43*(4), 401–414.

Nishimoto, Y. and Tamori, Y. (2017). CIDE family-mediated unique lipid droplet morphology in white adipose tissue and brown adipose tissue determines the adipocyte energy metabolism. *Journal of Atherosclerosis and Thrombosis* 24, 989-998.

Ohgami, N., Kuniyasu, A., Furukawa, K., Miyazaki, A., Hakamata, H., Horiuchi, S. and Nakayama, H. (2000). Glibenclamide acts as an inhibitor of Acyl-CoA:Cholesterol Acyltransferase enzyme. *Biochemical and Biophysical Research Communications* 277, 417-422.

Olzmann, J. A. and Carvalho, P. (2019). Dynamics and functions of lipid droplets. *Nature Reviews Molecular Cell Biology* 20, 137-155.

Ouji, M., Augereau, J. M., Paloque, L. and Benoit-Vical, F. (2018). *Plasmodium falciparum* resistance to artemisinin-based combination therapies: A sword of Damocles in the path toward malaria elimination. *Parasite* 25, 24.

Ouweneel, A. B., Thomas, M. J. and Sorci-Thomas, M. G. (2020). The ins and outs of lipid rafts: functions in intracellular cholesterol homeostasis, microparticles, and cell membranes: Thematic Review Series: Biology of Lipid Rafts. *Journal of Lipid Research* 61(5), 676-686.

Ouyang, Q., Chen, Q., Ke, S., Ding, L., Yang, X., Rong, P., Feng, W., Cao, Y., Wang, Q., Li, M., Su, S., Wei, W., Liu, M., Liu, J., Zhang, X., Li, J. Z., Wang, H. Y. and Chen, S. (2023). Rab8a as a mitochondrial receptor for lipid droplets in skeletal muscle. *Developmental Cell* 58, 289-305.e6.

Ozeki, S., Cheng, J., Tauchi-Sato, K., Hatano, N., Taniguchi, H. and Fujimoto, T. (2005). Rab18 localizes to lipid droplets and induces their close apposition to the endoplasmic reticulum-derived membrane. *Journal of Cell Science* 118, 2601-2611.

Palacpac, N. M., Hiramine, Y., Mi-ichi, F., Torii, M., Kita, K., Hiramatsu, R., Horii, T. and Mitamura, T. (2004a). Developmental-stage-specific triacylglycerol biosynthesis, degradation and trafficking as lipid bodies in *Plasmodium falciparum*-infected erythrocytes. *Journal of Cell Science* 117, 1469-1480.

Palacpac, N. M., Hiramine, Y., Seto, S., Hiramatsu, R., Horii, T. and Mitamura, T. (2004b). Evidence that *Plasmodium falciparum* diacylglycerol acyltransferase is essential for intraerythrocytic proliferation. *Biochemical & Biophysical Research Communications* 321(4), 1062-1068.

Parks, J. S., Huggins, K. W., Gebre, A. K. and Burleson, E. R. (2000). Phosphatidylcholine fluidity and structure affect lecithin:cholesterol acyltransferase activity. *Journal of Lipid Research* 41, 546-553.

Patel, H. H. and Insel, P. A. (2008). Lipid rafts and caveolae and their role in compartmentation of redox signaling. *Antioxidants & Redox Signaling* 11, 1357-1372.

Pearson, W. R. (2013). An introduction to sequence similarity ("homology") searching. *Current Protocols in Bioinformatics* 42(1), 3.1.1-3.1.8

Pelle, K. G., Oh, K., Buchholz, K., Narasimhan, V., Joice, R., Milner, D. A., Brancucci, N. M. B., Ma, S., Voss, T. S., Ketman, K., Seydel, K. B., Taylor, T. E., Barteneva, N. S., Huttenhower, C. and Marti, M. (2015). Transcriptional profiling defines dynamics of parasite tissue sequestration during malaria infection. *Genome Medicine* 7, 19.

Pennington, K. L., Chan, T. Y., Torres, M. P. and Andersen, J. L. (2018). The dynamic and stress-adaptive signaling hub of 14-3-3: emerging mechanisms of regulation and context-dependent protein–protein interactions. *Oncogene* 37, 5587-5604.

Phan, C. T. and Tso, P. (2021). Intestinal lipid absorption and transport. *Frontiers in Bioscience-Landmark* 26(5), D299-D319.

Pietsch, E., Niedermüller, K., Andrews, M., Meyer, B. S., Lenz, T. L., Wilson, D. W., Gilberger, T.-W. and Burda, P.-C. (2024). Disruption of a *Plasmodium falciparum* patatin-like phospholipase delays male gametocyte exflagellation. *Molecular Microbiology* 121, 529-542.

Pohnl, M., Trollmann, M. F. W. and Bockmann, R. A. (2023). Nonuniversal impact of cholesterol on membranes mobility, curvature sensing and elasticity. *Nature Communications* 14, 8038.

Pol, A., Gross, S. P. and Parton, R. G. (2014). Review: biogenesis of the multifunctional lipid droplet: lipids, proteins, and sites. *Journal of Cell Biology* 204, 635-46.

Polheim, D., David, J., Schultz, F. M., Wylie, M. B. and Johnston, J. M. (1973). Regulation of triglyceride biosynthesis in adipose and intestinal tissue. *Journal of Lipid Research* 14, 415-421.

Ponnudurai, T., Lensen, A. H., Meis, J. F. and Meuwissen, J. H. (1986). Synchronization of Plasmodium falciparum gametocytes using an automated suspension culture system. *Parasitology 93*, 263-274.

Prattes, S., Hörl, G., Hammer, A., Blaschitz, A., Graier, W. F., Sattler, W., Zechner, R. and Steyrer, E. (2000). Intracellular distribution and mobilization of unesterified cholesterol in adipocytes: triglyceride droplets are surrounded by cholesterol-rich ER-like surface layer structures. *Journal of Cell Science* 113, 2977-2989.

Prinz, W. A., Toulmay, A. and Balla, T. (2020). The functional universe of membrane contact sites. *Nature Reviews Molecular Cell Biology* 21, 7-24.

Quevillon, E., Spielmann, T., Brahimi, K., Chattopadhyay, D., Yeramian, E. and Langsley, G. (2003). The *Plasmodium falciparum* family of Rab GTPases. *Gene* 306, 13-25.

Rajendran, L., Le Lay, S. and Illges, H. (2007). Raft association and lipid droplet targeting of flotillins are independent of caveolin. *Biological Chemistry* 388(3), 307-314.

Rakotonirina-Ricquebourg, R., Costa, V. and Teixeira, V. (2022). Hello from the other side: Membrane contact of lipid droplets with other organelles and subsequent functional implications. *Progress in Lipid Research* 85, 101141.

Ramaprasad, A., Burda, P.-C., Koussis, K., Thomas, J. A., Pietsch, E., Calvani, E., Howell, S. A., MacRae, J. I., Snijders, A. P., Gilberger, T. W. and Blackman, M. J. (2023). A malaria parasite phospholipase facilitates efficient asexual blood stage egress. *PLOS Pathogens* 19, e1011449.

Ribaut, C., Berry, A., Chevalley, S., Reybier, K., Morlais, I., Parzy, D., Nepveu, F., Benoit-Vical, F. and Valentin, A. (2008). Concentration and purification by magnetic separation of the erythrocytic stages of all human *Plasmodium* species. *Malaria Journal* 7, 45.

Ridgway, M. C., Cihalova, D., Brown, S. H. J., Tran, P., Mitchell, T. W. and Maier, A. G. (2022). Analysis of sex-specific lipid metabolism of *Plasmodium falciparum* points to the

importance of sphingomyelin for gametocytogenesis. *Journal of Cell Science* 135(5), jcs259592.

Ridgway Melanie, C., Shea Kwong, S., Cihalova, D. and Maier Alexander, G. (2020). Novel method for the separation of male and female gametocytes of the malaria parasite *Plasmodium falciparum* that enables biological and drug discovery. *mSphere* 5(4), e00671-20.

Ross, A. C., Go, K. J., Heider, J. G. and Rothblat, G. H. (1984). Selective inhibition of acyl coenzyme A:cholesterol acyltransferase by compound 58-035. *Journal of Biological Chemistry* 259, 815-819.

Rousset, X., Vaisman, B., Amar, M., Sethi, A. A. and Remaley, A. T. (2009). Lecithin: cholesterol acyltransferase – from biochemistry to role in cardiovascular disease. *Current Opinion in Endocrinology, Diabetes and Obesity* 16, 163-171.

Rudlaff, R. M., Kraemer, S., Marshman, J. and Dvorin, J. D. (2020). Three-dimensional ultrastructure of *Plasmodium falciparum* throughout cytokinesis. *PLOS Pathogens* 16, e1008587.

Saha, S., Anilkumar, A. A. and Mayor, S. (2016). GPI-anchored protein organization and dynamics at the cell surface. *Journal of Lipid Research* 57, 159-175.

Salo, V. T., Li, S., Vihinen, H., Hölttä-Vuori, M., Szkalisity, A., Horvath, P., Belevich, I., Peränen, J., Thiele, C. and Somerharju, P. (2019). Seipin facilitates triglyceride flow to lipid droplet and counteracts droplet ripening via endoplasmic reticulum contact. *Developmental Cell* 50, 478-493. e9.

Sato, S., Fukasawa, M., Yamakawa, Y., Natsume, T., Suzuki, T., Shoji, I., Aizaki, H., Miyamura, T. and Nishijima, M. (2006). Proteomic profiling of lipid droplet proteins in hepatoma cell lines expressing hepatitis C virus core protein. *Journal of Biochemistry* 139(5), 921-930.

Schaffner, G. and Matile, P. (1981). Structure and composition of baker's yeast lipid globules. *Biochemie und Physiologie der Pflanzen* 176, 659-666.

Schroeder, B., Schulze, R. J., Weller, S. G., Sletten, A. C., Casey, C. A. and McNiven, M. A. (2015). The small GTPase Rab7 as a central regulator of hepatocellular lipophagy. *Hepatology* 61, 1896-907.

Schuldiner, M. and Bohnert, M. (2017). A different kind of love - lipid droplet contact sites. *Biochimica et Biophysica Acta (BBA) – Molecular & Cell Biology of Lipids* 1862, 1188-1196.

Schwartz, R. S., Olson, J. A., Raventos-Suarez, C., Yee, M., Heath, R. H., Lubin, B. and Nagel, R. L. (1987). Altered Plasma Membrane Phospholipid Organization in Plasmodium falciparum-Infected Human Erythrocytes. *Blood* 69, 401-407.

Scorrano, L., De Matteis, M. A., Emr, S., Giordano, F., Hajnoczky, G., Kornmann, B., Lackner, L. L., Levine, T. P., Pellegrini, L., Reinisch, K., Rizzuto, R., Simmen, T., Stenmark,

H., Ungermann, C. and Schuldiner, M. (2019). Coming together to define membrane contact sites. *Nature Communications* 10, 1287.

Sezgin, E., Levental, I., Mayor, S. and Eggeling, C. (2017). The mystery of membrane organization: composition, regulation and roles of lipid rafts. *Nature Reviews Molecular Cell Biology* 18, 361-374.

Shears, M. J., Botte, C. Y. and McFadden, G. I. (2015). Fatty acid metabolism in the Plasmodium apicoplast: Drugs, doubts and knockouts. *Molecular & Biochemical Parasitology* 199, 34-50.

Sheokand, P. K., Yamaryo-Botte, Y., Narwal, M., Arnold, C. S., Thakur, V., Islam, M. M., Banday, M. M., Asad, M., Botte, C. Y. and Mohmmed, A. (2023). A *Plasmodium falciparum* lysophospholipase regulates host fatty acid flux via parasite lipid storage to enable controlled asexual schizogony. *Cell Reports* 42(4), 112251.

Sherman, I. W. (1979). Biochemistry of *Plasmodium* (malarial parasites). *Microbiological Reviews* 43, 453-495.

Shihan, M. H., Novo, S. G., Le Marchand, S. J., Wang, Y. and Duncan, M. K. (2021). A simple method for quantitating confocal fluorescent images. *Biochemistry & Biophysics Reports* 25, 100916.

Shockey, J. M., Gidda, S. K., Chapital, D. C., Kuan, J.-C., Dhanoa, P. K., Bland, J. M., Rothstein, S. J., Mullen, R. T. and Dyer, J. M. (2006). Tung tree DGAT1 and DGAT2 have nonredundant functions in triacylglycerol biosynthesis and are localized to different subdomains of the endoplasmic reticulum. *The Plant Cell* 18, 2294-2313.

Shunmugam, S., Arnold, C. S., Dass, S., Katris, N. J. and Botte, C. Y. (2022). The flexibility of Apicomplexa parasites in lipid metabolism. *PLOS Pathogens* 18, e1010313.

Shunmugam, S., Quansah, N., Flammersfeld, A., Islam, M. M., Sassmannshausen, J., Bennink, S., Yamaryo-Botté, Y., Pradel, G. and Botté, C. Y. (2023). The patatin-like phospholipase PfPNPLA2 is involved in the mitochondrial degradation of phosphatidylglycerol during *Plasmodium falciparum* blood stage development. *Frontiers in Cellular & Microbiology 13*,997245.

Si, W., Zhao, Y., Qin, X., Huang, Y., Yu, J., Liu, X., Li, Y., Yan, X., Zhang, Q. and Sun, J. (2023). What exactly does the PfK13 C580Y mutation in *Plasmodium falciparum* influence? *Parasites & Vectors* 16(1), 421.

Siddiqui, A. A., Saha, D., Iqbal, M. S., Saha, S. J., Sarkar, S., Banerjee, C., Nag, S., Mazumder, S., De, R., Pramanik, S., Debsharma, S. and Bandyopadhyay, U. (2020). Rab7 of *Plasmodium falciparum* is involved in its retromer complex assembly near the digestive vacuole. *Biochimica et Biophysica Acta (BBA) - General Subjects* 1864(10), 129656.

Sidhu, A. B. S., Verdier-Pinard, D. and Fidock, D. A. (2002). Chloroquine resistance in *Plasmodium falciparum* malaria parasites conferred by pfcrt mutations. *Science* 298, 210-213.

Sinden, R. E., Canning, E. U., Bray, R. S., Smalley, M. E. and Garnham, P. C. C. (1997). Gametocyte and gamete development in *Plasmodium falciparum*. *Proceedings of the Royal Society of London. Series B. Biological Sciences* 201, 375-399.

Singh, P., Alaganan, A., More, K. R., Lorthiois, A., Thiberge, S., Gorgette, O., Guillotte Blisnick, M., Guglielmini, J., Aguilera, S. S., Touqui, L., Singh, S. and Chitnis, C. E. (2019). Role of a patatin-like phospholipase in *Plasmodium falciparum* gametogenesis and malaria transmission. *Proceedings of the National Academy of Sciences* 116, 17498-17508.

Singh, R., Kaushik, S., Wang, Y., Xiang, Y., Novak, I., Komatsu, M., Tanaka, K., Cuervo, A. M. and Czaja, M. J. (2009). Autophagy regulates lipid metabolism. *Nature* 458, 1131-1135.

Skarda, L., Kowal, J. and Locher, K. P. (2021). Structure of the human cholesterol transporter ABCG1. *Journal of Molecular Biology* 433(21), 167218.

Smilkstein, M., Sriwilaijaroen, N., Kelly, J. X., Wilairat, P. and Riscoe, M. (2004). Simple and inexpensive fluorescence-based technique for high-throughput antimalarial drug screening. *Antimicrobial Agents & Chemotherapy* 48(5), 1803-1806.

Smith, J. D., Rowe, J. A., Higgins, M. K. and Lavstsen, T. (2013). Malaria's deadly grip: cytoadhesion of *Plasmodium falciparum*-infected erythrocytes. *Cellular Microbiology* 15, 1976-1983.

Smith, S. J., Cases, S., Jensen, D. R., Chen, H. C., Sande, E., Tow, B., Sanan, D. A., Raber, J., Eckel, R. H. and Farese, R. V. (2000). Obesity resistance and multiple mechanisms of triglyceride synthesis in mice lacking Dgat. *Nature Genetics* 25, 87-90.

Song, J., Mizrak, A., Lee, C.-W., Cicconet, M., Lai, Z. W., Tang, W.-C., Lu, C.-H., Mohr, S. E., Farese, R. V. and Walther, T. C. (2022). Identification of two pathways mediating protein targeting from ER to lipid droplets. *Nature Cell Biology* 24, 1364-1377.

Sorci-Thomas, M., Babiak, J. and Rudel, L. L. (1990). Lecithin-cholesterol acyltransferase (LCAT) catalyzes transacylation of intact cholesteryl esters. Evidence for the partial reversal of the forward LCAT reaction. *Journal of Biological Chemistry* 265, 2665-2670.

Stone, S. J., Myers, H. M., Watkins, S. M., Brown, B. E., Feingold, K. R., Elias, P. M. and Farese, R. V. (2004). Lipopenia and skin barrier abnormalities in DGAT2-deficient mice. *Journal of Biological Chemistry* 279, 11767-11776.

Storch, C. H., Ehehalt, R., Haefeli, W. E. and Weiss, J. (2007). Localization of the human breast cancer resistance protein (BCRP/ABCG2) in lipid rafts/caveolae and modulation of its activity by cholesterol in vitro. *The Journal of Pharmacology & Experimental Therapeutics* 323(1), 257-264.

Sturley, S. L. and Hussain, M. M. (2012). Lipid droplet formation on opposing sides of the endoplasmic reticulum. *Journal of Lipid Research* 53, 1800-1810.

Su, W., Wang, Y., Jia, X., Wu, W., Li, L., Tian, X., Li, S., Wang, C., Xu, H., Cao, J., Han, Q., Xu, S., Chen, Y., Zhong, Y., Zhang, X., Liu, P., Gustafsson, J. Å. and Guan, Y. (2014).

Comparative proteomic study reveals 17β-HSD13 as a pathogenic protein in nonalcoholic fatty liver disease. *Proceedings of the National Academy of Sciences* 111, 11437-11442.

Suzuki, M., Shinohara, Y., Ohsaki, Y. and Fujimoto, T. (2011). Lipid droplets: size matters. *Journal of Electron Microscopy* 60, S101-S116.

Szilagyi, J. T., Vetrano, A. M., Laskin, J. D. and Aleksunes, L. M. (2017). Localization of the placental BCRP/ABCG2 transporter to lipid rafts: Role for cholesterol in mediating efflux activity. *Placenta* 55, 29-36.

Sztalryd, C. and Kimmel, A. R. (2014). Perilipins: Lipid droplet coat proteins adapted for tissue-specific energy storage and utilization, and lipid cytoprotection. *Biochimie* 96, 96-101.

Sztalryd, C., Xu, G., Dorward, H., Tansey, J. T., Contreras, J. A., Kimmel, A. R. and Londos, C. (2003). Perilipin A is essential for the translocation of hormone-sensitive lipase during lipolytic activation. *Journal of Cell Biology* 161, 1093-1103.

Tabata, N., Ito, M., Tomoda, H. and Ōmura, S. (1997). Xanthohumols, diacylglycerol acyltransferase inhibitors, from Humulus lupulus. *Phytochemistry* 46, 683-687.

Taku, I., Hirai, T., Makiuchi, T., Shinzawa, N., Iwanaga, S., Annoura, T., Nagamune, K., Nozaki, T. and Saito-Nakano, Y. (2020). Rab5b-Associated Arf1 GTPase Regulates Export of N-Myristoylated Adenylate Kinase 2 From the Endoplasmic Reticulum in *Plasmodium falciparum*. *Frontiers in Cellular & Infection Microbiology* 10, 610200.

Tan, Y.-j., Jin, Y., Zhou, J. and Yang, Y.-f. (2024). Lipid droplets in pathogen infection and host immunity. *Acta Pharmacologica Sinica* 45, 449-464.

Tapia, J. C., Kasthuri, N., Hayworth, K. J., Schalek, R., Lichtman, J. W., Smith, S. J. and Buchanan, J. (2012). High-contrast en bloc staining of neuronal tissue for field emission scanning electron microscopy. *Nature Protocols* 7, 193-206.

Tauchi-Sato, K., Ozeki, S., Houjou, T., Taguchi, R. and Fujimoto, T. (2002). The surface of lipid droplets is a phospholipid monolayer with a unique fatty acid composition. *Journal of Biological Chemistry* 277, 44507-44512.

Teo, W., Caprariello, A. V., Morgan, M. L., Luchicchi, A., Schenk, G. J., Joseph, J. T., Geurts, J. J. G. and Stys, P. K. (2021). Nile Red fluorescence spectroscopy reports early physicochemical changes in myelin with high sensitivity. *Proceedings of the National Academy of Sciences of the United States of America* 118(8), e2016897118.

To, H., Reinholdt, P., Bashawat, M., Luck, M., Lauritsen, L., Akkerman, V., Kroiss, M., Wüstner, D., Kongsted, J., Müller, P. and Scheidt, H. A. (2024). The impact of acyl-CoA:cholesterol transferase (ACAT) inhibitors on biophysical membrane properties depends on membrane lipid composition. *Molecular & Cellular Endocrinology* 594, 112385.

Toker, A. (2005). The biology and biochemistry of diacylglycerol signalling. *EMBO reports* 6, 310-314-314.

Tokumasu, F., Crivat, G., Ackerman, H., Hwang, J. and Wellems, T. E. (2014). Inward cholesterol gradient of the membrane system in P. falciparum-infected erythrocytes involves a dilution effect from parasite-produced lipids. *Biology Open* 3(6), 529-541.

Tran, P. N. (2014). A female-gametocyte-specific transporter plays a role in lipid metabolism in malaria parasites. *Doctoral thesis, La Trobe University*.

Tran, P. N., Brown, S. H., Mitchell, T. W., Matuschewski, K., McMillan, P. J., Kirk, K., Dixon, M. W. and Maier, A. G. (2014). A female gametocyte-specific ABC transporter plays a role in lipid metabolism in the malaria parasite. *Nature Communications* 5, 4773.

Tran, P. N., Brown, S. H., Rug, M., Ridgway, M. C., Mitchell, T. W. and Maier, A. G. (2016). Changes in lipid composition during sexual development of the malaria parasite *Plasmodium falciparum*. *Malaria Journal* 15, 73.

Turchetto-Zolet, A. C., Maraschin, F. S., de Morais, G. L., Cagliari, A., Andrade, C. M. B., Margis-Pinheiro, M. and Margis, R. (2011). Evolutionary view of acyl-CoA diacylglycerol acyltransferase (DGAT), a key enzyme in neutral lipid biosynthesis. *BMC Evolutionary Biology* 11, 263.

Turkish, A. and Sturley, S. L. (2007). Regulation of triglyceride metabolism. I. Eukaryotic neutral lipid synthesis: "Many ways to skin ACAT or a DGAT". *American Journal of Physiology, Gastrointerinal & Liver Physiology* 292(4), G953-G957.

Turkish, A. R. and Sturley, S. L. (2009). The genetics of neutral lipid biosynthesis: an evolutionary perspective. *American Journal of Physiology-Endocrinology and Metabolism* 297, E19-E27.

Turunen, S. (1979). Digestion and absorption of lipids in insects. *Comparative Biochemistry and Physiology Part A: Physiology* 63, 455-460.

Vallochi, A. L., Teixeira, L., Oliveira, K. D. S., Maya-Monteiro, C. M. and Bozza, P. T. (2018). Lipid Droplet, a Key Player in Host-Parasite Interactions. *Frontiers in Immunology* 9, 1022.

van Biljon, R., Niemand, J., van Wyk, R., Clark, K., Verlinden, B., Abrie, C., von Gruning, H., Smidt, W., Smit, A., Reader, J., Painter, H., Llinás, M., Doerig, C. and Birkholtz, L. M. (2018). Inducing controlled cell cycle arrest and re-entry during asexual proliferation of *Plasmodium falciparum* malaria parasites. *Scientific Reports* 8(1), 16581.

van Dooren, G. G., Marti, M., Tonkin, C. J., Stimmler, L. M., Cowman, A. F. and McFadden, G. I. (2005). Development of the endoplasmic reticulum, mitochondrion and apicoplast during the asexual life cycle of *Plasmodium falciparum*. *Molecular Microbiology* 57, 405-19.

van Dooren, G. G., Stimmler, L. M. and McFadden, G. I. (2006). Metabolic maps and functions of the *Plasmodium* mitochondrion. *FEMS Microbiology Reviews* 30(4), 596-630.

van Meer, G. (2001). Caveolin, Cholesterol, and Lipid Droplets? *Journal of Cell Biology* 152(5), 29-34.

van Meer, G., Halter, D., Sprong, H., Somerharju, P. and Egmond, M. R. (2006). ABC lipid transporters: Extruders, flippases, or flopless activators? *FEBS Letters* 580, 1171-1177.

van Meer, G., Voelker, D. R. and Feigenson, G. W. (2008). Membrane lipids: where they are and how they behave. *Nature Reviews Molecular Cell Biology* 9, 112-124.

Van Schravendijk, M. R., Pasloske, B. L., Baruch, D. I., Handunnetti, S. M. and Howard, R. J. (1993). Immunochemical characterization and differentiation of two ~300-KD erythrocyte membrane-associated proteins of *Plasmodium falciparum*, PfEMP1 and PfEMP3. *The American Journal of Tropical Medicine and Hygiene* 49, 552-565.

Vaughan, A. M., O'Neill, M. T., Tarun, A. S., Camargo, N., Phuong, T. M., Aly, A. S. I., Cowman, A. F. and Kappe, S. H. I. (2009). Type II fatty acid synthesis is essential only for malaria parasite late liver stage development. *Cellular Microbiology* 11, 506-520.

Veldhuis, J. D., Strauss, J. F., III, Silavin, S. L., Kolp, L. A., Klase, P. A., Juchter, D. and Garmey, J. (1985). The role of cholesterol esterification in ovarian steroidogenesis: studies in cultured Swine Granulosa cells using a novel inhibitor of Acyl Coenzyme A:Cholesterol Acyltransferase. *Endocrinology* 116, 25-30.

Vial, H. J. and Ben Mamoun, C. (2005). *Plasmodium* Lipids: Metabolism and Function. In *Molecular Approaches to Malaria*327-352.

Vial, H. J., Philippot, J. R. and Wallach, D. F. H. (1984). A reevaluation of the status of cholesterol in erythrocytes infected by *Plasmodium knowlesi* and *P. falciparum*. *Molecular and Biochemical Parasitology* 13, 53-65.

Vial, H. J., Thuet, M. J., Broussal, J. L. and Philippot, J. R. (1982). Phospholipid biosynthesis by *Plasmodium knowlesi*-infected erythrocytes: the incorporation of phospholipid precursors and the identification of previously undetected metabolic pathways. *The Journal of parasitology* 68(3), 379-391.

Vielemeyer, O., McIntosh, M. T., Joiner, K. A. and Coppens, I. (2004). Neutral lipid synthesis and storage in the intraerythrocytic stages of *Plasmodium falciparum*. *Molecular & Biochemical Parasitology* 135(2), 197-209.

Voß, Y., Klaus, S., Guizetti, J. and Ganter, M. (2023). Plasmodium schizogony, a chronology of the parasite's cell cycle in the blood stage. *PLOS Pathogens* 19, e1011157.

Wan, H.-C., Melo, R. C. N., Jin, Z., Dvorak, A. M. and Weller, P. F. (2007). Roles and origins of leukocyte lipid bodies: proteomic and ultrastructural studies. *The FASEB Journal* 21, 167-178.

Wang, F., Li, G., Gu, H. M. and Zhang, D. W. (2013). Characterization of the role of a highly conserved sequence in ATP binding cassette transporter G (ABCG) family in ABCG1 stability, oligomerization, and trafficking. *Biochemistry* 52, 9497-509.

Wang, H., Becuwe, M., Housden, B. E., Chitraju, C., Porras, A. J., Graham, M. M., Liu, X. N., Thiam, A. R., Savage, D. B. and Agarwal, A. K. (2016). Seipin is required for converting nascent to mature lipid droplets. *eLife* 5, e16582.

Wang, H., Sreenivasan, U., Hu, H., Saladino, A., Polster, B. M., Lund, L. M., Gong, D.-w., Stanley, W. C. and Sztalryd, C. (2011). Perilipin 5, a lipid droplet-associated protein, provides physical and metabolic linkage to mitochondria. *Journal of Lipid Research* 52, 2159-2168.

Ward, G. E., Tilney, L. G. and Langsley, G. (1997). Rab GTPases and the unusual secretory pathway of plasmodium. *Parasitology Today* 13, 57-62.

Watkins, P. A., Maiguel, D., Jia, Z. and Pevsner, J. (2007). Evidence for 26 distinct acyl-coenzyme A synthetase genes in the human genomes. *Journal of Lipid Research* 48, 2736-2750.

Watt, M. J. and Spriet, L. L. (2010). Triacylglycerol lipases and metabolic control: implications for health and disease. *Amerian Journal of Physiology. Endocrinology & Metabolism* 299(2), E162-E168.

Westerterp, M., Murphy, A. J., Wang, M., Pagler, T. A., Vengrenyuk, Y., Kappus, M. S., Gorman, D. J., Nagareddy, P. R., Zhu, X., Abramowicz, S., Parks, J. S., Welch, C., Fisher, E. A., Wang, N., Yvan-Charvet, L. and Tall, A. R. (2013). Deficiency of ATP-Binding Cassette Transporters A1 and G1 in macrophages increases inflammation and accelerates atherosclerosis in mice. *Circulation Research* 112, 1456-1465.

Wilfling, F., Thiam, A. R., Olarte, M. J., Wang, J., Beck, R., Gould, T. J., Allgeyer, E. S., Pincet, F., Bewersdorf, J., Farese, R. V., Jr. and Walther, T. C. (2014). Arf1/COPI machinery acts directly on lipid droplets and enables their connection to the ER for protein targeting. *eLife* 3, e01607.

Woehlecke, H., Pohl, A., Alder-Baerens, N., Lage, H. and Herrmann, A. (2003). Enhanced exposure of phosphatidylserine in human gastric carcinoma cells overexpressing the half-size ABC transporter BCRP (ABCG2). *Biochemical Journal* 376, 489-495.

Wu, A., Wojtowicz, K., Savary, S., Hamon, Y. and Trombik, T. (2020). Do ABC transporters regulate plasma membrane organization? *Cellular & Molecular Biology Letters* 25, 37.

Xie, C., Zhou, Z.S., Li, N., Bian, Y., Wang, Y.J., Wang, L.J., Li, B.-L. and Song, B.L. (2012). Ezetimibe blocks the internalization of NPC1L1 and cholesterol in mouse small intestine. *Journal of Lipid Research* 53, 2092-2101.

Xu, W., Wu, L., Yu, M., Chen, F.-J., Arshad, M., Xia, X., Ren, H., Yu, J., Xu, L. and Xu, D. (2016). Differential roles of cell death-inducing DNA fragmentation factor-α-like effector (cide) proteins in promoting lipid droplet fusion and growth in subpopulations of hepatocytes. *Journal of Biological Chemistry* 291, 4282-4293.

Yam, X. Y., Birago, C., Fratini, F., Di Girolamo, F., Raggi, C., Sargiacomo, M., Bachi, A., Berry, L., Fall, G., Currà, C., Pizzi, E., Breton, C. B. and Ponzi, M. (2013). Proteomic analysis of detergent-resistant membrane microdomains in trophozoite blood stage of the human malaria parasite *Plasmodium falciparum*. *Molecular & Cellular Proteomics* 12, 3948-3961.

Yamamuro, D., Yamazaki, H., Osuga, J.-i., Okada, K., Wakabayashi, T., Takei, A., Takei, S., Takahashi, M., Nagashima, S., Holleboom, A. G., Kuroda, M., Bujo, H. and Ishibashi, S. (2020). Esterification of 4β-hydroxycholesterol and other oxysterols in human plasma occurs independently of LCAT. *Journal of Lipid Research* 61, 1287-1299.

Yamazaki, T., Sasaki, E., Kakinuma, C., Yano, T., Miura, S. and Ezaki, O. (2005). Increased very low density lipoprotein secretion and gonadal fat mass in mice overexpressing liver DGAT1. *Journal of Biological Chemistry* 280, 21506-21514.

Yang, L., Ding, Y., Chen, Y., Zhang, S., Huo, C., Wang, Y., Yu, J., Zhang, P., Na, H., Zhang, H., Ma, Y. and Liu, P. (2012). The proteomics of lipid droplets: structure, dynamics, and functions of the organelle conserved from bacteria to humans. *Journal of Lipid Research* 53, 1245-1253.

Yang, Q., Loureiro, Z. Y., Desai, A., DeSouza, T., Li, K., Wang, H., Nicoloro, S. M., Solivan-Rivera, J. and Corvera, S. (2023). Regulation of lipolysis by 14-3-3 proteins on human adipocyte lipid droplets. *PNAS Nexus* 2(12), pgad420.

Yen, C. L., Stone, S. J., Koliwad, S., Harris, C. and Farese, R. V., Jr. (2008). Thematic review series: glycerolipids. DGAT enzymes and triacylglycerol biosynthesis. *Journal of Lipid Research* 49(11), 2283-2301.

Yoon, K., Han, D., Li, Y., Sommerfeld, M. and Hu, Q. (2012). Phospholipid:Diacylglycerol Acyltransferase is a multifunctional enzyme involved in membrane lipid turnover and degradation while synthesizing triacylglycerol in the unicellular green microalga Chlamydomonas reinhardtii *The Plant Cell* 24, 3708-3724.

Yu, J., Zhang, S., Cui, L., Wang, W., Na, H., Zhu, X., Li, L., Xu, G., Yang, F., Christian, M. and Liu, P. (2015). Lipid droplet remodeling and interaction with mitochondria in mouse brown adipose tissue during cold treatment. *Biochimica et Biophysica Acta (BBA) - Molecular Cell Research* 1853, 918-928.

Yuan, J., Cheng, K. C.-C., Johnson, R. L., Huang, R., Pattaradilokrat, S., Liu, A., Guha, R., Fidock, D. A., Inglese, J., Wellems, T. E., Austin, C. P. and Su, X. Z. (2011). Chemical genomic profiling for antimalarial therapies, response signatures, and molecular targets. *Science* 333, 724-729.

Yvan-Charvet, L., Ranalletta, M., Wang, N., Han, S., Terasaka, N., Li, R., Welch, C. and Tall, A. R. (2007). Combined deficiency of ABCA1 and ABCG1 promotes foam cell accumulation and accelerates atherosclerosis in mice. *The Journal of Clinical Investigation* 117, 3900-3908.

Zerial, M. and McBride, H. (2001). Rab proteins as membrane organizers. *Nature Reviews Molecular Cell Biology* 2, 107-117.

Zhang, P., Na, H., Liu, Z., Zhang, S., Xue, P., Chen, Y., Pu, J., Peng, G., Huang, X., Yang, F., Xie, Z., Xu, T., Xu, P., Ou, G., Zhang, S. O. and Liu, P. (2012). Proteomic study and marker protein identification of Caenorhabditis elegans lipid droplets. *Molecular & Cellular Proteomics* 11, 317-328.

Zhukovsky, M. A., Filograna, A., Luini, A., Corda, D. and Valente, C. (2019). Phosphatidic acid in membrane rearrangements. *FEBS Letters* 593, 2428-2451.

Zweytick, D., Athenstaedt, K. and Daum, G. (2000). Intracellular lipid particles of eukaryotic cells. *Biochimica et Biophysica Acta (BBA) - Reviews on Biomembranes* 1469, 101-120.